International PhD Program in Biomolecular Sciences – XXXIV cycle

Department of Cellular, Computational and Integrative Biology – CIBIO

Investigation of supernumerary centrosomes accumulation and Caspase-2 activation in human cell lines

PhD Thesis of:
Iva G. DZHILYANOVA
Mat. 205787

Tutor:
Prof. Massimo PIZZATO

Advisor:
Prof. Luca FAVA

Academic Year 2020/2021

DECLARATION

I, Iva Georgieva Dzhilyanova, confirm that this is my own work and the use of all materials from other sources has been properly and fully acknowledged.

ABSTRACT

Centrosomes are microtubule-based organelles composed of two centrioles and peri-centriolar material, involved in the formation and organization of the mitotic spindle, serving as microtubule-organizing center and involved in ciliogenesis. Supernumerary centrosomes are detrimental for cell physiology and activate the PIDDosome, a multi-protein complex that serves as a platform for the activation of Caspase-2, composed of: PIDD1, RAIDD and Caspase-2 itself. Caspase-2's preferred cleavage site based on peptide screening is VDVAD, however Caspase-2, when activated via the PIDDosome, cleaves its bona fide substrate MDM2 (negative p53 regulator) in the FDVPD sequence.

Here, I present evidence for VDVADase activity in apoptotic cells lacking Caspase-2, which suggests that this cleavage site is not Caspase-2 specific when the Caspase-2 activation occurs via the PIDDosome. In order to investigate if the mode of activation of Caspase-2 determines its substrate specificities I performed a Caspase-2 rescue experiment and introduced several mutations affecting the Caspase-2 autoproteolytic-processing. Furthermore, I present evidence that exogenous Caspase-2 is able to form the PIDDosome and cleaves MDM2 but when key autoproteolytic sites are mutated no MDM2 cleavage is detectable.

Supernumerary centrosomes also accumulate upon overexpression of PLK4 (a kinase regulator of the centriole duplication). Immunofluorescence images of cells overexpressing PLK4 were taken following the centrioles quantification over time. Consequently, a large amount of image data was accumulated, which necessitated the development of a semi-automated pipeline for centrioles counting. This pipeline was generated using the image processing and analysis tool ImageJ and the deep learning segmentation tool MitoS together with the pretrained MitoSegNet model, which was finetuned to count centrioles stained against different centrosomal epitopes, namely Centrin 1, γ-Tubulin and ANKRD26. This semi-automated method of centrioles quantification is easy to use, reproducible and faster than manual quantification. Using this pipeline to quantify centrioles in p53, SCLT1 or ANKRD26 lacking cells we demonstrate accumulation of supernumerary centrosomes in these cells similar to parental cells.

ABSTRACT

I centrosomi sono organelli cellulari a base di microtubuli, composti da due centrioli e dal materiale pericentriolare che li circonda. I centrosomi sono coinvolti nell'organizzazione dei microtubuli, nella formazione del fuso mitotico e nella ciliogenesi. I centrosomi soprannumerari sono dannosi per la fisiologia cellulare e attivano il PIDDosoma, un complesso multiproteico, composto da PIDD1, RAIDD e Caspasi-2, che funge da piattaforma per l'attivazione della caspasi stessa. Il sito preferenziale di proteolisi di Caspasi-2 è stato individuato tramite screening peptidico nella sequenza VDVAD. Nonostante ciò, quando attivata tramite il PIDDosoma, Caspasi-2 scinde il suo substrato di elezione MDM2 (regolatore negativo di p53) a livello della sequenza FDVPD.

In questa tesi presento evidenze di attività VDVAD-asica in cellule apoptotiche prive di Caspasi-2, suggerendo che questo sito di taglio non sia specifico di Caspasi-2 quando la sua attivazione avviene tramite il PIDDosoma. Al fine di indagare se la modalità di attivazione della proteasi determina le sue specificità di substrato, ho eseguito esperimenti di complementazione di Caspasi-2 facendo uso di diversi mutanti che influenzano il suo processamento autoproteolitico. Inoltre, presento prove che Caspasi-2 esogena è in grado di assemblare il PIDDosoma e proteolizzare MDM2 ma quando i suoi siti chiave di autoproteolisi sono mutati non è rilevabile il taglio di MDM2.

I centrosomi soprannumerari si accumulano anche in caso di sovraespressione di PLK4 (chinasi regolatrice della duplicazione dei centrioli). Immagini di immunofluorescenza di cellule che sovraesprimono PLK4 sono state acquisite seguendo la cinetica di accumulo dei centrioli nel tempo. Di conseguenza, l'ingente mole di dati generati ha reso necessario lo sviluppo di una procedura semiautomatica per la conta dei centrioli. Questa pipeline è stata generata utilizzando il programma di elaborazione e analisi di immagini ImageJ e il programma di segmentazione basato su deep learning MitoS, insieme al modello MitoSegNet, che è stato affinato per la conta dei centrioli evidenziati tramite immunofluorescenza diretta contro diversi epitopi centrosomiali, ossia: Centrin 1, γ-Tubulina e ANKRD26. Questo metodo semiautomatico di quantificazione dei centrioli è facile da usare, riproducibile e più veloce della quantificazione manuale. Utilizzando questa procedura per quantificare i centrioli nelle cellule prive di p53, SCLT1 o ANKRD26, dimostriamo che l'accumulo di centrosomi soprannumerari in queste cellule è simile a quello riscontrato nelle cellule parentali.

TABLE OF CONTENT

ABBREVIATIONS

°C	degree Celsius
µg	microgram
µl	microliter
µM	micromolar
Ab	antibody
ADP	Adenosine Diphosphate
AFC	7-Amino-4-trifluoromethylcoumarin
AI	Artificial Intelligence
ANKRD26	Ankyrin Repeat Domain 26
ANN	Artificial Neural Network
AOMK	Acyloxymethyl Ketone
APAF	Apoptotic Protease Activating Factor 1
AR	Ankyrin Repeat
ATP	Adenosine Triphosphate
AURBK	Aurora B Kinase
BCA	Bicinchoninic Acid
BCA	Brightness and Contrast Adjustment
BH3	BCL-2 Homology 3
BID	BH3-interacting Domain Death Agonist
bit	binary digit
BLD10	Basal Body protein
C2CD3	C2 Domain-containing Protein 3
CARD	Caspase Recruitment Domain
CASP	Caspase
CASP-2	Caspase-2
CASP-3	Caspase-3
CCDC120	Coiled-coil Domain Containing Protein
CD95	Cluster of Differentiation 95

CDC	Cell Division Cycle
CDK	Cyclin-dependent Kinase
CED	*C. elegans* Cell Death
CENPJ	Centromere Protein J
CEP	Centrosomal Protein
CHO	Aldehyde functional group (Carbon Hydrogen Oxygen)
CIP1	CDK-interacting Protein 1
CK2	Casein Kinase 2
cm	centimeter
CMV	Cytomegalovirus
CNN	Convolutional Neural Networks
CO_2	Carbon dioxide
CP110	Centriolar Coiled-Coil Protein of 110kDa
CPAP	Centrosomal P4.1-Associated Protein
CPP32	Cysteine Proteas Protein 32-kDa
CPU	Central Processing Unit
CRADD	Caspase-2 And RIPK1 Domain Containing Adaptor With Death Domain
CUX	Cut Like Homeobox 1
DED	Death Effector Domains
DEVD	Aspartic Acid Glutamic Acid Valine Aspartic Acid
DHCB	Dihydro Cytochalasin-B
DISC	Death-inducing Signaling Complex
DMEM	Dulbecco's Modified Eagle Medium
DMSO	Dimethyl Sulfoxide
DNA	Deoxyribonucleic Acid
DSCD	Aspartic Acid Serine Glycine Aspartic Acid
DXC	Doxycycline
E2F	E2 factor
E3	Enzyme 3
EB1	End binding 1

ECT2	Epithelial Cell Transforming 2
ER	Endoplasmatic Reticulum
ESPD	Glutamic Acid Serine Proline Aspartic Acid
FBF1	Fas-binding Factor 1
FDVPD	Phenylalanine Aspartic Acid Valine Proline Aspartic Acid
FL	Full length
FMK	Fluoromethyl Ketone
FRT	FLP Recombination Target
fw	forward
G 0/1/2	Gap 0/1/2
GEF	Guanine Nucleotide Exchange Factors
GFP	Green Fluorescent Protein
h	hours
H_2O	water
HEK293T	Human Embryonic Kidney 293 cells
HQPA	Hydroxyquinazoline-Pyrazol-Aniline
hTERT-RPE1	Human Telomerase-immortalized Retinal Pigment Epithelium 1
IETD	Isoleucine Glutamic Acid Threonine Aspartic Acid
INK4	Inhibitors of CDK4
kDa	kilodalton
KIF24	Kinesin Family Member 24
KO	knockout
LDESD	Leucine Aspartic Acid Glutamic Acid Serin Aspartic Acid
LEHD	Leucine Glutamic Acid Histidine Aspartic Acid
LQTD	Leucine Glutamine Threonine Aspartic Acid
LRDD	Leucine-rich Repeats and Death Domain
M	Mitosis
Man	manual
MDM2	Mouse Double Minute 2 homolog
MEF	Mouse Embryonic Fibroblasts
MetOH	Methanol

mL	milliliter
MOMP	Mitochondrial Outer Membrane Permeabilization
MSN	MitoSegNet
MT	microtubules
MTOC	Major Microtubule-organizing Center
NAP1L4	Nucleosome Assembly Protein 1-Like 4
NEDD	Neural precursor cell expressed developmentally downregulated
NEK2A	NIMA-related Kinase A
NES	Nuclear Export Signal
NF	Nuclear Factor
NLS	Nuclear Localization Signal
NT	non treated
o/n	over night
ODF2	Outer Dense Fiber protein 2
OE	overexpression
OFD1	Oral-Facial-Digital Syndrome 1 protein
P53	Tumor Protein P53
PARP	Poly (ADP-ribose) Polymerase
PBS	Phosphate-buffered Saline
PCM	Pericentriolar Material
PCNT	Pericentrin
PIDD	P53-Induced Death Domain Protein
PK	Protein Kinase
PKC	Protein Kinase C
PKCK2	Protein Kinase Casein Kinase 2 alpha
PLK	Polo-like Kinase
PP	Protein Phosphatase
qVDOPh	Quinoline-Val-Asp-Difluorophenoxymethylketone
RAIDD	RIP-Associated ICH1/CED3-Homologous Protein with Death
RB	Retinoblastoma Protein
RING	Really Interesting New Gene

RIP	Receptor-Interacting Protein
RNA	Ribonucleic Acid
RT	room temperature
rw	reverse
SA	Semi-automated
SAC	Spindle Assembly Checkpoint
SAS6	Spindle Assembly Abnormal Protein 6 Homolog
SCLT1	Sodium Channel and Clathrin Linker 1
Sdi1	Sulphur deficiency-induced gene 1
SDS	Sodium Dodecyl Sulphate
SEGD	Serine Glutamic Acid Glycine Aspartic Acid
SEVDG	Serine Glutamic Acid Valine Aspartic Acid Glycine
SFSD	Serine Phenylalanine Serine Aspartic Acid
Smac	Second Mitochondria-derived Activator of Caspases
SPICE	Spindle and Centriole-Associated Protein
STIL	SCL/TAL1-interrupting locus protein
STS	Staurosporine
TAL1	T-cell Acute Lymphocytic Leukemia Protein 1
TNFR	Tumor Necrosis Factor
TTBK2	Tau Tubulin Kinase 2
UM	Unsharp Masking
UV	Ultraviolet
VDTTD	Valine Aspartic Acid Threonine Threonine Aspartic Acid
VDVAD	Valine Aspartic Acid Valine Alanine Aspartic Acid
VEID	Valine Glutamic Acid Isoleucine Aspartic Acid
WEHI	Walter and Eliza Hall Institute
wt	wild type
ZYG	Zygote Defective Protein
γ-TuRC	γ-Tubulin Ring Complex

INTRODUCTION

1. Cell cycle

Cell division (mitosis) allows the duplicated single (mother) cell to generate two new (daughters) cells and to segregate its duplicated genome equally among them. The process was observed under a microscope for the first time in 1835 by the German botanist Hugo von Mohl (Mohl, 1837) and the term “mitosis” was firstly introduced by Walther Flemming (Flemming, 1878). Cell division is a highly regulated process of the cell cycle that involves many molecules and signals in order to achieve high precision. The cell division process plays a key role in the cell cycle and determines most of it. The cell cycle is the lifetime of a cell starting right after the mother cell’s division and ending with its own cell division or cell death. The concept for cell cycle and its main phases were developed by Alma Howard and Stephen Pelc in 1953, the same year Watson and Crick published their discovery of the molecular structure of the nucleic acids based on Rosalind Franklin's discovery (Howard, A. & Pelc, 1953; Howard & Pelc, 1986; Voorhees et al., 1976; Watson & Crick, 1953).

The animal cells’ interphase (taking approximately 24 hours (Alberts B, Johnson A, Lewis J, 2002; Israels & Israels, 2001)) is subdivided into three main stages: gap before DNA synthesis (G1) phase, DNA synthesis phase (S) and a gap post-DNA replication (G2) phase (Hartwell & Weinert, 1989; Howard & Pelc, 1986), followed by mitosis (M phase) which ends with cytokinesis (Fig. 1). G is indicative for a gap in the cell’s microscopic appearance between the two morphologically most distinctive phases: S phase and mitosis (Nurse, 2000; Prestige, 1972; Schafer, 1998). Thus, morphologically the cell cycle could be divided in two main phases: interphase (the preparation for the cell division) and mitosis (the process of cell division) (Fig. 1).

1.1 Phases of interphase

After cytokinesis the “new-born” cell enters the G1 phase which lasts approximately 12 hours (Israels & Israels, 2001; Nurse, 2000; Schafer, 1998). During G1 phase, also known as pre-

synthetic period, the cell prepares for the S phase (Pardee, 1989). The G1 phase is characterized by metabolic events leading to the initiation of the DNA replication. In order to assure high precision before the next phase initiation the cell needs to pass the first of several checkpoints in its cell cycle (Barnum & O'Connell, 2014). Cells that do not divide actively are considered to be in the G0 phase or quiescent state (Schafer, 1998).

During S (synthesis) phase the genetic material of an eucaryotic cell is doubled through active DNA and histone synthesis. The duration of the phase is approximately 5-6 hours (Israels & Israels, 2001). In each cell cycle's S phase the DNA is duplicated only once (Blow & Laskey, 1988; Diffley, 1996). The DNA duplication produces two identical copies of each chromosome, called sister chromatids (Barnum & O'Connell, 2014). After S phase the cell enters the G2 (duration: 2-4 hours) phase, which is the post-synthesis period of the cell cycle and ends with the beginning of the mitosis. In this phase the cell is tetraploid (see below). During G2 phase the cell prepares the for the following stage of the cell cycle - mitosis (Israels & Israels, 2001).

1.2 Mitosis

During mitosis (duration: 1-2 hours), a bipolar mitotic spindle (see below) is generated, the sister chromatids are segregated (separated), and the cell divides into two daughter cells. In this way identical chromosomal copies of the mother cell are precisely distributed to the two daughter cells (Israels & Israels, 2001). Mitosis is divided into several subphases (Fig. 1). The first subphase of the mitosis is the prophase I, when the DNA is compacted as condensed chromosomes. At this stage, cells are still tetraploid. Each chromosome is composed of two sister chromatids attached to each other via the centromere (Dalal, 2009). During the next subphase, prometaphase, the sister chromatids attach their centromere region to the spindle fibers through the kinetochore. Each chromatid of the same chromosome has its own kinetochore attached to the microtubules of the mitotic spindle emerging from one of the mitotic spindle poles (see below) (Nicklas, 1997; Nurse, 2000). The nuclear envelope breaks down (Beaudouin et al., 2002). The following phase is the metaphase. At this phase the sister chromatids are aligned along the central plane of the mitotic spindle (Tan et al., 2015). The sister chromatid resolution (appearing as rod-shaped structures) occurs and allows the partial

separation of the sister chromatids (Shintomi & Hirano, 2010). The next stage of mitosis is the anaphase. In this phase the compacted sister chromatids are oriented towards the opposite poles of the mitotic spindle and are being segregated and pulled in the opposite directions towards one of the poles (Nasmyth, 1999; Nurse, 2000). Anaphase is followed by telophase, when the chromosomes are positioned at the opposite poles and the microtubules of the mitotic spindle are disassembled, while a new nucleus starts to form in each of the new daughter cells (Xue & Funabiki, 2014). The cytoplasm begins its division with the formation of a tension-generating contractile ring (O'Shaughnessy & Thiyagarajan, 2018).

After the telophase, the last stage of the mitosis, follows the cytokinesis**.** This is the actual physical splitting of the cell cytoplasm and membrane of the mother cell among the two daughter cells (Green et al., 2012). The process is tightly regulated and orchestrated by the anaphase spindle and coordinated with the chromosomal segregation. A cleavage furrow separates the two daughter cells which already have their own nucleus and restored ploidy (Dorn & Maddox, 2011).

1.3 Cell cycle regulation

1.3.1 Cell cycle drivers and regulators

A major component of the cell cycle control system are the cyclin-dependent kinases (CDKs). More precisely, serine and threonine kinases, whose concentration in the cell varies according to the cell cycle phase and stage (Malumbres et al., 2009; E A Nigg, 1995; Nurse, 1990). CDKs complexes regulate the passage from one cell phase to another (Arellano & Moreno, 1997). They are highly regulated through post-translational modifications but also by many proteins, the major group of which are cyclins (E A Nigg, 1995)**.** CDKs are the catalytic partners of cyclins and only when bound to cyclins the inactive CDKs are activated (Israels & Israels, 2001).

Cyclins were discovered in the early 1980s by Timothy Hunt and Ruderman (T. Evans et al., 1983; Luca & Ruderman, 1989). After being synthesized, cyclins bind to CDKs and then are destroyed with the cell cycle progression (Arellano & Moreno, 1997; Johnson & Walker, 1999). The CDK-cyclin complexes phosphorylate different substrates in order to direct the

cell fate (Israels & Israels, 2001). Like CDKs, cyclins' concentration varies according to the cell cycle phase (Fig. 1).

Other CDK regulators are the CDKs inhibitors. They are divided into two big groups: INK4 (INhibitors of CDK4) and Cip/Kip inhibitors (Roussel, 1999; Xiong, 1996). The last one includes: $p21^{CIP1/WAF1/Sdi1}$ which is one of the most investigated inhibitors. (Hall et al., 1995; Schafer, 1998). P21 is a CDK inhibitor which suppresses the G1/S-CDKs and the S-CDKs and plays a major role in the cell fate regulation as an inhibitor of the cell cycle progression during the G1 phase and the S phase transition in mammal cells (Deng et al., 1995; Harper et al., 1993). p21 forms a p21-cyclin-CDK complex and thus prevents the kinase activity of the CDKs (Chen, Saha, et al., 1996; Hall et al., 1995). P21 is activated upon diverse upstream stimuli or indirectly (in a PIDDosome-p53-dependent manner) by supernumerary centrosomes (see below) (Abbas & Dutta, 2009; Fava et al., 2017).

1.3.2 Checkpoints

Checkpoints are rigid regulatory biochemical mechanisms enforcing dependency of late events in the cell cycle on early ones (Hartwell & Weinert, 1989). Checkpoints are operational at a precise moment in the cell cycle when several biochemical reactions, involving particular proteins, determine the cell faith (Pietenpol & Stewart, 2002). Only if the checkpoint is passed are downstream pathways activated leading to the transition into the next cell cycle phase. If the cell fails to pass the checkpoints due to irreparable damage or other errors, it might lead to cell cycle arrest or death. There are four main checkpoints in the cell cycle (Fig. 1). The first and the most important checkpoint is the G1/S checkpoint or restriction point (Voorhees et al., 1976). This mechanism senses the conditions in and outside the cell determining if there should be a progression or restrain of the cell cycle (Alberts B, Johnson A, Lewis J, 2002; Barnum & O'Connell, 2014). The next checkpoint, the intra-S checkpoint, is activated by cells upon DNA damage during S phase and aims to protect genomic integrity to ensure successful and correct DNA replication (Iyer & Rhind, 2017). The G2/M checkpoint prevents cells from initiating mitosis upon several factors like unresolved damages from the previous phases or DNA damage during G2 (Nyberg et al., 2002; B. Xu et al., 2002). If the cell passes all the other checkpoints it arrives to the phase when the spindle assembly checkpoint (SAC) is activated.

SAC or meta-to-anaphase transition checkpoint evolved as a measurement against errors during mitosis (Nicklas, 1997). The SAC components proteolytically cleave cyclins and proteins involved in the holding of the sister chromatids and other early mitosis protein families (Barnum & O'Connell, 2014; Bodrug et al., 2021). One of these families are the Polo-like kinases (PLKs) and the others are the Aurora kinases (see below). Their role is to prevent chromosome mis-segregation and aneuploidy and their miss-function is associated with tumorigenesis (Musacchio & Salmon, 2007). Once the proper biorientation of the chromosomes is sensed by SAC (thus the checkpoint is passed) series of reactions trigger the onset of anaphase and telophase and lead to cytokinesis and completion of the cell cycle (Musacchio & Salmon, 2007).

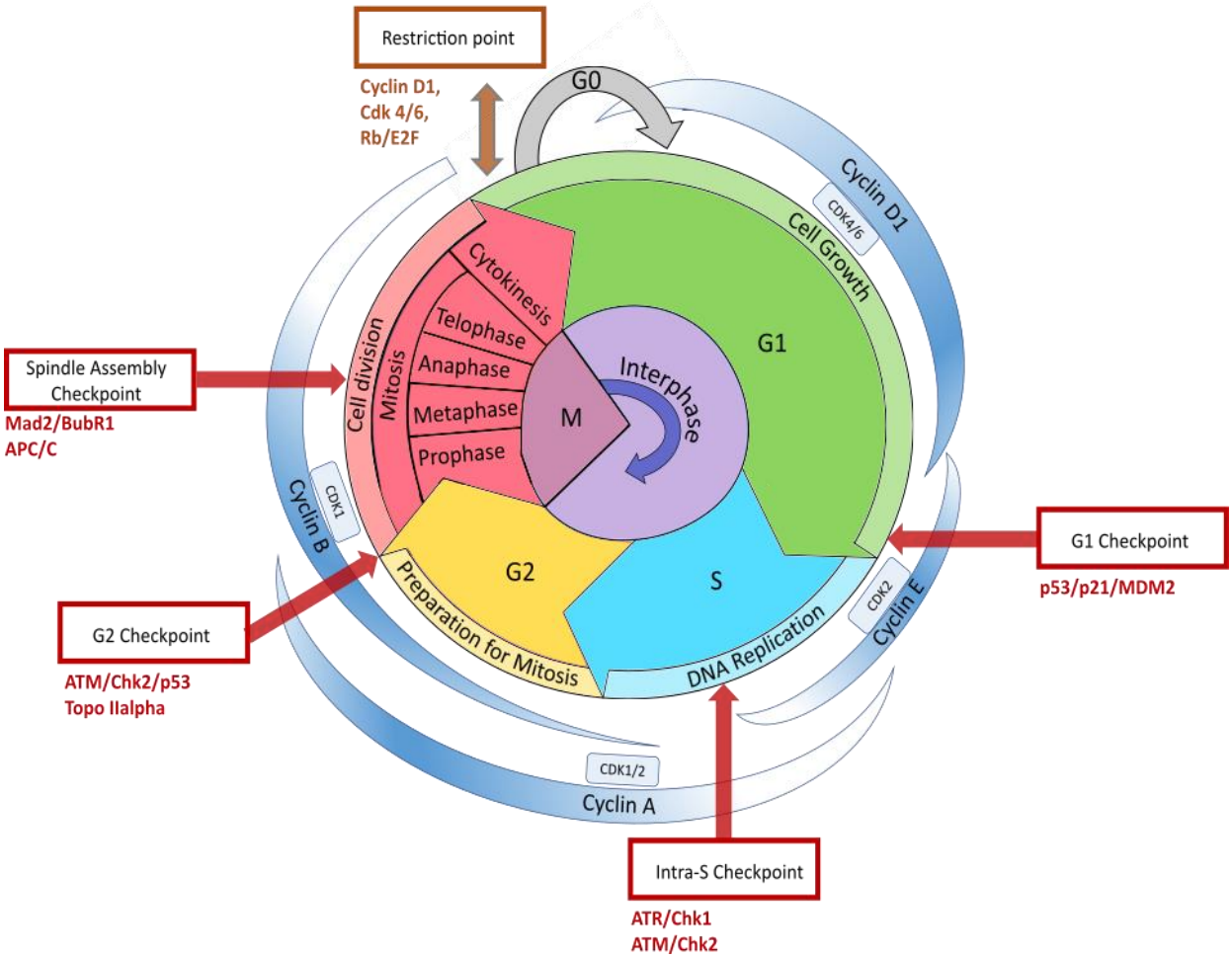

Figure 1. Cell cycle and its regulation.

The cell cycle is divided in two main phases - mitosis and interphase. The interphase begins with G1 - green, when cells grow in size, followed by S - light blue when the DNA replication occurs and G2 - yellow phases

when cells prepare for the mitosis (the cell division) - pink. The mitosis is subdivided into: prophase, metaphase, anaphase, telophase and cytokinesis marking the end of one cell cycle. G0, in grey, is indicative for a quiescent state of cells. Scheme based on: https://www.sciencefacts.net/cell-cycle.html. The cell cycle is regulated by cyclins and CDKs. The cell enters and exit different cell cycle phases in association with the synthesis and degradation of the cyclins indicated above each cell phase. Cyclins bind and activate specific CDKs which coordinate the progression of the cell cycle by phosphorylating a variety of substrates and catalyzing the process of cell division. At the beginning of G1 cyclin D activates CDK4 while during the second half it activates CDK6. At the end of G1 and beginning of S phase cyclin E is associated with CDK2 activation which is also be activated by cyclin A at the transition from S to G2. Cyclin A activates CDK1 during G2, so as cyclin B which activates CDK1 during G2 and M phases (Spoerri et al., 2015). Blue color and shape are indicative for relative intracellular cyclin concentration. Information for the scheme based on: (Schafer, 1998). G0 Restriction Point (in brown box) illustrates the reversible nature of the cell cycle re-entry of quiescent cells. Four checkpoints are indicated in red boxes. G1, intra-S and G2 checkpoints control for DNA damage. The G1 checkpoint controls the cell size, nutrition and growth factors availability. During the intra-S checkpoint the quality of the replicated DNA is controlled. The DNA and cell size are controlled during G2 before the initiation of M phase. Between metaphase and anaphase the SAC assures the correct chromosome attachment to the spindle and their proper arrangement. Major checkpoint regulators triggering each checkpoint are indicated in red below the checkpoint box (Bower et al., 2017).

1.4 Ploidy

Most normal human somatic cells are diploid (2N), i.e. they have two sets of chromosomes and each cell has two copies of each chromosome which are similar but slightly different, and called homologues chromosomes. Each homologue chromosome represents one copy of the DNA from each one of the parents. The ploidy of a cell is determined by the complete sets of chromosomes. Gain or loss of an individual whole chromosome (Ben-David & Amon, 2020) or gain or loss of chromosomal fragment (Lens & Medema, 2019) in a cell is called aneuploidy (Otto, 2007; Pollard et al., 2017). The origin of aneuploidy is diverse, mainly chromosomal instability, errors in the DNA repair or in the mitotic process like cytokinesis failure (see below) (Gordon et al., 2012; Lens & Medema, 2019). In diploid cells a tetraploid (with four sets of chromosomes) or polyploid state could be obtained upon prevention of cytokinesis, incomplete cell division after its initiation, fusion of two or more cells, endoreduplication or endomitosis (Storchova & Pellman, 2004). The presence of another set of chromosomes could contribute to genome instability and the predisposition for the

development of aneuploidy which is highly associated with pathologies (Lens & Medema, 2019). In fact, aneuploidy was long ago noticed as a hallmark of cancer (Theodor Boveri, 1914, 2008). Although 90% of solid tumors are aneuploid (Weaver & Cleveland, 2006) and aneuploidy occurs in 88% of cancers (Taylor et al., 2018) it is type specific and could have oncogenic and tumor suppressive functions depending on the cell type and context (Ben-David & Amon, 2020; Vasudevan et al., 2021).

2. Centriole cycle and biogenesis

2.1 Mitotic spindle

The mitotic spindle plays a key role in the cell division process and the precise distribution of the duplicated genome between the two daughter cells. Described in 1887 by Theodor Heinrich Boveri (T. Boveri, 1887; Hamoir, 1992; Scheer, 2014) as "a system of astral rays extending between the centrosomes" (Nurse, 2000; Wilson, 1925) its structure was not characterized until 1961, after the development of the electron microscopy allowed the discovery of its microtubules nature and its composition from tubulin polymers (Harris, 1961; Kiefer et al., 1966; Nurse, 2000). The mitotic spindle has three morphologically distinct components – the main ones are the microtubules, the others are the chromosomes and the centrosomes. The mitotic spindle is a highly dynamic molecular structure composed not only of tubulin but many other molecules like: nucleators, kinases, phosphatases, other microtubules-associated proteins and motor proteins, which are involved in the assembly of the spindles, the quality control and the subsequent segregation of chromosomes and its monitoring (Nazockdast & Redemann, 2020). The microtubules are arranged in two antiparallel arrays with their plus ends at the "equator", which attach to the chromosomes and their minus ends nucleated mainly at the centrosomes but also to other membrane organelles (Karsenti & Vernos, 2001; J. Wu & Akhmanova, 2017). The centrosomes are located at the opposite poles of the dividing cell and are the two main organizing centers of the mitotic spindle. Each centrosome nucleates a radial array of highly dynamic microtubules, which by shrinking and regrowth explore the space around them until they sense a kinetochore and

"capture" a chromosome. This establishes the connection between the pole and the chromosomes (O'Connell & Khodjakov, 2007).

2.2 Centrosome

The term "centrosomes**"** was also introduced by Boveri (T. Boveri, 1900), while the same structure was named *corpuscule central* by van Beneden and Neyt and was noted by several other scientist at the time, including W. Flemming (Flemming, 1878; Fürst, 1898; Hamoir, 1992; Hertwig, 1876; Scheer, 2014; van Beneden E, 1887). Centrosomes are initially described as permanent cell organelles that appear at both poles of the mitotic spindle and act as major microtubule-organizing center (MTOC) for the cell division. They play a crucial role in the division process and are involved in the initiation and organization of the mitotic spindle. Interestingly, centrosomes are dispensable and not all species have them (Karsenti & Vernos, 2001). However, in most somatic cells they play a crucial role in the cell division process and a change in their number, most commonly addition of an extra centrosome, often referred as supernumerary centrosomes causes multipolar mitotic figures noted already with their discovery by Boveri and associated with aneuploidy (T. Boveri, 1888, 1900; Gall, 2004; Scheer, 2014) and PIDDosome (see below) activation (Fava et al., 2017).

Centrosomes are subcellular, non-membrane bound organelles, which are self-assembling and approximately 1 μm in size (Schatten, 2008). Centrosomes assemble by attachment of pericentriolar material (PCM) around cylindrical structures named centrioles (Lawo et al., 2012; Mennella et al., 2012). A typical mammalian centrosome consists of a multiprotein scaffold of a large number of proteins (Schatten, 2008). Some centrosome proteins (γ-Tubulin, γ-TuRC and Centrin) are permanently associated with the centrosome core (Schatten, 2008). The main components of a centrosome can be morphologically distinguished into two main structures: two perpendicularly oriented centrioles and the surrounding PCM, which serves as a dynamic platform for microtubule nucleation, as well as for stabilization and attachment of microtubules minus ends.

2.3 Centriole

Centrioles are evolutionarily conserved microtubule-based structures, involved in the assembly of flagella, cilia (Sorokin, 1962; Vertii et al., 2016) and centrosomes. The name "centrioles" was also given by Boveri who described them as a "minute, cyclical and dense granule at the centrosome center" (Scheer, 2014). They are crucial for many fundamental processes that enable cells to move, sense their environment and transduce signals (Gönczy, 2012). They are called "centriole" typically in cycling cells and "basal body" in resting cells (Gönczy, 2012). A cell has typically two centrioles: a younger type, which is assembled in the previous cell cycle, called the daughter centriole and an older centriole - termed the parental or mother centriole. Centrioles are polarized along their long axis, so the base of their centriolar cylinder is referred as the proximal/minus end and the top as the distal/plus end (Fig. 2B) (R. Uzbekov & Alieva, 2018). The proximal end of the parental centriole only recruits and organizes the PCM required for the microtubule nucleation, while the distal end carries protuberances known as appendages, see below (Breslow & Holland, 2019).

2.4 Centriole architecture and markers

Centrioles' architecture is well studied through electron and super-resolution light microscopy (Anderson & Brenner, 1971; Bowler et al., 2019; Guichard et al., 2018; Sullenberger et al., 2020; R. Uzbekov & Alieva, 2018; Vasquez-Limeta & Loncarek, 2021; Woodruff et al., 2014). Images revealed that in human cells a mature centriole is composed of nine sets of interconnected microtubule triplets (A, B and C) which become doublets (A and B) towards the distal end where the appendages are located (Conduit et al., 2015; Viol, 2020). Each microtubule contains protofilaments (Anderson & Brenner, 1971; Gönczy, 2012) (Fig. 2A). The 13-protofilaments of A-tubules align with 10-protofilament of B- and C-tubules, while the A-tubule from one triplet connects to the C-tubule of the neighboring triplet through an A–C linker (J. T. Wang & Stearns, 2017) (Fig. 2C). Numerous studies contributed to define the protein components of the centrioles, the PCM and the centrosomes in the different stages of the cell cycle. Some key proteins have been known for almost two decades and are used as labeling markers in immunofluorescence assays. Centrin is a small protein member of a highly conserved superfamily of Ca^{2+}-binding proteins intrinsic for the

centrosomes and essential for their duplication (Schatten, 2008). Centrin is consistent and present in all centrioles inner centrosomal protein found at the distal part of the centriole (occupying larger domain of the centriole) and the procentriole (Fig. 2B) (Gönczy, 2012; Erich A Nigg & Holland, 2018). This makes it useful as a detective marker for immature and mature centrioles in immunofluorescence imaging assays (Baron et al., 1992; Paoletti et al., 1996). The centriole "cap" is presented at the very distal part of the centriolar cylinder and regulates the centrioles' length (Vasquez-Limeta & Loncarek, 2021).

An important component of the centriole's architecture is the cartwheel. The cartwheel is a central scaffold, crucial for building the proximal part of the centriole at the onset of the centriole assembly and it extends throughout the entire length of the centriole (Aydogan et al., 2018; Hirono, 2014). It is composed of three main structures: a hub, nine spokes and nine pinheads (Guichard et al., 2018; Vasquez-Limeta & Loncarek, 2021). The mother centriole usually loses the cartwheel (Conduit et al., 2015). Detailed schematic representation of parental centriole and procentriole with the key proteins is shown in Fig. 2.

The mother centriole possesses two types of appendages which are centriole-associated structures. The first type - the distal ones are located at the distal end of the centriole and serve to mediate the plasma membrane docking of centrioles during the ciliogenesis. The other type is subdistal, located more proximately and serve to anchor the minus-end for the microtubules in interphase centrosomes and contribute to centriole cohesion (Breslow & Holland, 2019). Distal appendages are constant in number and structure, while subdistal appendages can change morphologically (R. Uzbekov & Alieva, 2018). The distal and subdistal appendages proteins are numerous (Fig. 3) and the studies of their exact structure and components are still an ongoing process. Proteins of the distal and subdistal appendages could be used as markers for mature centrioles.

Recently a novel distal appendage protein - ANKRD26 was reported (Bowler et al., 2019). It plays an important role in the recognition of supernumerary centrosomes accumulation (see below) upon cytokinesis failure and the following PIDDosome activation by increasing PIDD1 (see below) concentration close to the centrosome (Burigotto et al., 2021).

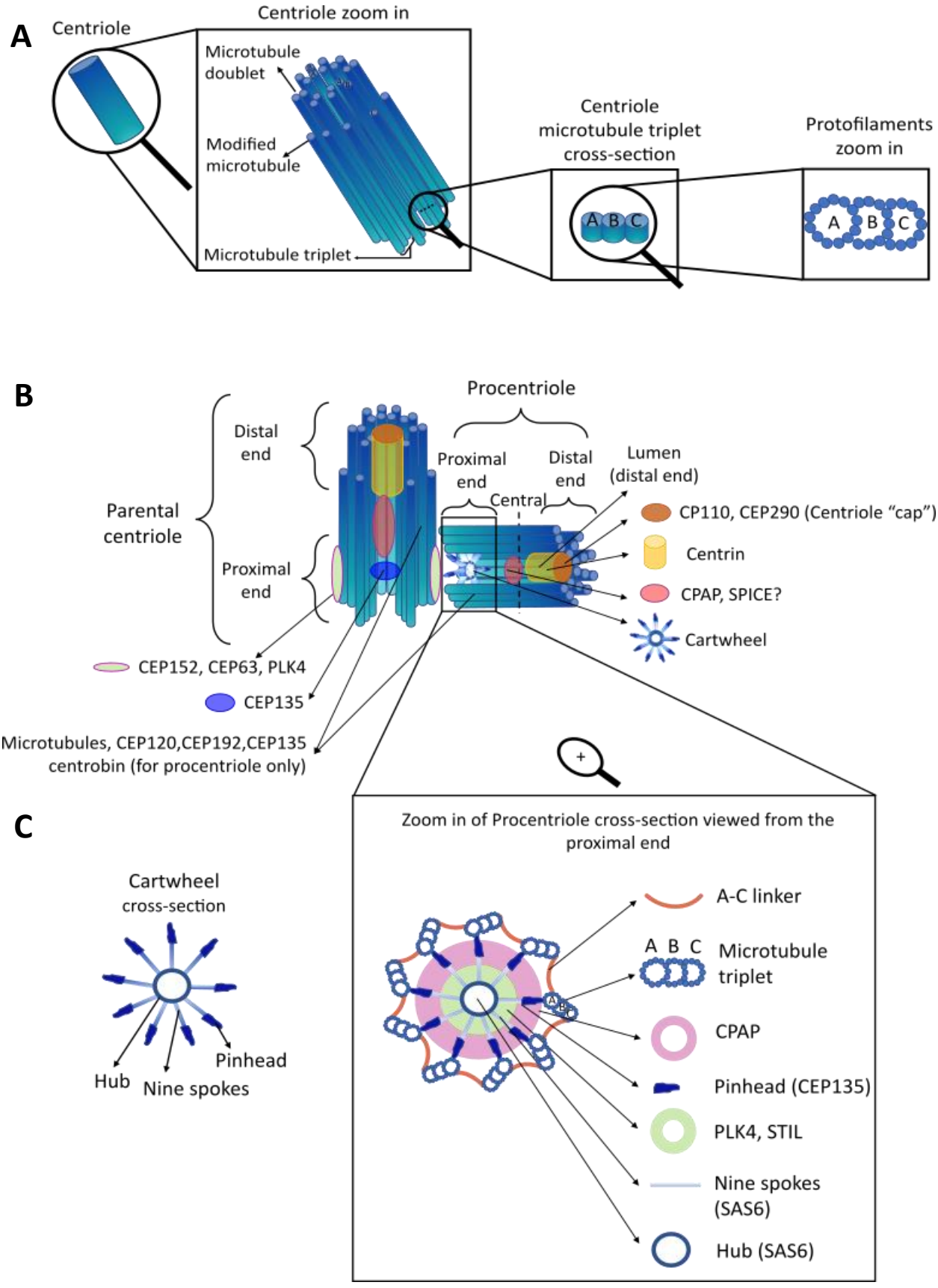
A
Centriole
Centriole zoom in
Microtubule doublet
Modified microtubule
Microtubule triplet
Centriole microtubule triplet cross-section
Protofilaments zoom in
A B C
B
Procentriole
Distal end
Proximal end
Parental centriole
Proximal end
Distal end
Central
Lumen (distal end)
CP110, CEP290 (Centriole "cap")
Centrin
CPAP, SPICE?
Cartwheel
CEP152, CEP63, PLK4
CEP135
Microtubules, CEP120,CEP192,CEP135 centrobin (for procentriole only)
C
Cartwheel cross-section
Hub
Nine spokes
Pinhead
Zoom in of Procentriole cross-section viewed from the proximal end
A-C linker
A B C
Microtubule triplet
CPAP
Pinhead (CEP135)
PLK4, STIL
Nine spokes (SAS6)
Hub (SAS6)

Figure 2. Centriole and procentriole structure.

(A) Schematic representation of human centriole without distal and subdistal appendages. A zoom in window shows the centriole wall composed of nine sets of nine-fold symmetrically arranged microtubule triplets and their protofilaments (Conduit et al., 2015). **(B)** Schematic structure of parental centriole with tightly associated and growing procentriole and key proteins/markers Distal and proximal ends are labeled for parental and procentriole. Central plane is shown on the procentriole. Lumen at the distal end is shown for the procentriole (Erich A Nigg & Holland, 2018). Microtubule and associated proteins are shown with arrows. Centriole "cap" composed of: CP110 and CEP290 is shown in brown (Vasquez-Limeta & Loncarek, 2021). Centrin is shown in yellow. Centrosomal p4.1-associated protein (CPAP) and spindle and centriole-associated protein (SPICE) which has not been precisely localized (question mark) are show in light pink. CEP135 is shown in blue. CEP152 and CEP63 (light green) form a ring around the proximal part of the centriole, PLK4 localizes in proximity. CEP120, CEP192 and CEP135 (parental centriole) and centrobin (procentriole only) are found close to the microtubules. Cartwheel located at the very proximal part of the procentriole lumen is shown in blue (Gönczy, 2012; Erich A Nigg & Holland, 2018). **(C)** Cartwheel and procentriole proximal part detailed structure. A schematic graph of cross-section of cartwheel is shown on left, pointing its three prominent components: pinheads (dark blue), nine spikes (light blue) and the hub (white circle with dark outline). A zoom in window with details of the structures of the cartwheel from a cross-section view shows components of the procentriole proximal part including the cartwheel. A-C linker is shown in brown color, microtubule triplets with their protofilaments are shown in blue, CPAP is shown in pink, pinheads (putative component CEP135) in dark blue, PLK4 and SCL/TAL1 interrupting locus (STIL) are shown in green. Spokes are shown in light blue, white a circle with dark outline shows the cartwheel hub, all composed of spindle assembly abnormal protein 6 (SAS6) (Vasquez-Limeta & Loncarek, 2021).

2.5 Pericentriolar material

The PCM is described as a fibrous scaffolding lattice mainly composed of coiled-coil centrosome proteins (Schatten, 2008). Several of the PCM components can recruit γ-Tubulin, the main component responsible for the microtubules nucleation and anchoring of the centrosome (Kollman et al., 2011). In animal cells, γ-Tubulin is part of a larger complex - γ-Tubulin ring complex (γ-TuRC) which caps the minus ends of the microtubule and nucleates them (J. Wu & Akhmanova, 2017). γ-Tubulin is a highly conserved protein in eukaryotes. It is essential for centrosome functions and nuclear division since its depletion is lethal to the cell and to the organism (Joshi & Zhou, 2001; Oakley et al., 1990).

A key player of the PCM components which plays role in the spindle organization in mammalian cells is an elongated coiled-coil protein extending away from the centriole - pericentrin. It serves as a multifunctional scaffold for anchoring numerous centrosomal proteins (Delaval & Doxsey, 2010). Pericentrin can bind γ-Tubulin (Dictenberg et al., 1998) and anchors γ-TuRC (Zimmerman et al., 2004). The proteins of the PCM form a porous lattice which incorporates functional components needed for the microtubule nucleation (Fig. 3).

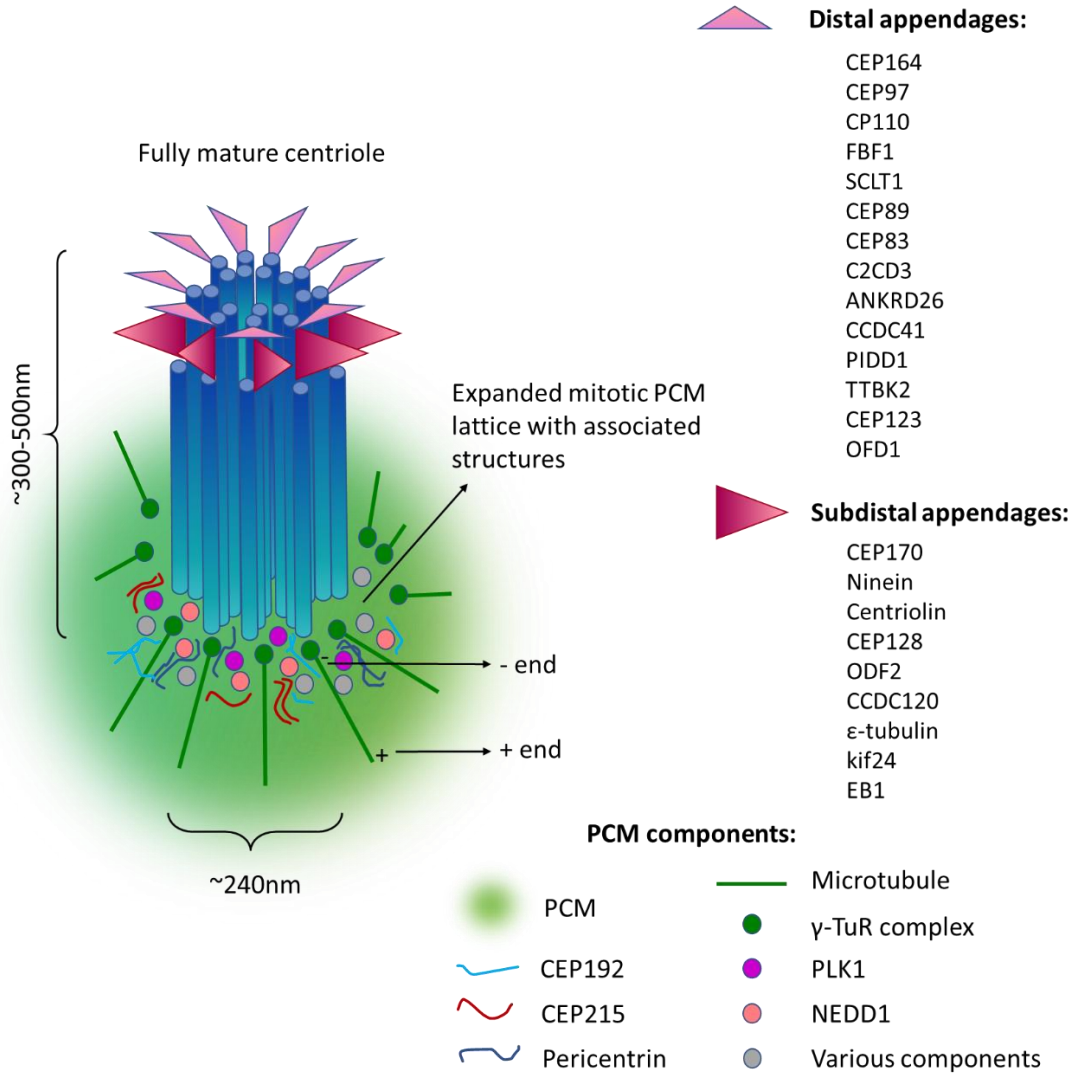

Figure 3. Appendages and pericentriolar material components of a mature centriole

The scheme shows fully mature single mammalian centriole with distal and subdistal appendages and PCM after centrosome maturation (G2 phase and mitosis). Centriole size is shown in nm (Gupta & Kitagawa, 2018; Vasquez-Limeta & Loncarek, 2021). Distal appendages reported proteins are listed: CEP164, CEP97, CP110, FBF1, SCLT1, CEP89, CEP83, C2CD3 (Chong et al., 2020; T. T. Yang et al., 2018), ANKRD26, CCDC41

(Bowler et al., 2019), PIDD1, TTBK2 (Vasquez-Limeta & Loncarek, 2021), CEP123 (Viol, 2020), OFD1 (Tischer et al., 2021). Subdistal appendages reported proteins are listed as follow: CEP170, Ninein, Centriolin, CEP128, ODF2 (Chong et al., 2020; Tischer et al., 2021), CCDC120 (Vasquez-Limeta & Loncarek, 2021), ε-Tubulin, kif24, EB1 (Pihan, 2013). PCM is enlarged after centrosome maturation. A model of the components of the mitotic PCM lattice is shown at the bottom of the scheme, based on information from: (Vasquez-Limeta & Loncarek, 2021).

2.6 Centriole cycle

2.6.1 Centrioles in G1

A new cell cycle starting with G1 phase, typically begins with a single centrosome and a complete set of chromosomes. This centrosome contains a pair of centrioles - the older parent centriole and a tightly associated younger procentriole. The two centrioles lose their orthogonal orientation in early G1 - a process known as centrosome disengagement and are re-connected through a flexible linker emanating from their base (Gönczy, 2012; P Meraldi & Nigg, 2002). During the whole interphase the centrosomes are juxtaposed and closely associated with the nucleus until the mitosis starts (Fig. 4) (Schatten, 2008). The PCM of interphase centrosomes appears more organized (Breslow & Holland, 2019).

In G1-S phase transition PLK4 (see below) is already recruited at the mother centriole and the process of centriole duplication begins. It is completed by the time the cell starts the mitosis. Interestingly this process begins before the DNA duplication, which occurs in S phase (R. Uzbekov & Alieva, 2010; R. E. Uzbekov, 2007). It is crucial that this process occurs once and only once per cell cycle similarly to the DNA replication. (Erich A Nigg & Holland, 2018). The centrosome duplication in mammalian somatic cells depends on the G1/S transition of the cell cycle and requires the phosphorylation of the retinoblastoma protein, activation of E2 transcription factors (E2F) and the activity of CDK2 in a complex with cyclin E and/or A (Hinchcliffe et al., 1999; Lacey et al., 1999; Matsumoto et al., 1999; Patrick Meraldi et al., 1999). Centrosome duplication is a highly regulated mechanism and a key requirement for a proper formation of the bipolar spindle and the proper chromosome segregation. Centrosome-intrinsic block prevents the reduplication of the mother centriole as long as the parent and procentriole remain tightly associated or engaged with each other

(Breslow & Holland, 2019). The molecules involved in the centriole duplication are discussed below.

2.6.2 Centrioles in S

The formation of a new centriole/procentriole occurs from a single site near the proximal end of the parental centriole (R. Uzbekov & Alieva, 2018). Each procentriole remains tightly engaged to the mother centriole in the orthogonal orientation during S and G2 phases until late mitosis (Breslow & Holland, 2019; Conduit et al., 2015). During S the procentriole elongates and reaches ~80% of its finale length (Gönczy, 2012). At the onset of S phase of the cell cycle a procentriole begins to assemble roughly orthogonal (at right angle) to each existing parental centriole (Fig. 2) (Gönczy, 2012). Although it is very little, the PCM is highly organized around the mother centriole (Conduit et al., 2015). The centrioles duplication is completed shortly before the G2 phase (Schatten, 2008). At this stage the cell has four centrioles - two mother centrioles and two daughter centrioles (Fig. 4). Errors in the centrosome duplication can lead to defects in the structure of the centrosomes like defect of the shape or the size of the centrosome.

2.6.3 Centrioles in G2

The procentriole continues to elongate in G2 until it reaches its finale dimensions (Gönczy, 2012). At the G2/M transition, also referred as centrosome maturation, several PCM proteins, particularly γ-TuRCs, gather to form a single layer of molecules around the mother centriole (Conduit et al., 2015). The mother centrioles recruit larger amounts of PCM organized by a scaffold structure. The amount of γ-Tubulin increases about three- to five-fold so as the microtubules nucleated at the centrosome (Khodjakov & Rieder, 1999). The immature parental centriole acquires maturation markers (P Meraldi & Nigg, 2002).

The cell cycle also controls the assembly of appendages, as they are lost from centrioles during the previous mitosis and reassembled during centriole maturation in G2 (Breslow & Holland, 2019). In addition to appendages the daughter centriole will need to acquire the ability to recruit PCM - process called centriole-to-centrosome conversion, which allows the recruitment of proteins necessary for the procentriole duplication in the next cell cycle (Erich A Nigg & Holland, 2018; W.-J. Wang et al., 2011). While the cell goes through

reorganization the two pairs of centrioles start to move apart as breaking of the linkage between them occurs. This is the first step of a process known as centrosome disjunction (Conduit et al., 2015; P Meraldi & Nigg, 2002). During the second step of the separation the sister centrosomes with the associated PCM are spatially separated around the nucleus (Schatten, 2008). The centrosomes mature into the mitotic poles of the spindle (Fig. 4A) and a γ-Tubulin ring complex is formed around the centrosome (Schatten, 2008).

2.6.4 Centrioles in Mitosis

At this stage the cell is bipolarized, each centrosome represents a pole of the mitotic spindle and the M-CDKs initiate the mitotic spindle assembly (Nurse, 2000). The centrioles move apart to the opposite directions of the spindle and start extending microtubules to form it until prometaphase-I when full maturation of the mitotic spindle is achieved. The PCM of the mitotic centrioles appears disordered and gel-like (Breslow & Holland, 2019).

At the late stage of mitosis, the procentriole disengages from the parent centriole so that the daughter centriole can mature to a mother centriole in the following cycle and become able to form its own daughter centriole (Conduit et al., 2015). After the disengagement the centrioles lose the tight orthogonal orientation but often remain loosely connected via flexible linker (Conduit et al., 2015). Each of the two newly created daughter cells inherits a pair of parent centrioles that are competent for duplication in the next cell cycle. Importantly, the parent centriole that was formed one and a half cell cycles ago reaches its full length in the following G1 phase and full maturity in the next G2 phase through the acquisition of subdistal and distal appendages that allow it to function as a basal body (Breslow & Holland, 2019; Erich A Nigg & Stearns, 2011). The process of centrosome duplication could be considered semi-conservative since each centrosome receives a newly generated centriole and an old/parental centriole.

2.6.5 Centrioles in G0

In quiescent cells the centriole pair of the cell migrates to the cell surface, where in proximity to the plasma membrane only the mother centriole docks and becomes converted to a basal body (Breslow & Holland, 2019; Vertii et al., 2016). The basal body serves as a base and anchors a cilium.

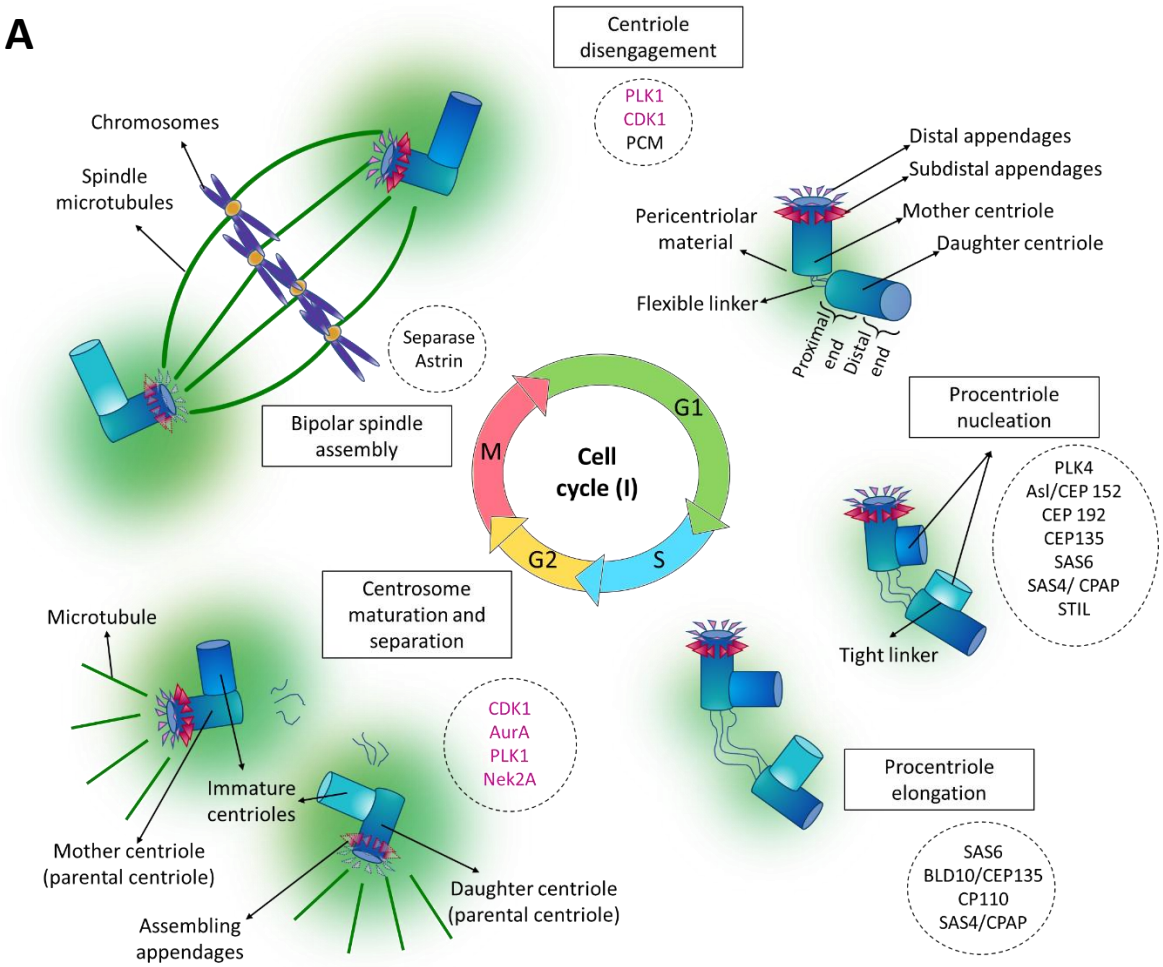
A
Centriole disengagement
PLK1
CDK1
PCM
Chromosomes
Spindle microtubules
Separase
Astrin
Bipolar spindle assembly
Distal appendages
Subdistal appendages
Pericentriolar material
Mother centriole
Daughter centriole
Flexible linker
Proximal end
Distal end
Procentriole nucleation
PLK4
Asl/CEP 152
CEP 192
CEP135
SAS6
SAS4/ CPAP
STIL
Tight linker
G1
S
G2
M
Cell cycle (I)
Centrosome maturation and separation
Microtubule
Immature centrioles
Mother centriole (parental centriole)
Daughter centriole (parental centriole)
Assembling appendages
CDK1
AurA
PLK1
Nek2A
Procentriole elongation
SAS6
BLD10/CEP135
CP110
SAS4/CPAP
B
Cell cycle (II)
G1
S
G2
M

Figure 4. Centriole cycle.

(A) Schematic representation of (first) centriole cycle tightly regulated and synchronizes with the cell cycle. In G1 the new-born cell inherits two centrioles - a mother (possessing distal and subdistal appendages) and a daughter centriole. Major events of the centrioles cycle are: 1) At the late M phase centriole disengagement/displacement takes place. After the disengagement a flexible proteinaceous linker is established. At the end of G1 the centriole duplication begins with the procentriole nucleation (G. Wang et al., 2014). 2) During S the procentriole elongates by adding α/β-Tubulin dimers. PLK4 induces its own phosphorylation in order to prevent centriole reduplication. After the centriole duplication each originally inherited centriole (the mother and the daughter) have become parental centriole generating their own centriole duplicates (procentrioles). 3) In G2 the cell possesses four centrioles in total: a mature mother centriole with its "newborn" immature centriole, a maturing daughter centriole with its own immature centriole. In G2 the daughter centriole starts assembling distal and subdistal appendages. Around each couple of centriole additional PCM is recruited (green). 4) The mature centrosomes serve as MTOCs to assemble the bipolar spindle necessary for the chromosome segregation during mitosis. Inner circle indicates the phases of the cell cycle in which the main centriole cycle events occur. Major events of the centriole cycle are given in boxes. Key proteins are shown in circles, mitotic kinases are shown in pink. Based on: (G. Wang et al., 2014). **(B)** Example of following (second) centriole cycle shows further maturation of one of the procentrioles (light blue) created in the previous cycles. This procentriole, created by the young parental (daughter) centriole in the previous cycle, is maturing into fully maturing parental centriole in this cycle acquiring distal and subdistal appendages in G2. Light pink and light orange show the new procentrioles created in the second cell cycle.

3. Miss regulation of the cell and centriole cycle

3.1 Cytokinesis failure

When a dividing cell, which has already prepared itself for division and has duplicated the genetic material and centrosomes (went through the S phase), is unable to physically divide its cytoplasm and genetic material into two daughter cells an error known as cytokinesis failure is observed (Fig. 5).

Cytokinesis failure could be naturally scheduled in some normal tissues. For example, cytokinesis is physiologically regulated in liver and heart where a large number of cells are tetraploid (Normand & King, 2010). In adult liver in humans many of the cells are polyploid with polyploidy increasing with age (Kudryavtsev et al., 1993; Toyoda et al., 2005). Importantly, liver polyploidization was found to be caused by cytokinesis failure (Guidotti et

al., 2003). Even though naturally occurring in proliferating hepatocytes cytokinesis failure leads to centrosome clustering and engages the PIDDosome (discussed in detail below) (Sladky & Villunger, 2020). Importantly, Caspase-2 and PIDD1 are barely expressed in adult hepatocytes but could be reactivated in an E2F-dependent manner in order to avoid hyper-polyploidization during liver regeneration (Sladky et al., 2020). Megakaryocytes are also naturally polyploid mainly due to endomitosis (an incomplete mitosis aborted after its initiation) which results from a late failure of cytokinesis (Mazzi et al., 2018).

Cytokinesis failure can be triggered by defect in several stages of the cell division process. Defects in the checkpoint, gene defects of tumor suppression genes or mutations of the cytokinesis drivers (Lens & Medema, 2019) can lead to cytokinesis failure. Exit of mitosis without initiating anaphase or cytokinesis due to prolonged mitosis could also result in cytokinesis failure (Gascoigne & Taylor, 2008). Errors in the cleavage furrow initiation or formation with following regression could also be the reason for cytokinesis failure (Lens & Medema, 2019).

Cytokinesis failure leads to duplication of the genetic material and thus to the duplication of the ploidy of a cell, a predisposition to aneuploidy. Moreover, it leads to a numerical defect of the centrosomes knows as centrosome amplification/supernumerary centrosomes This is also a long known and commonly observed phenomenon in tumors (Theodor Boveri, 1914; Breslow & Holland, 2019). The association between tumors and supernumerary centrosomes is supported by several studies demonstrating that supernumerary centrosomes can trigger tumorigenesis spontaneously even in the absence of any additional genetic defects (P. A. Coelho et al., 2021; Levine et al., 2017; Serçin et al., 2016). Supernumerary centrosomes are also associated with hyperproliferation of cells and tumor cell migration and invasion (Godinho et al., 2014). Furthermore, presence of supernumerary centrosomes can cause multipolar spindle which causes genomic instability and aneuploidy (Lens & Medema, 2019; M. S. Levine et al., 2017) due to unappropriated chromosome segregation or miss-attachment. Additionally, this leads to micronucleus formation (Crasta et al., 2012; Ganem et al., 2009; Silkworth et al., 2009).

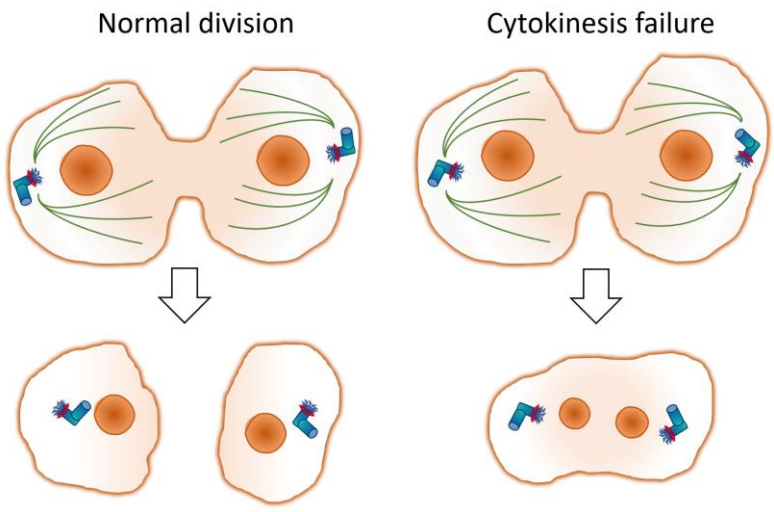

Figure 5. Cytokinesis failure.

Graphical representation of normal cell division and cytokinesis failure. Upon normal cell division the mother cell splits into two daughter cells each of which receives genetic material identical to the mother's and a centrosome (containing two centrioles). Upon cytokinesis failure the division of the mother cell into two daughter cells is perturbed, thus the duplicated genetic material and the duplicated centrosomes from the mother cell remain in a single cell.

3.2 Experimental triggers for cytokinesis failure

Aurora B (AURBK; Ipl1 in budding yeast) is an evolutionarily conserved serine/threonine protein kinase (Tanaka, 2005, 2008). It localizes at the kinetochores in prometaphase and metaphase and promotes turnover of kinetochore – microtubules attachments. Aurora B is also an inner centromere protein required for the bipolar attachment of chromosomes and involved in the activation of the SAC in case of attachment errors (Hauf et al., 2003; Krenn & Musacchio, 2015). Aurora B relocates from the kinetochores to the spindle upon anaphase onset (Tanaka, 2008), where it is necessary for the accurate chromosome segregation and completion of cytokinesis (Tanaka, 2002). Inhibition of Aurora B shows extensive chromosome missegregation, mal-oriented chromosomes and accumulation of synthetic (both sister kinetochores attached to one spindle pole) kinetochore–microtubule attachments (Hauf et al., 2003; Lampson et al., 2004), similar to cytokinesis failure. Aurora kinases can be inhibited by small molecules like: Hesperadin (Hauf et al., 2003), cytok-hydroxyquinazoline pyrazol anilide (HQPA) (Gully et al., 2012) or ZM447439 - selective

Aurora A and B kinase inhibitor (Ditchfield et al., 2003). Treated with ZM447439 cells enter mitosis but fail to divide or trigger mitotic exit by inactivating the SAC (Ditchfield et al., 2003). Cells that go under this process fail centriole disengagement (W.-J. Wang et al., 2011). ZM447439 inhibits chromosome alignment and compromises the SAC function (Ditchfield et al., 2003). The initiated mitosis without exit upon the treatment with ZM447439 leads to cytokinesis failure and accumulation of supernumerary centrosomes.

Another drug used to perturb the cytokinesis is with dihydrocytochalasin-B (DHCB) treatment. DHCB inhibits cell mobility and alters the cell morphology through interference with the actin polymerization (Atlas & Lin, 1978). Treatment of cells with DHCB triggers Caspase-2 activation and MDM2 cleavage (Fava et al., 2017).

Small (or short) interfering RNA (siRNA) is an established method to knockdown genes. It is used to trigger cytokinesis failure through inducing short-term silencing specifically on key cytokinesis genes. Such example are the guanine nucleotide exchange factors (RhoGEFs) that serve as activators of the Rho family (Cook et al., 2011). Cells treated with siRNA targeting the ECT2 (member of RhoGEFs) also show cytokinesis failure and Caspase-2 mediated MDM2 cleavage (Fava et al., 2017).

3.3 PLK4 overexpression

Polo-like kinases (PLKs) are required for multiple stages of mitotic progression and are key players in mitosis, meiosis and cytokinesis but also centrosome separation, organization and dynamics (Barr et al., 2004). Each kinase is activated in a particular cellular cycle event. An important member of the family is PLK4 (Sak) which has been identified as a key regulator and inductor of the centriole biogenesis (Habedanck et al., 2005). It is also referred as a master regulator of centriole duplication and biogenesis, and it was also used as the earliest known marker for the site of procentriole assembly (Bettencourt-Dias et al., 2005; Habedanck et al., 2005; Kleylein-Sohn et al., 2007; Sonnen et al., 2012).

For the initiation of the centriole duplication a set of five core proteins were originally identified in *C. elegans*: PLK4 (ZYG-1 in *C. elegans*), centrosomal protein of 192 kDa (CEP192; SPD-2 in *C. elegans*), centrosomal P4.1-associated protein (CPAP, also known as CENPJ; the microtubule binding protein SAS4 in *C. elegans*), SCL-interrupting locus protein

(STIL; SAS5 in *C. elegans*) and spindle assembly abnormal protein 6 (SAS6) (Gönczy, 2012; Strnad et al., 2007). In vertebrates PLK4 is recruited to parent centrioles already in G1 phase by binding to the centriole receptors: CEP152 and CEP192, localized as a ring throughout the cell cycle (Cizmecioglu et al., 2010). PLK4 transitions from an initial ring-like localization around the parent centriole in G1 phase to a single dot at the G1–S phase transition. The relocalization of PLK4 to this discrete locus on the wall of the parent centriole is critical for selecting a single site for procentriole assembly (Breslow & Holland, 2019). PLK4 initiates centriole assembly via the STIL phosphorylation, which recruits SAS6 to the side of the procentriole (Vasquez-Limeta & Loncarek, 2021). Their oligomerization forms the cartwheel (Moyer & Holland, 2019). The parental centriole forms exactly one centriole during one cycle and this is strictly controlled by: PLK4, STIL, and SAS6. Overexpression (OE) of any of these three initiator proteins results in the simultaneous production of multiple procentrioles around one parent centriole (Habedanck et al., 2005; Kleylein-Sohn et al., 2007). In unmodified cells PLK4 autoregulates its instability by phosphorylating itself to promote its degradation and limit the centriole duplication only once per cycle. In this way the abundance of endogenous PLK4 is regulated (Holland et al., 2012). However, experimentally triggered PLK4 OE in human cells causes the recruitment of electron-dense material like a ring onto the proximal walls of parental centrioles and leads to the accumulation of supernumerary centrosomes (Habedanck et al., 2005) by the simultaneous formation of multiple procentrioles around each pre-existing centriole (Kleylein-Sohn et al., 2007). These multiple centrioles form during S phase and appear as flower-like structures throughout G2, when they continue to elongate and persist engagement with the parental centriole until disengagement in late M phase and they disperse at mitotic exit (Kleylein-Sohn et al., 2007). Studies showed that SAS6, CPAP, CEP135, CP110 and γ-Tubulin are indispensable for centriole biogenesis following PLK4 OE, since upon their depletion PLK4 procentriole induction was suppressed (Gönczy, 2012; Kleylein-Sohn et al., 2007). The centrioles accumulation upon PLK4 OE makes it a useful tool for the study of the supernumerary centrosomes downstream events in cells. However, in order to obtain the accumulation of mature centrioles it is necessary for the cell to pass two cell cycles, approximately 48 h after the induction of PLK4 OE, to observe the accumulation of mature centrioles.

4. Caspases

4.1 Classification and structure

Caspases are a family of evolutionary conserved cysteine-dependent, aspartate-directed proteases (Earnshaw et al., 1999). They play an essential role in apoptosis (see below) and many other cellular processes (S Shalini et al., 2015). Structurally caspases are descendants of the ancient CD clan of cysteine peptidases (McLuskey & Mottram, 2015). The caspases involved in apoptosis are sub-divided in two major groups: apical initiator caspases (group II: caspases -2, -8, -9 and -10) and effector/executioner caspases (group III: caspases -3, -6 and -7), based on the presence or absence of a protein interacting prodomain at their N-terminus (S Shalini et al., 2015). Caspases with a long prodomain of more than 90 amino acids which contains a protein:protein interaction domain like: death effector domain (DED; for caspases -8 and -10) or caspase recruitment domain (CARD; for caspases-2 and -9) are considered initiators (Aravind et al., 1999; Hofmann et al., 1997; Kersse et al., 2011; S Shalini et al., 2015). Their N-terminus prodomain could encode signals for recruitment in multiprotein complexes and defines the type of activation mechanism that caspases use. Caspases containing a short prodomain of 20-30 amino acids are considered executioners (Chowdhury et al., 2008). The C-terminus protease catalytic unit is a single domain but is often split during maturation. The catalytic dyad residues (Cys and His) are positioned in the large chain while the substrate recognition groove is formed primarily through residues from the small chain (Chowdhury et al., 2008; Lamkanfi et al., 2002; Ramirez & Salvesen, 2018).

4.2 Activation

Caspases are synthesized as inactive single chain zymogens (enzymes awaiting activation) and need to be activated either: 1) by multiprotein scaffold-mediated transactivation which allows their recruitments for proteolysis (typical for the initiator caspases), 2) by auto-processing of the inactive form to an active form, or 3) by proteolytic cleavage via upstream proteases (for executioner caspases) upon appropriate apoptotic activation signals (Earnshaw

et al., 1999; Ramirez & Salvesen, 2018; Van Opdenbosch & Lamkanfi, 2019). This cleavage separates the C-terminal domain into two subunits: large p20 and small p10 subunits allowing their reassemble as an active heterotetramer (Lamkanfi et al., 2002; Wejda et al., 2012).

The zymogens of apoptotic initiator caspases are inert monomers. The activation steps for these caspases involve: 1) recruitment to oligomeric activation platforms following apoptotic signal, 2) dimerization, 3) cleavage in trans between the large and small catalytic subunits, and cleavage in trans after the large prodomain. It is widely accepted that the proximity-induced dimerization induces conformational changes within the multiprotein complexes and initiate an autocatalytic activation of the caspase zymogens into an active protease (Boatright & Salvesen, 2003; Salvesen & Dixit, 1999; Van Opdenbosch & Lamkanfi, 2019). The unusual ability of caspases to auto-process themselves depends on intrinsic activity that resides in the zymogens of the initiator caspases (Salvesen & Dixit, 1999). So far, the activating multiprotein complexes of several caspases are well described. For Caspase-2 this complex is the PIDDosome (Tinel & Tschopp, 2004). Cleavage in trans after the large prodomain releases the activated caspase from the multiprotein complexes (Lamkanfi et al., 2002; Wejda et al., 2012).

4.3 Apoptosis

Cell death is essential for the proper functioning of an unicellular organisms. It removes damaged or unnecessary cells allowing further growth and differentiation. There are several distinct cell death types based on the cellular changes but the most commonly studies ones are apoptosis and necrosis (S Shalini et al., 2015). The first report of cell death was in 1842 by Karl Vogt, while Rudolf Virchow firstly described apoptosis it in 1860s (Diamantis et al., 2008; Gerschenson & Geske, 2001). Mitotic catastrophe is another form of cell death that occurs during mitosis when there is a conflict between cell cycle progression and DNA damage (Castedo, Perfettini, Roumier, Andreau, et al., 2004). This is an important oncosupressive mechanism which aims to remove cells (through apoptosis or senescence) with aneuploidy or polyploidy due to the aberrant mitosis resulting of the inactivated control mechanisms of the cell. In such cases Caspase-2 is the main executor of mitotic catastrophe

and if suppressed the cell cycle progression is promoted (Castedo, Perfettini, Roumier, Valent, et al., 2004; Vitale et al., 2017)

The most investigated cell death, apoptosis, is a form of a regulated cellular suicide with particular morphological, regulatory and biochemical characteristics. It is a caspase-dependent cell death in contrast to autophagy, which is a caspase-independent programmed cell death. Under the effect of effector caspases apoptotic cells shrink and loose contact with other cells, the chromatin condenses (pyknosis) and degrades, cytoplasmic organelles become more tightly packed, the nucleus is destroyed, while cytochrome *c* is release, the cell membrane starts to fragment, and membrane blebbing and formation of apoptotic bodies are observed (Elmore, 2007; Kerr et al., 1972; Van Opdenbosch & Lamkanfi, 2019). There are two main ways of apoptosis initiation, depending on the provoking signals: external or intrinsic (Igney & Krammer, 2002). The first one, the extrinsic signaling pathway of apoptotic initiation, is activated through ligand binding of its specific membrane receptors like FasL (CD95yApo-1) receptors, tumor necrosis factor superfamily of receptors (TNFR) or others, which leads to the direct recruitment of Caspase-8 (initiator caspase). This assemblage of proteins is known as death-inducing signaling complex (DISC). This process is further followed by the direct activation of the executioner caspases -3, -6 and -7 through cleavage of the procaspases moiets (Cory & Adams, 2002; Earnshaw et al., 1999; Elmore, 2007; Riedl & Salvesen, 2007).

The other way of activation of apoptosis is the intrinsic apoptosis pathway, also known as mitochondrial and could be triggered by a variety of stimuli. These stimuli could act in a negative/lack of apoptotic suppression (absence of certain growth factors, hormones or cytokines) or in a positive/apoptosis activating fashion (DNA damage, toxins, hypoxia, other cell stress, viral infections and others) (Elmore, 2007). The intrinsic pathway requires the neutralization of the pro-survival and anti-apoptotic members of the big B-cell lymphoma 2 (Bcl-2) protein family by the pro-apoptotic BH3 (Bcl-2 homology 3)-only proteins (Cory & Adams, 2002). This allows the indirect activation and oligomerization of the Bax/Bak complex (Bcl-2 family members), which alternatively could also be directly activated by Bid (Bcl-2 family member). Upon ER (endoplasmic reticulum) stress Bid is cleaved by Caspase-2 (Upton et al., 2008) and induces the mitochondrial outer membrane permeabilization (MOMP) (Cory & Adams, 2002; Elmore, 2007). The MOMP causes cytochrome *c* release

from the mitochondria and the activation of a multimeric adaptor protein complex (involving Apaf-1, Smac and cytochrome *c*) called the Apoptosome (Chinnaiyan, 1999; Hill et al., 2004; Wei et al., 2000). The Apoptosome serves as a platform for the activation of Caspase-9 (an initiator caspase) which activates the executioner caspases -3, -6 and -7.

4.4 Caspase-3

Caspase-3 (CASP-3), also known as CPP32, apopain and Yama, is a key executioner caspase in apoptosis (Porter & Jänicke, 1999). Caspase-3 is synthesized as inactive cytosolic homodimer (procaspase-3 consistent of 277 amino acids) that is activated by proteolytic cleavage upon upstream signals as described above. The proteolytic cleavage in combination with cysteine 163 (C163) residue dephosphorylation leads to its complete activation (Yadav et al., 2021). However, proteolysis itself only is sufficient to activate the procaspase-3. Active Caspase-3 utilizes a Cys residue to cleave variety of substrates like: Poly (ADP-ribose) polymerase (PARP), DNA-dependent protein kinase (PK) like PKC- gamma and delta, other procaspases like caspases -6, -7, -9, beta catenin, huntingtin, gelsolin and others (Cai et al., 1998; Chowdhury et al., 2008; Du et al., 2000; Elmore, 2007; Yadav et al., 2021). Caspase-3 cleaves it substrates at a high specificity for amino acid sequence – DEVD (Aspartic acid-Glutamic acid-Valine-Aspartic acid) (Agard et al., 2012; Thornberry et al., 1997). However, it can cleave, although less efficiently, after other substrate specificities like VEID, IETD, LEHD and importantly VDVAD (see below) (McStay et al., 2008). Caspase-3 specifically cleaves PARP (116 kDa) (Boulares et al., 1999; Nicholson et al., 1995; Tewari et al., 1995) at a very conserved sequence of residues- DEVD216-G217 (cleavage occurs between aspartate 216 and glycine 217) which results in the separation of the two zing-fingers DNA-binding motifs at the N-terminus (25 kDa) of PARP and the auto modification of the catalytic domain at the C-terminus (85 kDa) of PARP (Kaufmann et al., 1993; Nicholson et al., 1995). This cleavage is indicative for apoptosis and it is used as a confirmation marker of chemotherapeutically-induced apoptosis (Kaufmann et al., 1993) since the PARP cleavage inactivates its enzyme activity and its ability to respond and promote DNA breaks. The PARP cleavage is a critical point that directs death receptor signaling promoting further approach towards apoptosis or necrosis (Boulares et al., 1999; Los et al., 2002).

5. Caspase-2

5.1 Classification in the Caspases group

Caspase-2 (CASP-2, ICH-1 (L. Wang et al., 1994) or Nedd2 (S Kumar et al., 1994)) is a highly conserved among species cysteine-driven, aspartate-directed protease evolutionarily most closely related to CED-3, the *C. elegans* protease, then any other of the caspase family (S Kumar et al., 1994; Lamkanfi et al., 2002; Yuan et al., 1993). It is mainly associated as an initiator of apoptosis caspase, based on phylogenic analysis (Lamkanfi et al., 2002), since pro-Caspase 2 (51 kDa) shares sequence homology with some of the initiator caspases (-9 and -1) and possesses long pro-domain but its cleavage specificity is more closely related to that of executioner caspases (-3, -6 and -7), which makes Caspase-2 unique among the caspase family (Julien et al., 2016; Julien & Wells, 2017; Kitevska et al., 2014; Talanian et al., 1997; Tang et al., 2011; Thornberry et al., 1997; Wejda et al., 2012). Like other initiator caspases, Caspase-2 has a long N-terminus CARD domain, most similar to that of Caspase-9, followed by large (p19) catalytic subunit and small catalytic subunit (p12) at the C-terminus (Fava et al., 2012; Ramirez & Salvesen, 2018; S Shalini et al., 2015; Van Opdenbosch & Lamkanfi, 2019). But unlike the initiator caspases (-9 or -8) it does not cleave apoptosis effectors such as the executioner caspases (-3, -6 and -7), which need to be cleaved in order to be activated, and rather activates the executioner caspases in undirect way through the MOMP induction (Lisa Bouchier-Hayes, 2010; Fava et al., 2012; Guo et al., 2002; Van de Craen et al., 1999).

Caspase-2 could induce directly MOMP or have an upstream initiator function for the mitochondrial permeabilization process through cleavage of the pro-apoptotic Bcl-2 family protein Bid and/or upregulation of Bim, a BH3-only protein (Bonzon et al., 2006; Franklin & Robertson, 2007; Guo et al., 2002; Upton et al., 2008). Moreover, Caspase-2 mediated cleavage of MDM2 allows the stabilization of p53, permitting the induction of other mitochondrial apoptogenic factors (like the BH-3 only proteins) into the cell cytoplasm causing apoptosis (Oliver et al., 2011; Villunger et al., 2003). Caspase-2 deletion prevents the Bax/Bak translocation to the mitochondria (Boris Zhivotovsky & Orrenius, 2005). When

overexpressed the *Caspase-2/Nedd2* gene and its zymogens are shown to be sufficient for the Caspase-2 activation in cultured cells leading to apoptosis (S Kumar et al., 1994; L. Wang et al., 1994). Nuclear Caspase-2 could trigger the MOMP, which could be blocked by expression of the anti-apoptotic and preventing MOMP genes (Guo et al., 2002; S Kumar et al., 1994; Paroni et al., 2002; Troy & Shelanski, 2003; Vakifahmetoglu-Norberg & Zhivotovsky, 2010; L. Wang et al., 1994) suggesting alternative way for apoptosis in case of inhibition of the effector caspases (Troy & Shelanski, 2003). However, depending on the mode of activation Caspase-2 can act both upstream and downstream of MOMP (Lisa Bouchier-Hayes, 2010; Fava et al., 2012; Sharad Kumar, 2009; Sonia Shalini & Kumar, 2015; Troy & Shelanski, 2003).

Meanwhile, Caspase-2 itself is processed by Caspase-8 and Caspase-9 (in Caspase-2 knockout (KO) mice the Caspase-2 cleavage is dependent on the Apoptosome (O'Reilly et al., 2002)), and could be cleaved by Caspase-3 and to some extend by Caspase-7 (Paroni et al., 2001; Van de Craen et al., 1999). Due to the controversial role of Caspase-2 in apoptosis it is difficult to correctly place Caspase-2 in the apoptotic cascade (L Bouchier-Hayes & Green, 2012; Krumschnabel et al., 2008).

5.2 Function

In addition to its apoptotic function Caspase-2 is involved in many other processes including cell cycle regulation and signaling pathways (Vigneswara & Ahmed, 2020). Caspase-2 activation was reported to occur upon several diverse stimuli like DNA damage, ER stress and others, but it is also associated with differentiation and non-apoptotic cellular processes (Bouchier-Hayes, 2010; Fava et al., 2012; Miles et al., 2017; Boris Zhivotovsky & Orrenius, 2005). Caspase-2 function as a cell death effector varies in different cell types and its regulation of apoptosis could have a positive or negative effect depending on the cell type. Although it is processed upon apoptotic stimuli Caspase-2 is not required for apoptosis (Claudia Manzl et al., 2009; O'Reilly et al., 2002). However, Caspase-2 deficient mouse embryonic fibroblasts (MEF) have high rates of proliferation (Lien Ha Ho et al., 2009). Caspase-2 deficient mice develop normally and do not show any explicit phenotype, which suggest that Caspase-2 is not indispensable for apoptosis and its function can be replaced by

other functionally similar caspases (Bergeron et al., 1998; Marsden et al., 2004; O'Reilly et al., 2002). However, Caspase-2 is required for cell death induced by cytoskeletal disruption (L H Ho et al., 2008) and has been implicated to function as a regulator of the G2/M checkpoint (Dorstyn et al., 2012; Parsons et al., 2013). An important function of the Caspase-2-dependent apoptosis is to clean aneuploidy in cells (Dawar et al., 2017; Miles et al., 2017; Vitale et al., 2017). Moreover, Caspase-2 is selectively activated via the PIDDosome (see below) following cytoskeletal disruption and cytokinesis failure upon Aurora B inhibition or accumulation of supernumerary centrosomes upon PLK4 OE. This activation leading to a series of events that result in p21-dependent cell cycle arrest is used as an alternative mechanism to prevent aneuploidy and polyploidy (Fava et al., 2017).

An important function of Caspase-2 is its tumor suppression role. Caspase-2 KO MEFs have shown genomic instability, impaired DNA damage response and abnormal cycling. Moreover, Caspase-2 was shown to be indispensable for sensitization of tumor cells to chemotherapeutic drugs (Schmelz et al., 2004). Importantly, the tumor suppression function of Caspase-2 could be PIDDosome-independent (C Manzl et al., 2012; Peintner et al., 2015; Ribe et al., 2012). Taken together, Caspase-2 has shown to have an apoptotic and non-apoptotic function and makes it one of the most enigmatic caspases (Bergeron et al., 1998).

5.3 Caspase-2 localization

Caspse-2 has another unique feature among the caspases - its nuclear localization (Belinda C Baliga et al., 2003; Colussi et al., 1998). Procaspase-2 is found in the cytoplasm and the Golgi complex, but controversial reports indicate its presence in the mitochondria (Susin et al., 1999; van Loo et al., 2002). Importantly, it is present constitutively in the nucleus (Vakifahmetoglu-Norberg & Zhivotovsky, 2010; B Zhivotovsky et al., 1999). Studies show that both precursor and processed Caspase-2 localize to the cytoplasmic and the nuclear compartments. Moreover, the nuclear localization is strictly dependent on the presence of the prodomain. Using a fluorescent reporter fused with Caspase-2 it was shown that prodomain containing Caspase-2 forms dot- and fiber-like structures mainly in the nucleus, whereas Caspase-2 lacking the prodomain was concentrated in the cytoplasm (Belinda C Baliga et al., 2003). Interestingly, an amino-terminal fusion of the prodomain of Caspase-2 to Caspase-3

mediates nuclear transport of Caspase-3 (which like other caspases is strictly cytoplasmic) suggesting nuclear transportation function of the Caspase-2 prodomain (Colussi, Harvey, & Kumar, 1998). The nuclear import of Caspase-2 is regulated by two nuclear localization signals (NLS) in the prodomain. Mutation of the NLS of the cytosolic form of Caspase-2 is not able to prevent apoptosis upon OE of Caspase-2 and OE of the nuclear pool of the Caspase-2 results in apoptosis-related mitochondrial changes (Paroni et al., 2002; Robertson et al., 2002).

5.4 Caspase-2 – key residues, activation and inhibition

Caspase-2 is activated by proximity-induced oligo(di)merization, similar to other large-prodomain caspases, followed by autoproteolytic processing at aspartate 333 (D333) by cleavage in *trans* between the large and small catalytic subunits that remain associated. Already at this stage the Caspase-2 has 20% of the catalytic activity of the fully maturated wild type Caspase-2 (B C Baliga et al., 2004). Further step of auto-processing involves dimerization-induced cleavages at D169 which removes the inhibitory prodomain and a cleavage at D347 which removes the interdomain linker, generating the fully mature and active p19/p12 heterotetramer (Troy & Shelanski, 2003). The last cleavage in *trans* releases the caspase from the activation complex (Butt et al., 1998; Harvey et al., 1997; Lamkanfi et al., 2002; Read et al., 2002). Another important residue for the Caspase-2 function is the catalytic residue C320 at the C-terminus catalytic domain. Its mutation completely abolishes the catalytic activity of the enzyme, unlike the wild type form which is catalytically active or the D333 mutant which is partially active (B C Baliga et al., 2004; Dawar et al., 2017). Although auto proteolytic cleavage is not necessary for the initial activation of the caspase but for its full activation the autocatalytic processing seems to stabilize the active enzyme (B C Baliga et al., 2004). Uncleavable Caspase-2 showed that the dimerization and not processing is the key event for the activation, and after dimerization the auto catalytic cleavage stabilizes the dimer and enhances the catalytic activity of the enzyme. Importantly, only fully activated Caspase-2 is able to reach the levels necessary to induce apoptosis upon OE (B C Baliga et al., 2004). Interestingly, when overexpressed Caspase-2 activation occurs by an autoproteolytic mechanism (Butt et al., 1998).

Under crystallization conditions, the two Caspase-2 monomers are covalently linked by a central disulfide bridge, another unique feature of Caspase-2 (Schweizer et al., 2003). However, the dimerization of Caspase-2 is not dependent on the linkage between the two monomers, but its disruption leads to reduced catalytic efficiency (B C Baliga et al., 2004). Unlike caspases -8 or -9, unbound Caspase-2 is a stable dimer in solution (Schweizer et al., 2003). After dimerization Caspase-2 is ubiquitinated at three distinct lysine residues (K15, K152, K153). This promotes further dimer stability and activation (Robeson et al., 2018).

Inhibition by phosphorylation is one of the mechanisms of Caspase-2 regulation. There are three main phosphorylation sites. The first one, serine 135 (S135) suppresses the Caspase-2 activation and is metabolic-dependent (Nutt et al., 2005). The second one is the evolutionary conserved S340 (Andersen et al., 2009) which when phosphorylated suppresses the Caspase-2-mediated apoptosis upstream of the MOMP. The third, S157 of procaspase is shown to suppress the Caspase-2 activation in human cells. This phosphorylation is induced by casein kinase 2 (PKCK2, a serine/threonine protein kinase) and its inhibition induces the Caspase-2 dimerization and activation in a PIDDosome-dependent manner (Shin et al., 2005).

Recently, a mass spectrometry-based study reported other six phosphorylation sites, among which is the phosphorylation at the highly conservative S384 on the small subunit (p12). It is mediated by Aurora B kinase. This phosphorylation results upon mitotic insults and inhibits the apoptotic and catalytic activity of Caspase-2 by affecting the conformation of the binding pocket but not the dimerization. This phosphorylation fails to cleave MDM2 or Bid and shows increased polyploidy following Aurora B kinase inhibition (Lim et al., 2021).

The *Caspase-2* gene could be spliced alternatively in two distinct isoforms. One is Caspase-2L (or ICH-1_L of 435 amino acids) containing the sequence for both p19 and p12 subunits and it is proapoptotic. The other is Caspase-2S (or ICH-1_S 312 amino acid) is a truncated anti-apoptotic version containing only the p19 subunit sequence. The expression of the different isoforms is tissue specific (L. Wang et al., 1994).

5.5 PIDDosome

Caspase-2 was shown to be spontaneously recruited and activated via a large molecular weight protein complex (Read et al., 2002; Tinel & Tschopp, 2004). This complex is known

as the PIDDosome and it is consistent of the CARD- and death domain (DD)-containing adaptor protein RAIDD (also known as receptor-interacting protein (RIP)-associated ICH-1/CED-3 homologous protein with a DD (CRADD)) (Duan & Dixit, 1997), the p53-inducible DD-containing protein PIDD1 (also LRDD) (Lin et al., 2000; Telliez et al., 2000) and Caspase-2 itself (Tinel & Tschopp, 2004). PIDD1 binds and induces oligomerization of RAIDD through a protein-protein interaction via their DDs. RAIDD binds to Caspase-2 via its N-terminus CARD domain which recruits it via the Caspase-2 CARD domain into the PIDDosome by homophilic DD-fold interaction (Duan & Dixit, 1997). This recruitment induces the proximity of the Caspase-2 zymogens and facilitates its dimerization. The crystal structure of the DDs of PIDD1 and RAIDD revealed that five DDs monomers of PIDD1 bind seven DDs monomers of RAIDD allowing the recruitment of totally seven Caspase-2 molecules (Fig. 6) leading to the proximity-induced oligomerization and activation of Caspase-2 (H. H. Park et al., 2007). When within the PIDDosome the activation of Caspase-2 in the cytoplasm is RAIDD-dependent but PIDD1-independent, while in the nucleus the activation platform requires both PIDD1 and RAIDD (Ando et al., 2017).

Caspase-2 could be activated in variety of modes. Interestingly, its activation could be in a PIDDosome-dependent and -independent manner since deletion of PIDD or RAIDD did not affected the enzyme's activation (Claudia Manzl et al., 2009). Moreover, PIDD1 KO mice do not show dramatic phenotype suggesting that PIDD1 is not essential for the processing of Caspase-2 (Claudia Manzl et al., 2009). However, OE of RAIDD results in the generation of active Caspase-2 and OE of PIDD1 leads to the early Caspase-2 activation followed by caspases -3 and -7 activation, slowed apoptosis and increased sensitivity of cells to genotoxic stimuli (Berube et al., 2005; Lin et al., 2000; Tinel & Tschopp, 2004).

Interestingly when the PIDDosome is formed it could either trigger cell survival through NF-κB activation or alternatively triggers Caspase-2 activation and apoptosis (Tinel et al., 2007). However, in the presence of supernumerary centrosomes the PIDDosome, activated through ANKRD26-dependent recruitment of PIDD1 to the distal appendages of the mother centriole (Burigotto et al., 2021; L. T. Evans et al., 2021) leads to the Caspase-2 mediated MDM2 cleavage, which allows the stabilization of p53 in a positive feedback loop (see below) and the following p21-dependent cell cycle arrest (Fava et al., 2017).

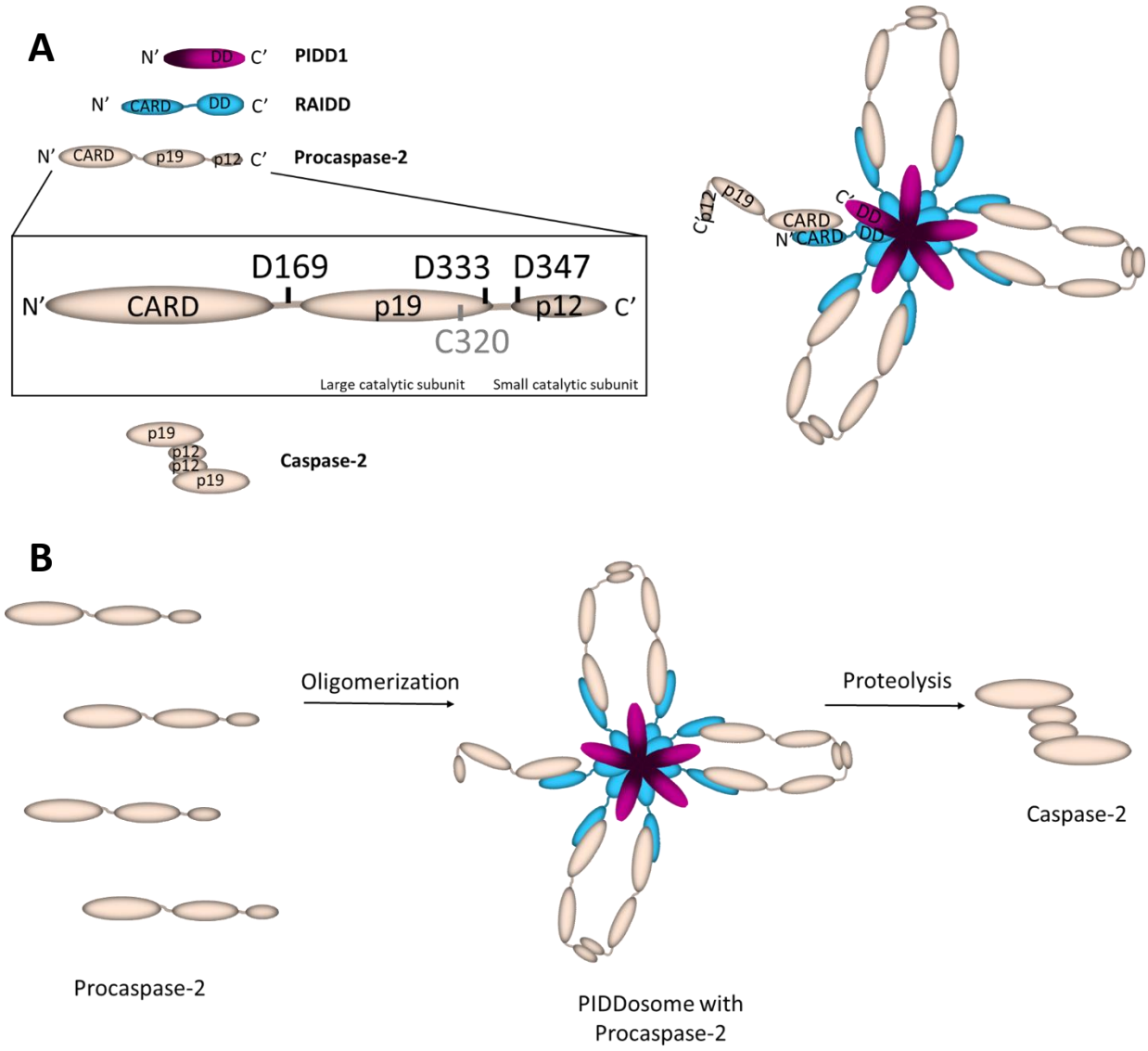

Figure 6. PIDDosome and PIDDosome-mediated Caspase-2 activation.

(A) Components of the PIDDosome are given on the left. PIDD1's DD is located at its C-terminus. RAIDD1's DD is at its C-terminus and its CARD is at the N-terminus. Caspase-2 has CARD domain at its N-terminus and possesses large and small catalytic subunits. Key cleavage sites residues (D169, 333, 347) and the active site residue (C320) of Caspase-2 are shown on the procaspase-2 zoom in window. Active fully mature Caspase-2 heterotetramer is composed of two small (p12) and two large (p19) catalytic units. A model of the PIDDosome composed of five molecules of PIDD1, seven molecules of RAIDD1 and seven molecules of procaspase-2 is shown on the right. Based on: (B C Baliga et al., 2004; Fava et al., 2017; Tinel & Tschopp, 2004)**. (B)** A model shows the steps in the activation of procaspase-2 via the PIDDosome. Based on: (B C Baliga et al., 2004; Fava et al., 2012; V. C. Sladky & Villunger, 2020).

5.6 Caspase-2 substrate specificity

Proteases cleave their protein substrates specifically. The cleavage could occur at the N- or C-terminus, or in the middle of the substrate protein, through the binding of the protease active site to the substrate residues flanking the cleavage site. The active site residues in the protease are composed of pockets termed subsites. Nomenclature labels the amino acids residues of the substrate surrounding the protease cleavage side as Pn towards the N-terminus and Pn' towards the C-terminus: NH_2. . . P3-P2-P1↓P1′-P2′-P3'. . .COON (cleavage site or proteolytic cut of the scissile bond happens between P1 and P1'). The subsites pockets of the active site of the proteases are correspondingly to the cleavage site named: NH_2. . . S3-S2-S1-S1′-S2′-S3'. . .COON (Schechter & Berger, 1967). The preferred sequence cleavage site is usually being reported as an amino acids sequences from the N-terminus towards the cleavage site (for example Caspase-3's indicative substrate is reported to be the tetrapeptide DEVD (P4=D, P3=E, P2=V, P1=D). All caspases cleave after an aspartate residue at the P1 position but have different preferences for the 3-4 residues preceding it (P2-P5) (Bouchier-Hayes, 2010). However, caspases -2, -3 and -7 show a strong preference for aspartate residue in P4 position compared to other caspases which can tolerate it (Talanian et al., 1997; Thornberry et al., 1997).

Caspase-2 preferences for amino acid residues sequence based on peptide screening is the pentapeptide VDVAD (Valine-Aspartic acid-Valine-Alanine-Aspartic acid) (Benkova et al., 2009; McStay et al., 2008; Talanian et al., 1997; Tang et al., 2011) with preferred P1 as aspartate. According to some the primary sequence specificity for the Caspase-2 cleavage is DEVD (Julien et al., 2016). These suggestions are based on a human recombinant Caspase-2 protein cleavage sites screen experiment, which revealed that the preferred cleavage substrate motif for Caspase-2 is DEVD↓G (P4-P1'), without strong specificity for the P5 residue, remarkably similar sequence to the cleavage site of the executioner Caspase-3 and Caspase-7 (Julien et al., 2016; Seaman et al., 2016). Other study reports the DEVD sequence as a consensus site for caspases -2 -3 and -7, which shows that Caspase-2 might function as an executioner/apoptotic caspase after disassembled from the activation complex (Wejda et al., 2012). A study using yeast-based transcriptional reporter system determined the minimal specificity for the Caspase-2 cleavage and suggest Acetyl (Ac)-VDTTD-AFC (7-amino-4-

trifluoromethylcoumarin (AFC)) as a peptide with better selectivity for Caspase-2 compared to Caspase-3 (Kitevska et al., 2014), which is a result consistent with several other peptide screening studies (McStay et al., 2008; Talanian et al., 1997).

Caspase-2 has a variety of substrates (Fava et al., 2012). It has 235 protein cell substrates with potential 277 cleavage sites (Julien et al., 2016). Among the identified cellular substrates for Caspase-2 are: Golgin-160, which protects cells from stress-induced apoptosis and it's cleaved by Caspase-2 in vitro at a specific site - $ESPD^{59}$ and a site common with other caspases - $SEVD^{311}G$ confirming the already reported capability of Caspase-2 to show some preferences for the DEVD cleavage site (Maag et al., 2005; Mancini et al., 2000; Troy & Shelanski, 2003). Other substrates are: Bid (cleavage site LQTD), nucleosome assembly protein 1-like 4 (NAP1L4; cleavage site SFSD), CUX-1 (cleavage site SEGD and/or DSCD), cleaved also by other caspases (Truscott et al., 2007) and others (Miles et al., 2017). However, the substrate that could be considered as a bona fide substrate for Caspase-2 is MDM2 (see below). In response to DNA damage and/or supernumerary centrosomes PIDDosome-dependent Caspase-2 mediated cleavage of MDM2 occurs. Importantly, the cleavage site of Caspase-2 for MDM2 is $FDVPD^{367}$ (Oliver et al., 2011; Pochampally et al., 1998).

5.7 Caspase-2 inhibitors

A known wide-range Caspase inhibitor, which also binds irreversibly to Caspase-2 is the bVAD (Biotin-Val-Ala-Asp (Ome)-fluoromethylketone) or the closely related pan caspase inhibitor z-VAD-FMK (benzyloxycarbonyl (z-), fluoromethyl-ketone (FMK)) (Gregoli & Bondurant, 1999; Tinel & Tschopp, 2004). The z-VAD-FMK inhibitor has moderate activity suppression for Caspase-2 and Caspase-3, while its suppression for caspases -8, -9 and -10 is efficient (Poreba et al., 2019). The bVAD binds covalently to the first caspase activated in response to a stimulus (Bouchier-Hayes, 2010). A crystal structure-based study revealed that fully processed Caspase-2 binds to the Ac-LDESD-aldehyde inhibitor and forms a $(p19/p12)_2$ dimer that contains two active sites, one on each monomer (Schweizer et al., 2003). Another pan-caspase inhibitor - Q-VD-OPh (Quinoline-Val-Asp-Difluorophenoxymethyl ketone) was developed for treatment strategy is widely used to inhibit apoptosis and caspases (Keoni & Brown, 2015). AF-D-AFC-base (N-Acetyl-S-farnesyl-L-cysteine (AFC)) inhibitor of

Caspase-2 was reported for treatment of neuronal diseases (H. Lee et al., 2018). Since the preferred cleavage for Caspase-2 is widely believed to be VDVAD, a Z-VDVAD-FMK and an Ac-VDVAD-CHO (N-acetyl-L-valyl-L-alpha-aspartyl-L-valyl-L-alanyl-L-aspart-1-al) inhibitors are also available (Maillard et al., 2011).

Recently, a potent, cell-permeable and selective for Caspase-2 inhibitor, named NH-23-C2 (non-acetylated at the P5 position acyloxymethyl ketone (AOMK) electrophile that reacts covalently with the caspases' catalytic cysteine), was shown to selectively inhibit Caspase-2 and to prevent the MDM2 cleavage (Poreba et al., 2019).

Importantly, a study performed by Gruetter's Laboratory reported an ankyrin based, highly specific for Caspase-2 inhibitor named AR_F8 (Schweizer et al., 2007). AR_F8 is ankyrin repeat based small artificial protein designed to bind the surface of Caspase-2 in allosteric way which provokes an inhibiting conformation for the active site of the enzyme and shows remarkably selective specificity towards Caspase-2.

5.8 Downstream events of the PIDDosome activation - MDM2 and p53

The ubiquitin-ligase murine double-minute 2 (MDM2; the murine homolog of hdm2) is a product of an evolutionary conserved gene - *murine double minute 2*, which encodes a cellular phosphoprotein with molecular mass of 95 kDa and 491 amino acids length (Barak & Oren, 1992; Cheng & Cohen, 2007). The *mdm-2* gene overexpression exhibits tumorigenic potential for the cells and it is accumulated in cancer cells (Fakharzadeh et al., 1991; Momand et al., 1992). Importantly, the *mdm-2* gene has a p53 responsive region (X. Wu et al., 1993). MDM2 protein has a DNA and p53 binding domain, so as nuclear localization signal (Manfredi, 2010; X. Wu et al., 1993). MDM2 has a variety of functions in the cell but one of the most crucial is to regulate p53.

The tumor protein p53 (TP53), also known as the guardian of the genome or gatekeeper is a transcription factor and a tumor suppressor that plays crucial role in the process of division since it monitors the integrity of the genome (Bieging & Attardi, 2012). In normal cells its levels of expression are kept low, almost undetectable but upon genomic damage, oncogene activation, oxidative stress and other stress stimulus its levels are upregulated (Kastenhuber & Lowe, 2017; Lohrum & Vousden, 1999; Luo et al., 2017). P53 loss of function is a key

event in tumor formations and 50% of the malignancies are associated with p53 mutations (Greenblatt et al., 1994; Shaw, 1996). P53 could be inactivated due to mutation or binding to oncogenic proteins, like MDM2 (Hainaut et al., 1998; Oliner et al., 1993; Prives & Hall, 1999).

MDM2 constantly shuttles between the nucleus and the cytoplasm and this event is independent of its interaction with p53 (Roth et al., 1998). However, shortly after its discovery it was shown that MDM2 directly binds p53 and inhibits its transcriptional function (G1 cell cycle arrest and apoptotic function) by forming a tight complex with p53 (Chen, Wu, et al., 1996; Haupt et al., 1997; Momand et al., 1992; Oliner et al., 1993). The E3-ubiquitin ligase activity of MDM2 further targets p53 for ubiquitination and subsequent degradation through the 26S proteasome (multi-catalytic ATP-dependent protease complex that serves for degradation of proteins (Livneh et al., 2016)) (Haupt et al., 1997; Honda et al., 1997; Kubbutat et al., 1997). MDM2 is a negative regulator of the p53 activity but p53 regulates the transcription levels of the *mdm-2* gene too. Thus, in normal cells p53 induces the expression of the *mdm-2* gene promoting its own degradation and creating a negative feedback loop for itself (Nag et al., 2013). However, in the presence of DNA damage or other stress factors p53 suppresses the expression of the *mdm2* gene, inhibits the MDM2-mediated p53 degradation and creates an autoregulatory positive feedback loop (Moll & Petrenko, 2003; Picksley & Lane, 1993).

Previous studies have demonstrated that MDM2 can be cleaved directly by Caspase-2 activated in a PIDDosome-dependent manner and this also creates a p53-mediated positive feedback loop (Oliver et al., 2011). The PIDDosome-mediated MDM2 cleavage leads to loss of the C-terminal RING domain of MDM2 responsible for the p53 ubiquitination. Cleaved MDM2 results in 60 kDa N-terminal protein doublet (Pochampally et al., 1998). Consequently, the N-terminally truncated MDM2, containing the p53-binding domain, binds p53 and instead of promoting its degradation it promotes the p53 stability and lead to its elevated levels (Kubbutat et al., 1997; Oliver et al., 2011). Moreover, the MDM2 cleavage induced by the PIDDosome is notable in cells without PARP cleavage, thus without apoptosis, suggesting that in this situation the stabilized p53 leads to upregulation of the CDK inhibitor p21 (inhibiting active CDKs 2, 4, and 6) and the p21-dependent cycle arrest (Benson et al., 2014; Fava et al., 2017; Pochampally et al., 1998).

6. Semi-automated pipeline for centrioles counting

6.1 Image processing

Immunofluorescence is a widely used technique for biological imaging of tissues and cells (Coons & Kaplan, 1950). It uses labeled with fluorophores antibodies against specific antigen in a cell. The signal of the fluorophores is used to generate an optical image which is transformed into a digital raster image composed of pixels (Lichtman & Conchello, 2005). Each pixel has assigned a number corresponding to intensity value. Pixel values are used to process images and extract relevant biological information. One of the simplest image processing techniques is global (applies to all pixels of the image) thresholding, when pixels of an image above or below a certain value (threshold) are excluded or only pixels in a given numerical (minimal and maximal value) range are left (Uchida, 2013).

Another important field of image processing is image segmentation. Image segmentation (similar to image pattern recognition (J. Yang & Yang, 2009)) is the process by which pixels are grouped (segmented) in regions which correspond to visually meaningful object or feature. After specific for the task and the image's characteristics processing the image could be converted into binary image (also binary mask). This is the simplest image - binary image and can display only two possible intensity values, usually black (0) and white (1 or 255) (Fisher R., Perkins S., Walker A., 2004). Image segmentation serves for many important purposes in image processing: to count objects, measure their size, analyze their shape or appearance, track or localize them. However, it is the most difficult of all image processing tasks. Typical image segmentation methods are: background subtraction, watershed method (L. P. Coelho et al., 2009) and others (Uchida, 2013). The term "watershed" means the ridge lines of a three-dimensional surface like a ground-surface. The method considers a region surrounding a closed ridge line as a partitioned region (Uchida, 2013). Thresholding is also considered a segmentation method but it is applicable only when the objects of interest have very bright signal that is easily distinguishable from other objects or background and are well separated from each other (Torborg & Feller, 2004). Thresholding segmentation can be

improved through preprocessing of the images with feature enhancing algorithms like Difference-of-Gaussians (Fischer et al., 2020).

Image segmentation is of a high importance for the automated image processing for certain tasks. Recently, the computationally based data and image analysis are becoming more and more important with the increasing amount of generated scientific data and images. Automated image analysis is necessary also for time-saving reasons, since manual image analysis is a laborious, time-consuming approach and requires high concentration for repetitive work at the computer. Moreover, manual approach is subjective. The automated image analysis not only reduces the workload and saves time but also assures consistency in the annotation, unbiased objectivity and easier reproducibility. For those reasons a high effort is invested in the improvement of image segmentation. However, since many bioimage analysis methods, including the ones for image segmentation, have been developed for specific biological assays, they are unapplicable for other assays. Importantly, often they require manual software adaptation, which is an obstacle for most biological laboratories, where the knowledge of the mathematics behind the image analysis algorithms is limited so as the experience in software engineering (Sommer & Gerlich, 2013). Furthermore, the complexity of biological images often results in poor performance when applying the most common segmentation methods.

6.2 Machine learning

Recently, an innovative and fast-evolving discipline in the computational sciences - machine learning is proving its powerful capabilities in scientific and medical image segmentation and analysis and offers a solution to the above-mentioned obstacle since it doesn’t require additional programming and instead learns how to achieve a task on its own. Moreover, it is superior to conventional image processing programs for complex multi-dimensional data analysis (like most biological ones) (Sommer & Gerlich, 2013). Machine learning is a field of artificial intelligence (AI). Historically AI goes back to the 1950s when Allan Turing published his work on machines (Turing, 1950). AI includes what was later called machine learning, however the first AI algorithms didn’t learn but generated a set of rules large enough to manipulate knowledge. However, for more diffuse and complex tasks like image

recognition and manipulation the introduction of machine learning was necessary (Iglesias et al., 2021). Computer vision is a more advanced field of AI for machine-based image processing which combines interdisciplinary approaches and it is dealing with the theory behind artificial systems that extract information from images. Machine learning has a high impact on the improvement of computer vision.

Machine learning methods are approaches for knowledge extraction, dating in the 1980s and already then they were used to support progress in the field of medicine and science (Zorman & Verlic, 2009). The term "machine learning" describes the study of computer algorithms that improve automatically through experience (Mitchell, 1997). These algorithms are self-adaptive and improve the quality of the analysis with more experience or newly added data. Other approaches that try to extract generalized knowledge from examples by induction are: symbolic approaches, computational learning theory and neural networks. In these approaches the goal is to learn how to classify objects by analyzing data of already classified sets of data for which the classes and decision criteria are known (Zorman & Verlic, 2009).

Machine learning proceeds in two phases. The first one, a training phase, is when training data set is used to build and improve the computer system learning from the inherent structures and relationships within this data set. A common approach of machine learning is feature extraction, which aims to characterizing an object by its properties or features like dimensions, shape, color, texture or others. These features are then used for the classification - distinguishing all the objects and assigning them to a specific category (Veronese et al., 2013). The other phase is the application of the knowledge learned by the computer system to a new data set used to predict features or properties of the data. There are two main types of machine learning – unsupervised and supervised. Supervised learning is guided by a user, who generates annotated representative examples of the data set which in the case of image analysis is the manual image annotation or segmentation of key objects from a representative image. This data set is used as training data. Subsequently, the "learned" by the machine algorithm knowledge, automatically generated rules for classes discrimination, is used to perform similar task to the rest of the unseen data of the full set.

An important subtype of machine learning is deep learning, which is based on artificial neural networks (ANN). Deep learning refers to multiple hidden layers that perform information processing in the neural network (deep neural network). It creates patterns used in decision

making and utilizes a hierarchical level of artificial neural networks able to learn from unstructured and unlabeled data with or without supervision, similar to the machine learning. In ANN the processing units are interconnected by nodes like a web and are composed of input and output units. A class of ANN are the convolutional neural networks (CNN). The CNN can take an input image with assigned objects and differentiate them without the necessity of pre-processing. This is done through convolution and pooling. CNN reduces the input image into resized image easier to process preserving critical features necessary for a good prediction. Then they load the first part of convolutional layer, which extracts high level features by applying filters across the image. The following layer is the pooling layer where the spatial size of the convolved features is reduced, necessary to decrease the computational power. Lastly, the final output is flattened and fed to a regular neural network for classification purposes. This last fully connected layer is necessary to learn non-linear and high-level features combinations generated by the previous convolutional layer.

Semantic image segmentation is a method that aims to label each pixel of an image with a corresponding class of what is being represented and can be achieved using a fully convolutional network (trained end-to-end, pixels-to-pixels). Fully convolutional networks take input of arbitrary size and produce correspondingly sized output with efficient inference and learning (Jonathan Long, Evan Shelhamer, 2015). A popular fully convolutional network is the U-Net architecture which consists of a contracting path to capture context and a symmetric expanding path that enables precise localization and could be trained end-to-end from few images. This architecture uses data augmentations - random elastic deformations of the training samples as a key concept for learning and it was shown to outperform other convolutional network-based approaches for image segmentation (Ronneberger et al., 2015). Recently, a user-friendly deep learning software MitoS and a model based on U-net called MitoSegNet were developed for the segmentation of cellular organelles like mitochondria and was adapted for the image processing in this thesis (C. A. Fischer et al., 2020).

6.3 ImageJ

Fiji (Schindelin et al., 2012) is an ImageJ (https://imagej.nih.gov/nih-image/) distribution that contains many image analysis and machine learning plugins. ImageJ is an open source public

domain image software for processing and analyzing scientific and medical images created by Wayne Rasband. Developed in 1997 ImageJ has been continuously updated and improved by its creators and users. It's open source structure allows the generation and loading of small code modules (macros and plugins) performing automatically simple or more complicated tasks, which extends the built-in capabilities of ImageJ. Macros are written in ImageJ's Java-like macro programming language while plugins are written in the Java programming language. Macros and plugins are easy to install and could be combined with the main ImageJ capabilities. An example of plugins and macros using some of the built-in functions of Fiji and adding new functions is the BioVoxxel Toolbox (https://www.biovoxxel.de/development/) developed by Jan Brocher (Brocher, 2015) which has features like particle analysis, feature extractor, Speckle inspector, watershed irregular features and binary masking.

AIMS OF THE THESIS

Centrosome amplification is often found in tumors and it is a predisposition for aneuploidy (Godinho et al., 2014; Levine et al., 2017). Previous studies showed that supernumerary centrosomes accumulation activates a multiprotein complex composed of: PIDD1, RAIDD and Caspase-2 leading to the cleavage of the negative p53 regulator MDM2, followed by p53 stabilization and p21-dependent cell cycle arrest (Fava et al., 2017). The PIDDosome activation upon supernumerary centrosomes accumulation is dependent on the ANKRD26 (centriolar distal appendage protein)-mediated PIDD1 recruitment (Burigotto et al., 2021). Moreover, Caspase-2 has been reported to possess tumor suppressive function (Lisa Bouchier-Hayes, 2010; Lien Ha Ho et al., 2009).

Detection of PIDDosome-mediated Caspase-2 activation

PIDDosome-activating cues have been reported (Burigotto et al., 2021) but finding a reliable tool to detect the activated PIDDosome *in vivo* could contribute to the further understanding of the localization, mode and timing of the PIDDosome activation. One way to develop such tool would require the knowledge of precise substrate specificities of Caspase-2 when activated in the PIDDosome. Numerous reports indicate VDVAD as a specific and preferred substrate cleavage site of Caspase-2 (Benkova et al., 2009; McStay et al., 2008; Talanian et al., 1997; Tang et al., 2011). Investigation of the VDVAD-based fluorescent substrates for the detection of PIDDosome activation would facilitate the development of such tool and the profound understanding of the PIDDosome activation. One of the main goals of this project is to find a reliable PIDDosome-activated Caspase-2 read out tool.

Determination of the Caspase-2's substrate preferences dependance of its mode of activation

Caspase-2's preferred substrates cleavage site based on peptide screening is reported to be VDVAD, however the bona fide PIDDosome substrate MDM2 is cleaved at the FDVPD site

(Pochampally et al., 1998). Difference in the Caspase-2 substrate preferences could be due to its mode of activation, which relies on PIDDosome-dependent and independent autoproteolysis. We hypothesize that the PIDDosome-activated Caspase-2 cleaves after the FDVPF motif and the fully active Caspase-2 heterotetramer cleaves after the VDVAD motif. Developing a strategy to investigate the Caspase-2 substrate preferences upon PIDDosome-activation stimuli in non-autoproteolytically cleavable Caspase-2 would reveal the potential mechanism behind the difference of the substrate specificities of Caspase-2.

Automated quantification of supernumerary centrosomes

Development of a fast and easy mode of centriole quantification would facilitate the processing of large amounts of image data generated for the purpose of investigations of supernumerary centrosomes accumulation and the following PIDDdosome-p53 signaling axis. The last part of this project is dedicated to the development of a semi-automated pipeline for the centrioles quantification with different antibody staining across different genetic perturbations designed to impinge on centriole abundance.

MATERIALS AND METHODS

1. Tissue Culturing

Cell lines

A549 (ATCC® CCL-185) and HEK293T (gift by Dr. Ulrich Maurer, University of Freiburg) cells were cultured in Dulbecco's Modified Eagle's Medium (DMEM, Corning, 15-017-CVR) media completed with 10 % v/v fetal bovine serum (Gibco, 10270-106), 2 mM L-glutamine (Gibco, 25030-024) and 5 % v/v Penicillin (100 UI/mL)/Streptomycin (100 µg/mL) solution (Gibco, 15070-063). hTERT-RPE1 (hereafter referred to as RPE1; gift by Stephan Geley, Medical University of Innsbruck) cells were cultured in F12 (Gibco, 21331-020) completed with 10 % v/v fetal bovine serum (Gibco, 10270-106), 2 mM L-glutamine (Gibco, 25030-024) and 5% v/v Penicillin (100 UI/mL)/Streptomycin (100 µg/mL) solution (Gibco, 15070-063). Single cell clones of Caspse-2 KO were used: for A549 - clone 13#2 and for RPE1 - clones 12#2 and 13#9 generated by the laboratory using the CRISPR/Cas9 system. For Fig. 9 and 11 Caspase-2 KO clone 12#2 was used. For culturing, the cells were passaged, using Trypsin (Gibco™, 25200056), after reaching full confluency. Cells were treated and incubated in sterile conditions, in an incubator in humid environment, at 37°C with 5% CO_2. Before treatments with drugs cells were split and the necessary amount was calculated in order to seed 1.2 million cells of RPE1 or 0.8 million cells of A549 in 6 cm dishes. Before transfection 4 million HEK293T cells were seeded in 10 cm petri dishes in media without Pen/Strep solution. After 4-8 h. when cells were attached to the petri dish bottom the media was exchanged with fresh one containing drugs or transfection reagents.

Drugs

Cells were treated with media containing 2 µM ZM447439 (Selleck Chemicals, S1103) for 24 hours. For untreated controls DMSO (Sigma-Aldrich, 472301)- the solvent used in the same concentration as for the corresponding drug was used. Treatment of A549 was done with the following compounds: 10 µM Staurosporine (ApexBio, 62996-74-1), 10 µM WEHI-539 (ApexBio, 1431866-33-9) or both with the indicated concentration contemporaneously for 7 hours. Treatment of RPE1 was done with the following compounds: 5 µM

Staurosporine, 10 µM WEHI-539 or both with the indicated concentration contemporaneously for 4 hours. For cells treated with doxycycline (Acros Organics, AC446060050) concentration of 1.9 µM was used for 24, 48, 72, 96 or 120 hours.

2. Molecular cloning

Human Caspase-2 gene followed by a sequence corresponding to a GS linker and an in-frame V5-tag was synthesized in the pEX-A258 backbone (Eurofins Genomics), see Table 1. The synthetic Caspase-2 cDNA was flanked at 5' by KpnI and BamHI restriction sites and at 3' by XbaI and NotI restriction sites. Silent mutations have been introduced within the Caspase-2 sequence in order to remove an internal BamHI restriction site and to render the construct resistant to Cas9 cleavage mediated by guide 1 (AGGACTCACACACCGGAAAA) and guide 2 (TGGTGAGCAACATATCCTCC).

Caspase-2 cDNA was digested from the pEX-A258 backbone with BamHI/XbaI and ligated into dephosphorylated with Antarctic Phosphatase pcDNA^{TM} 5/FRT/TO (Invitrogen, V652020) backbone plasmid in order to generate the following constructs: pcDNA5/FRT/TO-KpnBam-hCASP2-D169A-V5-XbaNot, pcDNA5/FRT/TO-KpnBam-hCASP2-D333A-V5-XbaNot, pcDNA5/FRT/TO-KpnBam-hCASP2-D347A-V5-XbaNot and pcDNA5/FRT/TO-hCASP2-L132D-V5. Point mutations were introduced via single-primer reactions in parallel, a modified Quick Change protocol (Edelheit et al., 2009) with primers listed in Table 4. Enzymes DpnI and Phusion DNA polymerase were used for the reaction (see Table 2). Additional single point mutations were subsequently introduced via the same protocol. The cDNA of each construct was further cloned into lentiviral vector CMVmin-TetO (Gift of Alessandra Fasciani (Alessio Zippo); Modified version of Addgene plasmid FUW-tetO-MCS (Plasmid #84008); lentiviral vector with a CMV minimum promoter and a TetON operator). All constructs were verified by Sanger Sequencing (Eurofins), for sequencing primers refer to Table 3. Designed Ankyrin Repeat Caspase-2 inhibitor based on the AR_F8 (Schweizer et al., 2007) was synthesized in pEX-A128 backbone (Eurofins Genomics), see Table 1. The designed ankyrin repeat cDNA was flanked at 5' by BamHI, 6x His tag and at 3' by in frame V5-tag and XhoI. cDNA was digested from the pEX-A128 backbone with BamHI/XhoI and subsequently cloned in dephosphorylated

with Antarctic Phosphatase pcDNA^{TM} 5/FRT/TO backbone in order to create pcDNA5/FRT/TO-CASP2-inhib. Construct sequence was verified by Sanger Sequencing (Eurofins).

Table 1. Synthesized cDNA sequences

cDNA	Sequence
Human CASP-2	GGTACCggatccACCATGGCGGCGCCGAGCGCGGGGTCTTGGTCCACCTTCCAG CACAAGGAGCTGATGGCCGCTGACAGGGGACGCAGGATATTGGGAGTGTGT GGCATGCATCCTCATCATCAGGAAACTCTAAAAAAGAACCGAGTGGTGCTAG CCAAACAGCTGTTGTTGAGCGAATTGTTAGAACATCTTCTGGAGAAGGACAT CATCACCTTGGAAATGAGGGAGCTCATCCAGGCCAAAGTGGGCAGTTTCAGC CAGAATGTGGAACTCCTCAACTTGCTGCCTAAGAGGGGTCCCCAAGCTTTTG ATGCCTTCTGTGAAGCACTGAGGGAGACCAAGCAAGGCCAtCTtGAGGATATG TTGCTCACCACCCTTTCTGGGCTTCAGCATGTACTCCCACCGTTGAGCTGTGA CTACGACTTGAGTCTaCCTTTTCCGGTGTGTGAGTCCTGTCCCCTTTACAAGA AGCTCCGCCTGTCGACAGATACTGTGGAACACTCCCTAGACAATAAAGATGG TCCTGTCTGCCTTCAGGTGAAGCCTTGCACTCCTGAATTTTATCAAACACACT TCCAGCTGGCATATAGGTTGCAGTCTCGGCCTCGTGGCCTAGCACTGGTGTT GAGCAATGTGCACTTCACTGGAGAGAAAGAACTGGAATTTCGCTCTGGAGG GGATGTGGACCACAGTACTCTAGTCACCCTCTTCAAGCTTTTGGGCTATGAC GTCCATGTTCTATGTGACCAGACTGCACAGGAAATGCAAGAGAAACTGCAG AATTTTGCACAGTTACCTGCACACCGAGTCACGGACTCCTGCATCGTGGCAC TCCTCTCGCATGGTGTGGAGGGCGCCATCTATGGTGTGGATGGGAAACTGCT CCAGCTCCAAGAGGTTTTTCAGCTCTTTGACAACGCCAACTGCCCAAGCCTA CAGAACAAACCAAAAATGTTCTTCATCCAGGCCTGCCGTGGAGATGAGACTG ATCGTGGGGTTGACCAACAAGATGGAAAGAACCACGCAGGcTCCCCTGGGTG CGAGGAGAGTGATGCCGGTAAAGAAAAGTTGCCGAAGATGAGACTGCCCAC GCGCTCAGACATGATATGCGGCTATGCCTGCCTCAAAGGGACTGCCGCCATG CGGAACACCAAACGAGGTTCCTGGTACATCGAGGCTCTTGCTCAAGTGTTTT CTGAGCGGGCTTGTGATATGCACGTGGCCGACATGCTGGTTAAGGTGAACGC ACTTATCAAGGATCGGGAAGGTTATGCTCCTGGCACAGAATTCCACCGGTGC AAGGAGATGTCTGAATACTGCAGCACTCTGTGCCGCCACCTCTACCTGTTCC CAGGACACCCTCCCACAGGCAGCGGCAAGCCCATCCCCAACCCCCTGCTGGG CCTGGACAGCACCTAGtctagaGCGGCCGC
Designed Ankyrin Repeat CASP-2 inhibitor	GGATCCACCATGAGGGGAAGTCACCACCACCATCACCATGGCTCTGATCTGG GCAAGAAGTTGCTCGAAGCAGCTAGAGCAGGGCAAGACGACGAAGTACGGA TACTCATGGCAAATGGGGCTGATGTCAACGCCACCGATTGGCTTGGACACAC ACCGCTCCATCTTGCCGCCAAGACAGGTCACTTGGAGATTGTCGAAGTTCTG CTGAAGTATGGCGCAGATGTGAATGCGTGGGATAACTACGGTGCTACTCCTC TGCACCTTGCCGCTGACAATGGGCATCTGGAGATCGTTGAGGTCCTGCTGAA ACACGGTGCAGATGTGAACGCCAAAGACTACGAGGGGTTTACGCCACTGCA TCTCGCTGCCTATGACGGCCATCTGGAAATCGTGGAAGTGCTGCTGAAGTAC GGAGCTGACGTGAATGCGCAGGATAAGTTCGGGAAAACCGCCTTCGACATC AGCATCGACAACGGCAATGAGGACTTGGCCGAGATTCTGCAGAAACTCAAC GGATCAGGCAAACCCATTCCCAACCCTCTTCTGGGACTGGATTCCACTTGAC TCGAG

Table 2. List of used enzymes		
Enzyme	**Company**	**Reference**
5 BamHI	Anza™, Thermo Fisher Scientific	IVGN0058
17 KpnI	Anza™, Thermo Fisher Scientific	IVGN0176
12 XbaI	Anza™, Thermo Fisher Scientific	IVGN0126
1 NotI	Anza™, Thermo Fisher Scientific	IVGN0016
8 XhoI	Anza™, Thermo Fisher Scientific	IVGN0086
Antarctic Phosphatase	New England Biolabs	MO289S
T4 DNA Ligase	Anza™, Thermo Fisher Scientific	IVGN2104
DpnI	Thermo Fisher Scientific	ER1701
Phusion DNA polymerase	Thermo Fisher Scientific	F530-L

Table 3. List of sequencing primers		
Backbone	**Primer**	**Sequence (5'-3')**
pcDNA™ 5/FRT/TO	Fw	GTGAACCGTCAGATCGCCT
	Rw	GCTATTGTCTTCCCAATCCTCCC
CMVmin-TetO	Fw	AGCTCGTTTAGTGAACCGTC
	Rw	CCACATAGCGTAAAAGGAGCAA

Table 4. List of mutagenesis primers		
Construct	**Primer**	**Sequence (5'-3')**
pcDNA5/FRT/TO-KpnBam-hCASP2-D169A-V5-XbaNot	Fw	CTCCCTAGACAATAAAGCTGGTCCTGTCTGCCTTC
	Rw	GAAGGCAGACAGGACCAGCTTTATTGTCTAGGGAG
pcDNA5/FRT/TO-KpnBam-hCASP2-D333A-V5-XbaNot	Fw	GGGGTTGACCAACAAGCTGGAAAGAACCACGC
	Rw	GCGTGGTTCTTTCCAGCTTGTTGGTCAACCCC
pcDNA5/FRT/TO-KpnBam-hCASP2-D347A-V5-XbaNot	Fw	GGGTGCGAGGAGAGTGCTGCCGGTAAAGAAAAG
	Rw	CTTTTCTTTACCGGCAGCACTCTCCTCGCACCC
pcDNA5/FRT/TO-hCASP2-L132D-V5	Fw	CAGCATGTACTCCCACCGGATAGCTGTGACTACGACTTG
	Rw	CAAGTCGTAGTCACAGCTATCCGGTGGGAGTACATGCTG

Bacteria transformation

E. coli strain DH5α were used for transformation, thus plasmid multiplication. 1 ng of the desired plasmid and KCM solution (KCl 100 mM, $MgCl_2$ 50 mM, $CaCl_2$ 30 mM) 20 µl/1 ng DNA and were incubated on ice for 10 min. 100 µl saturated culture of bacteria were added to the transformation mix and incubated 20 min on ice, followed by 1 min incubation at 42°C. After heat shock bacteria were left on ice for 3-5 min and recovered at 37°C, at 500 rpm for 1 hour in liquid Luria Bertani (LB, Sigma-Aldrich, L3522) without antibiotics. Approximately 1/4 of bacteria cells were plated on a petri dish with LB agar 15 g/L (Acros

Organics) completed with 100 µg/mL Ampicillin (Fisher BioReagents, BP1760) and incubated at 37°C over night (o/n). Only when transformed with freshly ligated constructs all bacteria were plated. Antibiotic selected positive for the transformation colonies were picked and cultured additionally in Ampicillin completed LB at 500 rpm 37°C o/n. Cells were processed with NucleoSpin Plasmid Mini kit for plasmid DNA purification (Macherey-Nagel, 740588) or CompactPrep Plasmid Maxi Kit (Qiagen, 12863) according to manufacturer's protocols. Plasmid concentration and purity was evaluated at 230/260/280 nm with Nanodrop 200c (Thermo Fisher Scientific).

Generation of lentiviral particles, titration and transduction

HEK293T cells were seeded in antibiotic-free medium and co-transfected with pCMV-VSV-G (a gift from Bob Weinberg, Addgene plasmid #8454), psPAX2 (a gift from Didier Trono, Addgene plasmid #12260), pcDNA5/FRT/TO-CASP2-inhib (5 µgr or 10 µgr) or small molecule inhibitors of Caspase-2 and the desired construct (transfer plasmid) using calcium phosphate as described in (Burigotto et al., 2021). Small molecule Caspase-2 inhibitor NH-23-C2 (gift from Poreba et al., 2019) with concentration 30 mM was used. Transfection mix was kept for 7-8 hours. 48 and 72 hours post-transfection cell supernatant was collected and filtered with 0.22 µm Primo® Syringe Filters (EuroClone, EPSPE2230). Viral titer was measured as already reported (Pizzato et al., 2009). Virus containing supernatant was stored at -80°C. For transduction the virus containing supernatant was diluted with fresh medium at a concentration of 0.2 reverse transcriptase units per mL (U/mL, for A549 cells) or 0.1 U/mL (for RPE1 cells), supplemented with 4 µg/mL hexadimethrine bromide/Polybrene (Sigma-Aldrich, H9268) and administered to A549 or RPE1 cells (Fig. 9A) for 48 h (Burigotto et al., 2021).

3. Fluorometric assay and substrates

Fluorimetric Activity Assay was performed with Caspase-2 Fluorometric Assay Kit (Enzo Life Sciences, ALX-850-214) and Caspase-3/CPP Fluorimetric Assay kit (Enzo Life Sciences, ALX-850-216) according to the manufacturer's protocol with few modifications. Parental and Caspase-2 KO cells treated with drugs were collected via centrifugation at

5000G. Cell pellets were washed with PBS and resuspended in 50ul chilled Cell Lysis Buffer (included in the kit). Cells were incubated on ice for 10 min. Then centrifugation was performed for 1.5 min. at 4°C, 11000xG. Supernatant was transferred into fresh tube. 5 µl of the supernatant were used for BCA protein quantification (see Immunoblotting). The rest 45 µl were used for the fluorimetric measurement. 45 µl 2xReaction Buffer containing freshly added 10 mM DTT (included in the kit) was added to each sample. Finale concentration of 25 µM VDVAD-AFC/DEVD-AFC substrate was used for each sample. Cell lysate with the fluorimetric substrates were incubated at 37°C, for 1-2 hours, in dark. 65 µl of the samples were carefully transferred in 96-well microplate with clear bottom. Fluorescence was read with microplate reader (Tecan, Infinite® 200 PRO) with 400 nm excitation wavelength and 505 nm emission wavelength. At least three technical measurements were performed. The fluorimetric measurements for RPE1 cells were performed with home-made 2x Reaction Buffer (50 mM Tris-HCl pH 7.4 (Tris base, Fisher Bioreagents BP152), 150 mM NaCl, 0.1% v/v Triton X-100 and 5% v/v Glycerol freshly completed with 10 mM DTT) as described in (Liccardi et al., 2019). The third biological replicated for RPE1 cells was measured with the following substrates: Ac-VDVAD-AFC (Cayman chemicals, 14988) and Ac-DEVD-AFC (Cayman chemicals, 14459) following the same protocol (Fig. 8A).

4. Cell lysis and Immunoblotting

Cells were collected via trypsinization and lysed in Lysis buffer: 50 mM Tris-HCl pH 7.4, 150 mM NaCl, 0.5% v/v NP-40, 50 mM NaF, 1 mM Na_3VO_4, 1 mM PMSF, one tablet/10 mL Pierce™ Protease Inhibitors Mini Tablets, EDTA-free (Thermo Fisher Scientific, #A32955), 2 mM MgCl2 and 0.2 mg/mL DNase I (Thermo Fisher Scientific, #89836) and ddH_2O as described in (Burigotto et al., 2021). Concentration of proteins was determined with bicinchoninic acid assay (Pierce™ BCA Protein Assay Kit, Thermo Fisher Scientific, 23225), following the manufacturer's protocol and measuring the absorption of each lysate using microplate reader (Tecan, Infinite® 200 PRO).

Immunoblotting was performed as follows:

Equal amount of protein concentration was obtained via dilution of the lysates with Lysis buffer (see above) and SDS Loading Buffer 5X (Saturated solution of bromophenol blue

0,08% v/v, Glycerol 42% v/v, SDS 5% w/v, Tris-HCl 200 mM, pH 6,8) completed with 5% v/v β-mercaptoethanol (SCHARLAU, ME00950250). Proteins were denatured at 95°C for 7 min. Between 35 μgr and 55 μgr total proteins were loaded on self-made 8%, 10% or 12% polyacrylamide gels, used for protein separation via electrophoresis (Running buffer: TGS 10% v/v, ddH_2O). Proteins were wet transferred (Transfer buffer: Tris-Glycine 10% v/v (Tris 25 mM, Glycine 192 mM (Carlo Erba Reagents, 453807), ddH_2O), Ethanol 20% v/v, ddH_2O) via electroblotting at 4°C for 1 hour, on nitrocellulose membranes (GE Healthcare, RPN3032D). Successful transferring was verified with Red Ponceau (Ponceau S solution, Sigma-Aldrich, 6226-79-5) staining. Blocking of non-specific binding sites of the membranes was done with 5% w/v fat-free milk in PBS-Tween-20 0.1% v/v, which was also used for antibodies dilution. List of used antibodies and their dilutions are given in Tables 4 and 5. Primary antibody incubation was done o/n at 4° at 18rpm. On following day membranes were washed with PBS-Tween 0.1% v/v and incubated with HRP-conjugated secondary antibody for 1 hour at room temperature. Membranes were again washed with PBS-Tween 0,1% v/v. Chemiluminescence was detected in Alliance LD2 Imaging System (UVITEC, Cambridge) after short incubation with Amersham™ ECL Select™ Western Blotting Detection Reagent (GE Healthcare, RPN2235).

Table 5. Primary antibodies used for immunoblotting

Primary antibody	Host	Dilution	Company	Reference
α-Tubulin (YL12)	Rat	1:1000	Thermo Fisher Scientific	MA1-80017
Caspase-2 (11B4)	Rat	1:1000	Enzo Life Sciences	ALX-804-356
Caspase-3	Rabbit	1:1000	Cell Signaling	9662
HSP90	Mouse	1:10000	SCBT	sc13119
MDM2 (IF2 clone)	Mouse	1:1000	Invitrogen	MA1-113
PARP1	Rabbit	1:1000	Cell Signaling	9542
V5-tag (D3H8Q)	Rabbit	1:1000	Cell Signaling	13202

Table 6. Secondary antibodies used for immunoblotting

Primary antibody	Host	Dilution	Company	Reference
anti-mouse IgG/HRP	Rabbit	1:5000	Dako	P0161
anti-rabbit IgG/HRP	Goat	1:5000	Dako	P0448
anti-rat IgG/HRP	Goat	1:5000	Thermo Fisher Scientific	31470

5. Microscopy

Bright field microscopy

Images were taken with Leica DMi8 inverted wide-field fluorescence microscope equipped with Leica DFC450C (729933914) camera using the 5x (HI PLAN I 5x/0.22, Leica) objective. For the image acquisition the LAS X Life Science (Leica Microsystems) software was used. Image processing was done with Fiji.

Immunofluorescence

RPE1 and A549 cells were seeded on glass coverslips (Marienfeld-Superior, 0117580), washed in PBS 1x and fixed. Fixation and permeabilization was performed: 1) For anti-V5-tag antibody staining - with direct application of 4% v/v formaldehyde (Sigma-Aldrich, F8775) in PTEM buffer (0.2% Triton™ X-100, 20 mM PIPES at pH 6.8, 1 mM MgCl2, 10 mM EGTA in ddH2O) for 12 min at room temperature. 2) For all other antibodies - with application of ice-cold MetOH for at least 20 min at -20°C. After fixation cells were washed with PBS and blocked with blocking solution - 3% w/v BSA in PBS for 20 min at room temperature. Cells were stained with rabbit primary antibody against V5-tag (Cell Signaling, 13202), with dilution 1:500 in blocking solution, for 1 hour at room temperature, in dark. Cells were further washed with PBS and stained with fluorescent secondary goat anti-rabbit antibody (IgG Alexa Fluor 555, Invitrogen, A21429) or goat anti-mouse antibody (IgGAlexa Fluor 488, Invitrogen, A11029) with dilution 1:1000 and 1 µg/mL Hoechst 33342 (Invitrogen, H3570) for 15 min, at room temperature, in dark. Additional PBS wash was performed. Cells were washed with ddH_2O and mounted in ProLong™ Gold Antifade Reagent (Invitrogen, P36934). Image acquisition was done on a spinning disk Eclipse Ti2 inverted microscope (Nikon Instruments Inc), equipped with Lumencor Spectra X Illuminator as LED light source, an X-Light V2 Confocal Imager and an Andor Zyla 4.2 PLUS sCMOS monochromatic camera applying a plan apochromatic 100x/1.45 oil immersion objective.

Table 7. Primary antibodies used for immunostaining					
Primary antibody	**Host**	**Dilution**	**Company**	**Reference**	**Fixation Protocol**
V5-tag (D3H8Q)	Rabbit	1:500	Cell Signaling	13202	FA+PTEM
Centrin 1	Mouse	1:1000	Millipore	041624	MetOH
ANKRD26	Rabbit	1:800	GeneTex	GTX128255	MetOH
γ-Tubulin	Mouse	1:1000	Termo Fischer	MA1-19421	MetOH

6. MitoSegNet Models and Centrioles masks generation

Model I was generated by finetuning the pretrained MitoSegNet model using the MitoS segmentation tool with 3 (for Centrin 1, hereafter referred to as Centrin) or 4 (for each: γ-Tubulin and ANKRD26) augmented (20 augmentations per image) ground truth (hand-labeled) images. The pretrained MitoSegNet model was trained for 1 epoch (number of cycles of passing the entire training dataset the machine learning algorithm has completed). The finetuning for γ-Tubulin and ANKRD26 was performed simultaneously and one finetuned model (Model I-γ-Tubulin/ANKRD26) for both antibodies staining was generated.

Model II was generated in the same fashion as Model I for each individual antibody staining. For the generation of Model II-Centrin, a total of 24 augmented (15 augmentations per image) ground truth images were used. For the fine tuning of Model II-γ-Tubulin, a total of 36 augmented (10 augmentations per image) ground truth images were used. Model II-ANKRD26 was generated by finetuning of the pretrained MitoSegNet model with 92 augmented (10 augmentations per image) ground truth images.

For the generation of the predictions with Model I few images required adjustment of the Brightness/Contrast. For the generation of the predictions with Model II less than 10 % of the images required preprocessing with the built-in filter of Fiji Unsharp Mask filter application with Radius (Sigma) 3 pixels and Mask Weight of 0.6. Few images required manual generation of the binary masks using and adjusting the built-in Fiji Thresholding function due to disrupted image quality following precipitation.

Centrioles predictions were generated with the CPU version of MitoS tool (Fischer et al., 2020) using Model I (for Centrin or γ-Tubulin/ANKRD26) or Model II (for each individual antibody). All predictions for Centrin were performed with Minimum Object size 1. All predictions for ANKRD26 and γ-Tubulin were performed with Minimum Object size 3.

All predictions with Model I were post-processed with the built-in Classic Watershed of Fiji. The few predictions generated by manual thresholding (included in the Model II counts) were post-processed with the Watershed function.

7. Statistics

For the fluorimetric activity assay the mean value of three technical measurements were taken and normalized to the protein concentration measured via BCA assay (described above). This value was then normalized to the untreated (DMSO only) wild type parental cells. Data are presented as dot plots with mean value and standard deviation generated with GraphPad Prism 8.0 (GraphPad, San Diego, CA, USA).

For the semi-automated centrioles counts the number of samples/cells (n), total sum of centrioles, mean (M), the standard deviation (SD) and the *p* value of unpaired two-tailed t-test were calculated with GraphPad Prism 8.0 (GraphPad, San Diego, CA, USA). Mode and effect size were calculated with Microsoft Excel (Version 2109). Graphical summary of the *p* value are shown on the dot plots. Statistical significance is represented as number of asterisks (none or 1 to 4). For *p* values > 0.05 no statistical significance is shown on the dot plots, for *p* values ≤ 0.05 one asterisks is shown, for *p* values ≤ 0.01 two asterisks are shown, for *p* values ≤ 0.001 three asterisks are shown and for *p* values ≤ 0.0001 four asterisks, showing highest statistical significance.

Effect size (Lakens, 2013) was calculated by subtracting the mean value of the control group (manually counted centrioles) and each individual experimental group (semi-automatically counted centrioles with Model I or with Model II). The mean difference was divided by the pooled Standard Deviation in order to obtain the Cohen's *d* effect size in standard deviations as shown in the following equation:

$$|d| = \frac{M_A - M_B}{SD\ pooled}$$

where *d* is the Cohen's *d* effect size, M_A is the mean of the control group and M_B is the mean of the experimental group. SD *pooled* is the pooled standard deviation defined as:

$$SD\ pooled = \sqrt{\frac{(n_1 - 1) \times SD_1^2 + (n_2 - 1) \times SD_2^2}{n_1 + n_2 - 2}}$$

where n_1 is the number of samples of the control group, SD_1 is the standard deviation of the control group, while n_2 is the number of samples of the experimental group and SD_2 is the standard deviation of the experimental group. Effect size below 0.2 standard deviations is considered low, effect size between 0.2 and 0.8 is considered as medium and effect size above 0.8 is considered as large.

RESULTS

Could VDVADase fluorimetric assays be exploited to detect Caspase-2-PIDDosome activity?

Based on numerous peptide screening studies using mainly recombinant Caspase-2 the preferred cleavage substrate for Caspase-2 is reported to be the peptide sequence VDVAD, which is used for commercially available fluorescently labeled substrates for Caspase-2 activity detection like the Ac-VDVAD-AFC. I decided to test these substrates and try to use them for the detection of the Caspase-2 activation within the PIDDosome. As a comparison I selected Caspase-3, an executioner apoptotic caspase, whose reported substrate from peptide screening studies is DEVD (Agard et al., 2012; Thornberry et al., 1997), commercially available as Ac-DEVD-AFC. In order to activate Caspase-2 and Caspase-3 I selected specific drugs and drug combinations.

Cells were treated with ZM447439 in order to provoke cytokinesis failure and PIDDosome activation. A combination of simultaneous use of Staurosporine (STS) and WEHI-539 was necessary to provoke apoptosis in two cell lines used for this study: lung adenocarcinoma A549 (tumor-like cells) and in the commonly used non-transformed retinal cells of the pigmented epithelium (RPE1). STS on its own, despite causing morphological changes and affecting the shape of the cells (Fig. 7 A and B) didn't result in PARP1 cleavage (a common marker for apoptosis and immunoblot-detectable result of successful apoptosis) in A549, neither in RPE1. WEHI-539 on its own did not result in the typical for apoptosis cell morphology, neither resulted in PARP1 cleavage (Fig. 7 C and D). The simultaneous use of STS and WEHI-539 resulted in apoptosis-related cell morphology - cell shrinkage, rounding and detachment with results consistent for both cell lines (Fig. 7 A and B). Moreover, only in the condition when both drugs were used was PARP1 cleavage observed (Fig. 7 C and D). In the apoptotic cells reduced levels of Caspase-2 (full length) is observable (Fig. 7 C and D, Caspase-2 immunoblot). Cells treated with ZM447439 show cleavage of MDM2 as consequence of the cytokinesis failure, which leads to accumulation of supernumerary centrosomes and the PIDDosome activation. As expected MDM2 cleavage is

observed only in the parental cells treated with ZM447439 and no cleavage is observable in the *Caspase-2*$^{-/-}$ (Caspase-2 KO) cells for both cell lines (Fig. 7 C and D).

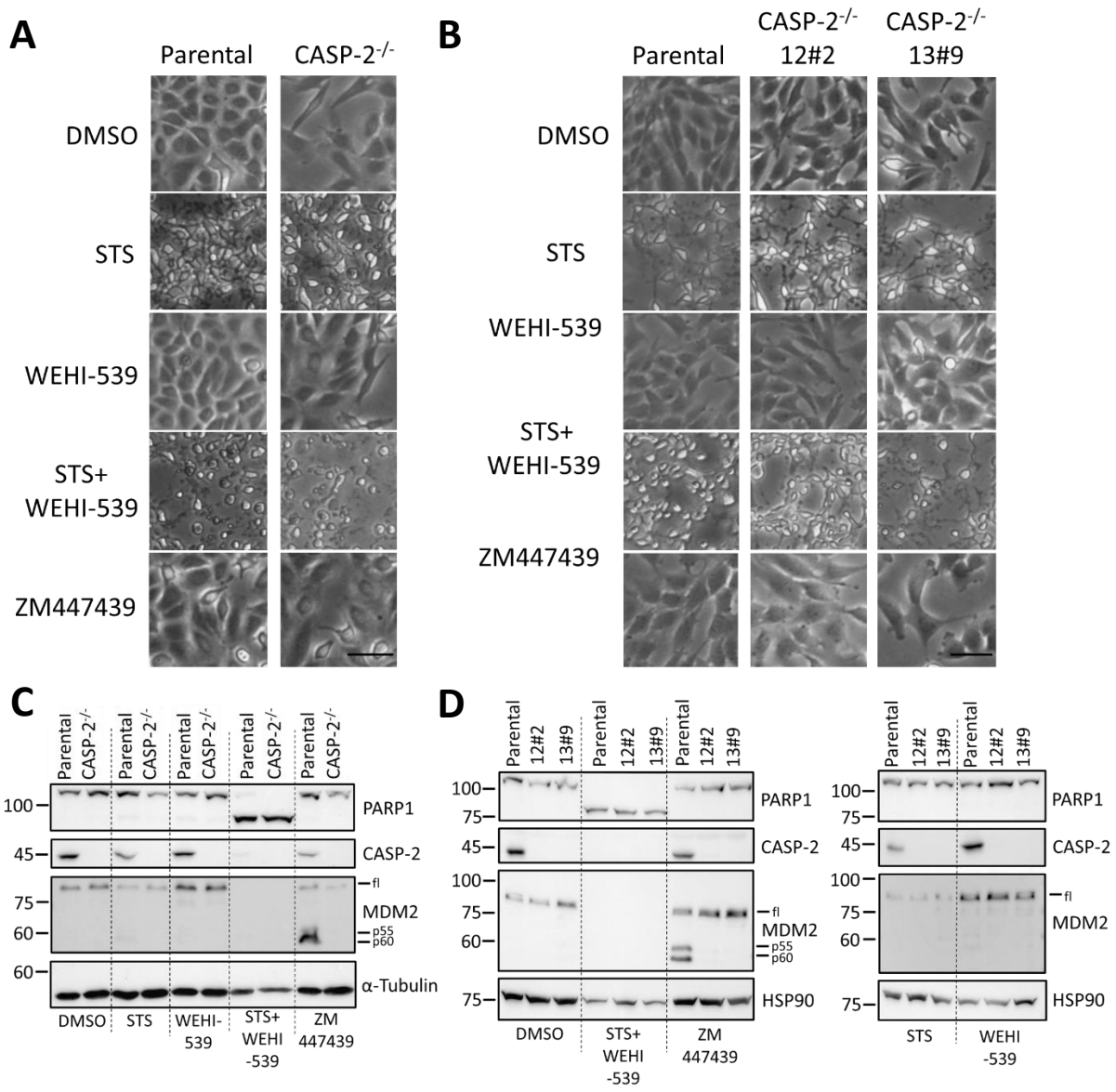

Figure 7. Assessment of drug-induced cytokinesis failure and apoptosis in A549 and RPE1.

(A) Differences in the cell morphology upon drug treatments are shown on bright field microscopy images of A549. Two genotypes of cells were used: wild type (parental) and *Caspase-2*$^{-/-}$. Control (DMSO) cells and WEHI-539 treated cells show no visible differences in the cell morphology. Cells treated with STS and the combination of STS and WEHI-539 show cell shrinkage. Cells treated with ZM appear doubled due to lack of physical separation after mitosis. Scale bar corresponds to 100 µm. **(B)** Bright field microscopy images of RPE1

cells show similar morphological changes as for A549. Two *Caspase-2*$^{-/-}$ clones – 12#2 and 13#9 were used in this experiment. Scale bar corresponds to 100 μm. **(C)** Immunoblot of A549 cells. Effect of drugs was controlled with Western Blot for parental and *Caspase-2*$^{-/-}$ cells. DMSO are used as control cells. Pro-Caspase-2 immunoblot confirms the lack of expression of Caspase-2 in the KO clone. Cleavage of PARP is indicative for apoptosis induction and is noticeable only in cells treated simultaneously with STS and WEHI-539. STS or WEHI-539 are not able to induce apoptosis in A549 cells. Upon ZM447439 treatment cleavage of MDM2 is observed only in the parental cell line. No such cleavage is visible for the *Caspase-2*$^{-/-}$ cells. **(D)** Immunoblot of RPE1 cells. Results are consistent with the ones for A549. (Left blot) DMSO are control cells. Pro-Caspase-2 immunoblot confirms the lack of expression of Caspase-2 in the KO clones (12#2 and 13#9). Cleavage of PARP1 is observed only in cells treated simultaneously with STS and WEHI-539. Upon ZM447439 treatment cleavage of MDM2 (p55/p60) is observed only in the parental cell line and no cleavage of MDM2 is visible in any of the *Caspase-2*$^{-/-}$ clones. (Right blot) STS or WEHI-539 are not able to induce apoptosis in RPE1 cells and no PARP1 cleavage is observed.

Cells were pelleted and subjected to the Fluorimetric Activity Assays. After incubation with the fluorescently labeled substrates the difference in the fluorescence between controls (DMSO) and treated cells was compared (Fig. 8A). As expected, the results for DEVDase activity (Caspase-3 activation fluorimetric assay) were confirmed with higher levels of fluorescence in the STS+WEHI-539 treated cells, where apoptosis was provoked. Control cells and cells treated with ZM447439 didn't show any significant fluorescence increase for each genotype (wild type and *Caspase-2*$^{-/-}$) in both cell lines (Fig. 8B). The VDVADase activity assay was supposed to show the activation of Caspase-2, based on previous studies. To our surprise, AFC (from cleaved VDVAD-AFC) fluorescent signal was not detected in parental cells treated with ZM447439. However, as expected increase in fluorescence was not detected in the Caspase-2 KO cells. Interestingly, a significantly strong VDVADase signal was detected in STS+WEHI-539 treated cells. Furthermore, this signal was not reduced in cells which lack Caspase-2. We confirmed this result in both tested cell lines (Fig. 8C). These results demonstrate that VDVAD is not the preferred cleavage site for Caspase-2 activated by the PIDDosome and that the PIDDosome-activated Caspase-2 does not elicit any measurable VDVADase activity. Thus, VDVAD-AFC is not a reliable fluorogenic reporter for the PIDDosome-activated Caspase-2.

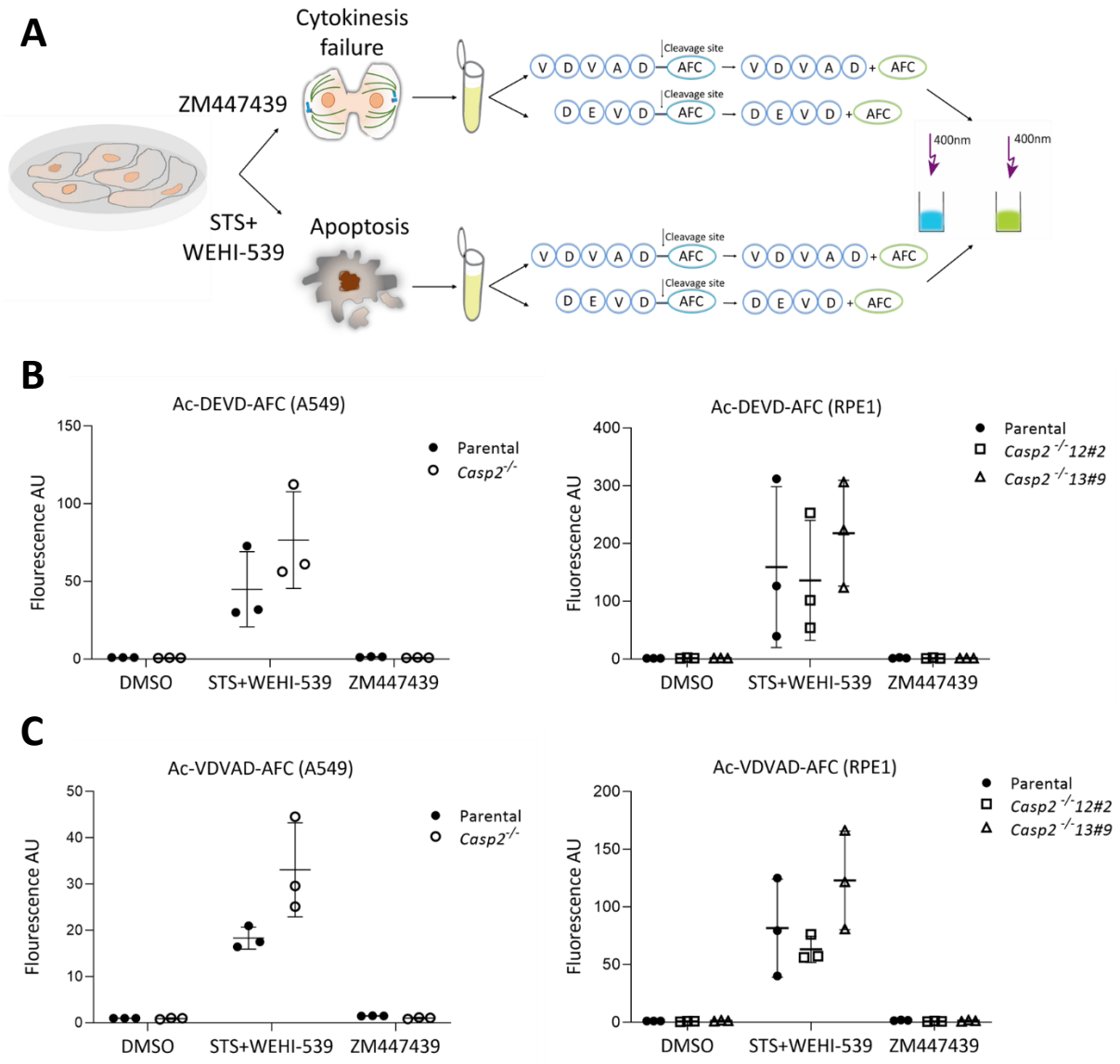

Figure 8. VDVAD is not the preferred cleavage site for Caspase-2 activated by the PIDDosome.

(A) Experimental layout scheme. Cells from two cell lines: A549 and RPE1 were used for this experiment. From each cell line two genotypes were used: wild type (parental) and *Caspase-2*$^{-/-}$. For RPE1 *Caspase-2*$^{-/-}$ two clones were used: 12#2 and 13#9. All cells were treated with ZM447439 for 24 h in order to cause cytokinesis failure. Cells were treated with STS, WEHI-539 and simultaneously with STS and WEHI-539 for 4-7 hours in order to induce apoptosis. DMSO treated cells were used as a control. Cell lysates were incubated with VDVAD or DEVD substrates labeled with fluorescent molecule - AFC. Upon caspases activation the cleaved AFC emits yellow-green fluorescence with λmax=505nm. After incubation the fluorescent signal of the control and treated with drugs cells was quantified in fluorescence plate reader with excitation light λ=400nm. Differences between the fluorescent emitted signal of control and treated cells was compared. **(B)** Fluorimetric Activity Assay results

for Caspase-3 for: A549 (left) and RPE1 (right). Control cells (DMSO), apoptotic cells (STS+WEHI-539) and cells with cytokinesis failure (ZM447439) were tested for DEVDase activity by measuring the difference in the signal between the different conditions. No signal was detected for the DMSO and ZM447439 treated cells. Significant signal was observed in STS+WEHI-539 treated cells for both genotypes of each cell line. Note the y axis scale differs between plots. Fluorescence signal intensity is shown in arbitrary units (AU); n = 3 independent experiments. **(C)** Fluorimetric Activity Assay results for Caspase-2 for A549 (left) and RPE1 (right). Control cells (DMSO), apoptotic cells (STS+WEHI-539) and cells with cytokinesis failure (ZM447439) were tested for VDVADase activity by measuring the difference in the signal between the different conditions. No signal was detected for the DMSO and ZM447439 treated cells. Significant signal though was observed in STS+WEHI-539 treated cells for both genotypes of each cell line. The presence of high signal of cleaved VDVAD-AFC in the *Caspase-2*$^{-/-}$ cells demonstrates that VDVAD is not a specific for PIDDosome-activated Caspase-2. Note the y axis scale differs between blots. Fluorescence signal intensity is shown in arbitrary units (AU); n = 3 independent experiments.

Does Caspase-2 display different substrate specificity depending on its mode of activation?

Since VDVAD-base activity assay failed to detect PIDDosome activation we decided to test if Caspase-2 displays different substrate specificity depending on its mode of activation. We hypothesized that fully activated and mature Caspase-2 heterotetramer cleaves the Ac-VDVAD-AFC substrate but not the PIDDosome activated Caspase-2 and that the PIDDosome-activated Caspase-2 cleaves MDM2.

In order to test our hypothesis, I performed a Caspase-2 rescue experiment - the complementation of cells genetically manipulated to lack the expression of the protein of interest via the exogenous expression of protein variants. So far, no successful rescue attempt for Caspase-2 was reported in the literature. Since the Caspase-2 precursor is known to undergo cleavage at D169, D333 and D347 in order to become a fully processed enzyme (Butt et al., 1998) I generated an uncleavable Caspase-2 triple mutant which does not allow the autoproteolytic cleavage and release from the PIDDosome. This mutant (CASP-2TriA) carries three point mutations on the key residues necessary for the auto proteolytic cleavage of Caspase-2: D169A, D333A, D347A (Fig. 9C). To perform the rescue experiment, I aimed to use lentiviral-mediated protocol which requires HEK293T cells transfection, necessary for the production of viral particles used in transduction of Caspase-2 KO cells (Fig. 9A).

HEK293T cells were transfected with lentiviral constructs carrying a wild type (wt) Caspase-2 labeled with an epitope tag V5 at the C-terminus (wtCASP-2-V5). At this step, however, the transfected with the wtCASP-2-V5 carrying construct HEK293T cells showed apoptotic morphology like shrinkage and detachment (Fig. 9B). Moreover, the viral titer was too low to proceed with the next steps of the protocol. In order to overcome this obstacle, we decided to inhibit the wt Caspase-2 during the transfection process. Our experience with Z-VDVAD-FMK, a known Caspase-2 inhibitor, lacks efficacy in inhibiting the caspase in any of our experimental assays consistently with our previous data demonstrating lack of selectivity for Caspase-2 of the VDVAD substrate. Another recently reported selective for Caspase-2 inhibitor - NH-23-C2 (Poreba et al., 2019) also failed to inhibit the wt Caspase-2 (data not shown). Since the chemical and small peptide inhibitors for the Caspase-2 did not show sufficient effect for the wt Caspase-2 inhibition, thus not allowing the production of the viral particles, I searched the literature for alternative means of inhibiting Caspase-2. Interestingly, an artificial protein ankyrin repeat protein AR_F8 was reported to allosterically inhibit Caspase-2 (Schweizer et al., 2007): Thus, we cloned it in a suitable mammalian expression vector and used it in conjunction with the lentiviral plasmid carrying the wtCASP-2-V5 and the packaging plasmids for cotransfection of the HEK293T (Fig. 9A). This successfully allowed the viral particles production and the successful transduction of Caspase-2 KO cells, thus the Caspase-2 rescue. Cells were treated with ZM447439 to trigger cytokinesis failure and activate the Caspase-2 in a PIDDosome-dependent manner. MDM2 cleavage was used as a read-out for the functional activation of the Caspase-2. The results show that the cells transduced with the wtCASP-2-V5 carrying construct recovered functional activity as shown in Fig. 9 D and E, comparable with the treated parental cells. Moreover, the exogenous Caspase-2 could be activated by the PIDDosome way. However, the outcome from the cells transduced with CASP-2TriA show no cleavage of MDM2 and thus lack of functional recovery for the triple mutant. The experiment was performed in two cell lines-A549 and RPE1, for both of which the results are consistent (Fig. 9 D and E). Results show that contrary to our hypothesis non-autoproteolytically cleavable Caspase-2 activated within the PIDDosome cannot cleave MDM2.

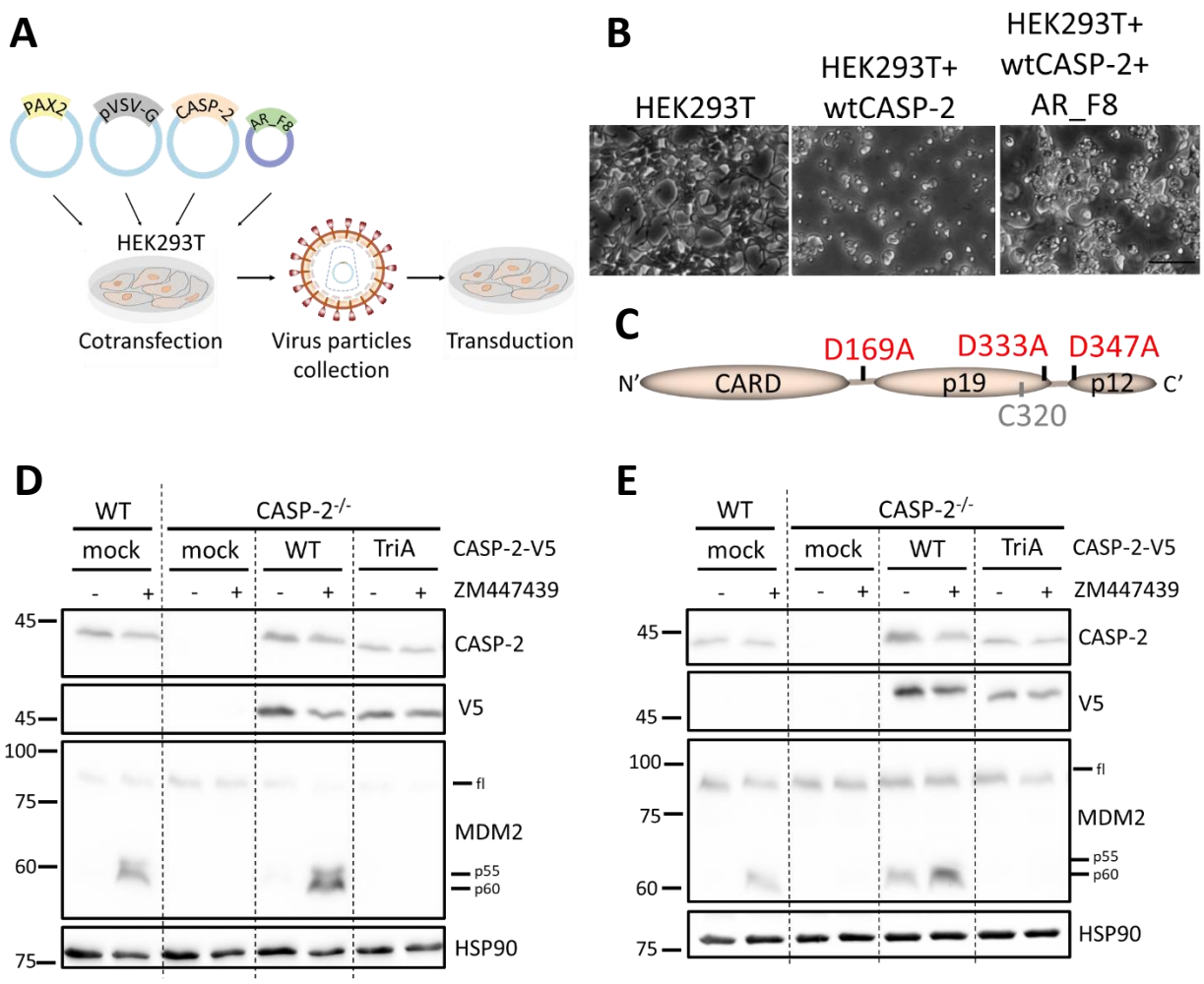

Figure 9. Non-autoproteolytically cleavable exogenous Caspase-2 activated within the PIDDosome cannot cleave MDM2.

(A) Experimental layout scheme. HEK293T cells were cotransfected with packaging (PAX2), envelope (pVSV-G), transfer vector CMVmin-TetO carrying exogenous wt Caspase-2 labeled with V5-tag or Caspase-2 triple mutant (D169/333/347A) labeled with V5-tag and pcDNA5/FRT/TO vector carrying AR_F8 (designed ankyrin repeat protein inhibitor of Caspase-2). Viral particles were collected, tittered and used for transduction of A549 or RPE1 cells. **(B)** Bright field images show the effect of OE of exogenous wt Caspase-2 labeled with V5-tag in HEK293T after transfection. Left image shows control, untransfected HEK293T cells with regular morphology. Middle image show shrunken apoptotic HEK293T cells 48 h after transfection with wtCASP-2-V5 carrying viral vector. Right image shows the cotransfection of designed ankyrin repeat protein inhibitor of Caspase-2 (AR_F8) and wtCASP-2-V5 carrying viral vector. Scale bar corresponds to 100 µm. **(C)** Caspase-2 triple mutant. Scheme indicating the triple mutant of Caspase-2 carrying three point mutations of aspartate residues: 169, 333 and 347 to alanine. **(D)** Immunoblot of A549 cells. Two genotypes of each cell lines were

used - parental (as a control) and *Caspase-2*$^{-/-}$. Cells were treated with ZM447439 for 24 hours in order to cause cytokinesis failure and activate the PIDDosome, which resulted in Caspase-2 activation leading to MDM2 cleavage visible as p55/p60 cleavage product. Treated and untreated cells were compared. Western Blot confirms the pro-Caspase-2 presence and the cleavage of MDM2 in parental cells. *Caspase-2*$^{-/-}$ cells lack Caspase-2 expression and cleavage of MDM2 upon drug-induced cytokinesis failure. *Caspase-2*$^{-/-}$ cells transduced with wtCASP-2-V5 carrying viral particles (Caspase-2 rescue) show exogenous Caspase-2 and V5-tag expression. Upon treatment with ZM447439 MDM2 cleavage is observed. *Caspase-2*$^{-/-}$ cells transduced with CASP-2TriA-V5 mutant carrying viral particles also show exogenous expression of Caspase-2 and V5-tag but no MDM2 cleavage is observed upon ZM447439 treatment. Experiment was repeated in three biological replicates. **(E)** Immunoblot of RPE1 cells. Experimental conditions and results are consistent with the ones for A549. Only cells carrying endogenous or exogenous wt Caspase-2 show cleavage of MDM2 upon treatment with ZM447439. Experiment was repeated in three biological replicates.

Can the newly established Caspase-2 rescue be exploited to perform structural/functional analyses?

Caspase-2 has a unique, among the other caspases, nuclear localization (Belinda C Baliga et al., 2003; Colussi et al., 1998). The Caspase-2 nuclear localization has also been detected by our laboratory using Caspase-2-V5 knock-in cells generated via CRISPR/Cas9 (Ghetti et al., 2021). The strong nuclear Caspase-2-V5 signal in untreated cells disappears upon PIDDosome activation (DNCB or ZM treatment), as shown in Fig. 10 A and B (IF images, courtesy of Matteo Burigotto). Importantly, the Caspase-2 activation most likely occurs in the cytoplasm near the centrosomes (Burigotto et al., 2021). Nuclear export pathways use nuclear export signal (NES) motifs to direct cargoes to the nucleus (Lee et al., 2019; Rhee et al., 2000; D. Xu et al., 2012). The active transportation is mediated via Exportin 1 (Lee et al., 2019; Ullman et al., 1997). Depletion of a non-canonical Exportin results into PIDDosome loss of function (Andreas Villunger, personal communication). This suggests that transportation of the Caspase-2 from the nucleus to the cytoplasm might be required for its activation via the PIDDosome. Interestingly, Caspase-2 carries non-canonical nuclear export sequence that has not been explored and which we identified (LPPL) based on previous studies (Rhee et al., 2000). Comparison of the non-canonical Caspase-2 NES (^{127}HVLPPLSCDYD^{137}) with an example of leucin rich canonical NES sequence, the one of the Rev protein (^{73}LQLPPLERLTL^{83}) (D. Xu et al., 2012) is shown on Fig. 10D.

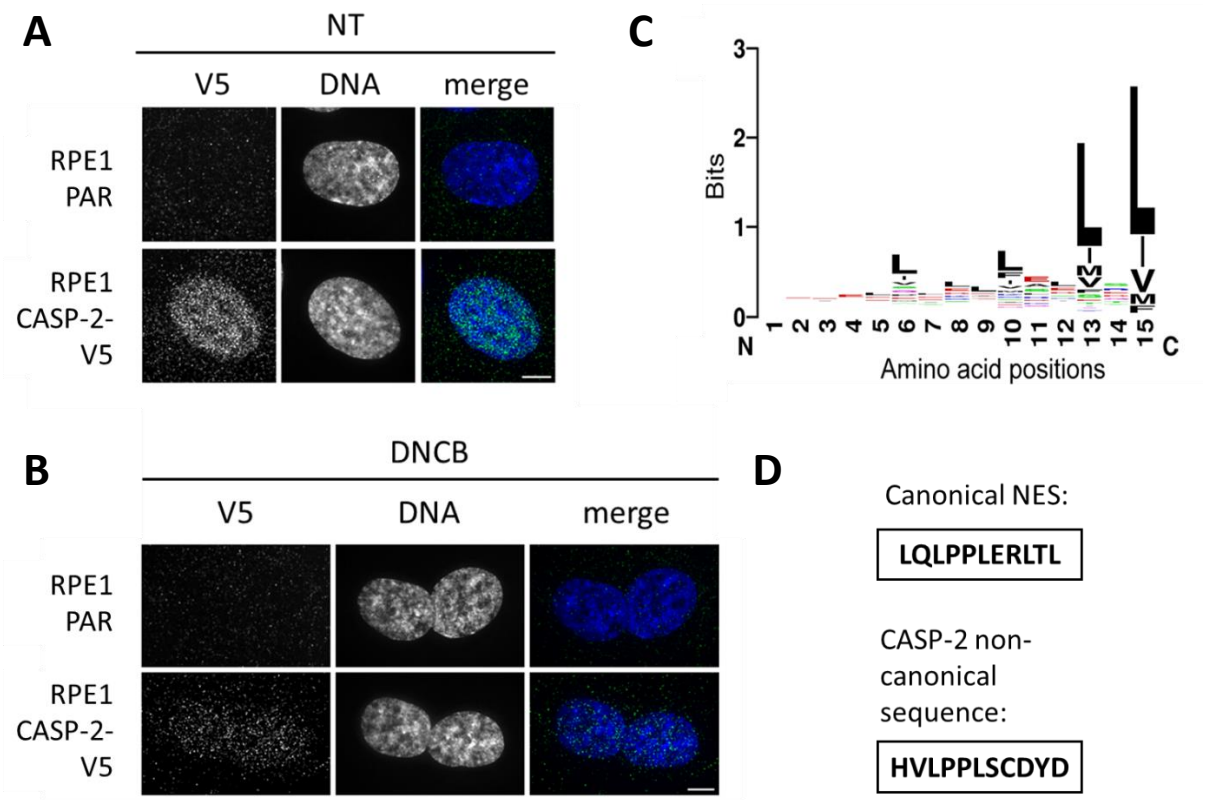

Figure 10. Caspase-2 nuclear localization and NES sequences

(A) Immunofluorescence images from parental PRE1 and Caspase-2-V5 knock-in RPE1 cells, DAPI staining (DNA) and merged demonstrate the Caspase-2 localization. Scale bar corresponds to 5μm. **(B)** Immunofluorescence images from parental PRE1 and Caspase-2-V5 knock-in RPE1 cells, DAPI staining (DNA) and merged demonstrate that upon PIDDosome activation (treatment with DNCB) the nuclear Caspase-2 signal disappears. Scale bar corresponds to 5μm. **(C)** Sequence logo of experimental Nuclear Export Signal (NES)s in NESdb, knowns as leucin-rich NES. Adapted from (D. Xu et al., 2012). **(D)** Comparison of Rev protein canonical NES and Caspase-2's non-canonical NES sequence.

In order to test this hypothesis, I introduced L132D mutation and generated the CASP-2L132D-V5 mutant, affecting the non-canonical nuclear export sequence aiming to to address the capability of CASP-2L132D-V5 and CASP-2L132D-TriA-V5 to be excluded from the nucleus upon cytokinesis failure. A549 and RPE1 cells expressing the CASP-2-L132D-V5 exogenous mutant demonstrate Caspase-2 activation within the PIDDosome, shown by the MDM2 cleavage (Fig. 11). Interestingly, an elevated MDM2 cleavage is

observed in RPE1 cells with the L132D mutation, even without treatment. However, upon PIDDosome activation induced by ZM447439 treatment MDM2 cleavage is observed in both cell lines, indicating that the PIDDosome activation was not perturbed by the L132D mutation. The uncleavable mutant with mutated nuclear export sequence (CASP-2L132D-TriA-V5) was not able to show any functional rescue neither in A549 nor in RPE1 (Fig. 11).

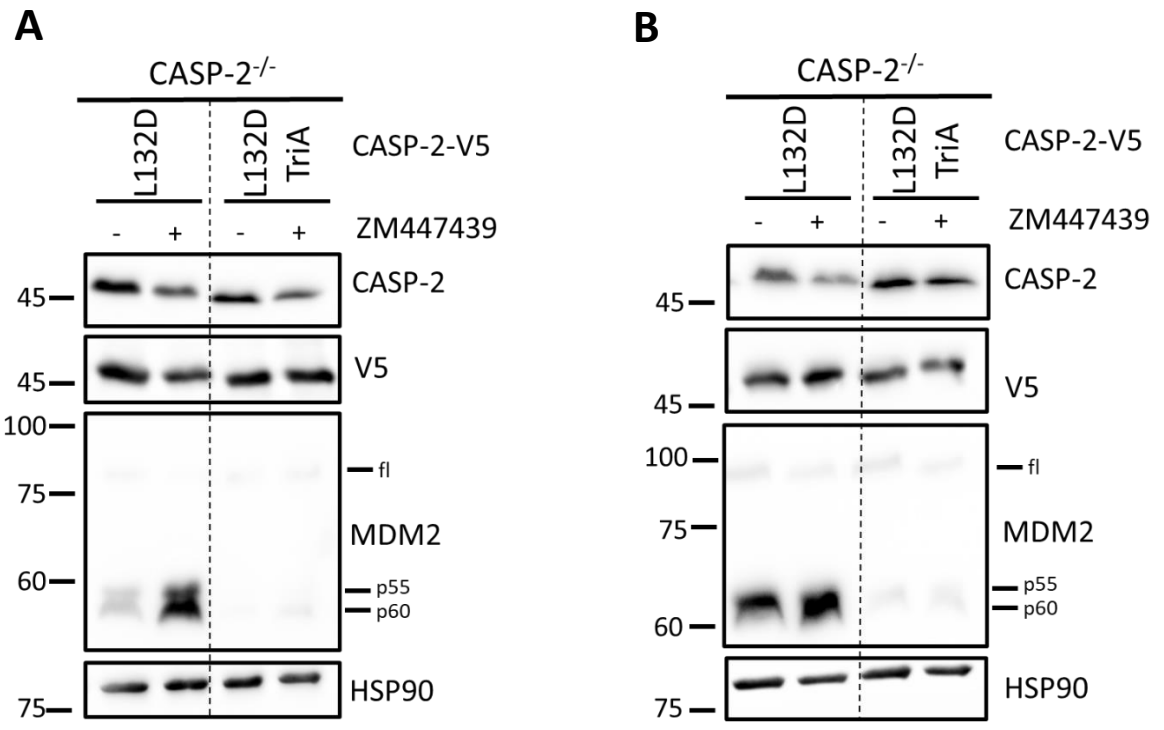

Figure 11. Caspase-2 non-canonical NES mutant upon PIDDosome activation.

(A) Immunoblot of A549 cells. Exogenous expression of CASP-2L132D-V5 mutant and CASP-2L132D-TriA-V5 mutant in *Caspase-2*$^{-/-}$ cells show that MDM2 cleavage (p55/p60) upon ZM447439 treatment is possible only in the autoproteolytically processed CASP-2L132D-V5 mutant independently of the non-canonical NES mutation L132D. Experiments were performed in two biological replicates. **(B)** Immunoblot of RPE1 cells. Results are consistent with the ones for A549. Experiments were performed in two biological replicates.

Development of a semi-automated centriole counting pipeline

Given the fact that supernumerary centrosomes are frequently found in human tumors (Erich A Nigg & Holland, 2018) as well as in preneoplastic lesions (Chan, 2011), our laboratory set out to study the consequences of an aberrant number of centrosomes in non-transformed cells. To this end, our laboratory engineered hTERT-RPE1 cells to inducibly overexpress the master centriole biogenesis regulator PLK4, which results in accumulation of procentrioles in the first S-phase that cells traverse after doxycycline (DXC) addition. Moreover, those centrioles mature to MTOC competent centrioles and in fully mature mother centrioles, carrying distal and subdistal appendages, during the two subsequent cell divisions. While in normal cells supernumerary mature centrosomes cause PIDDosome activation followed by MDM2 cleavage and p53-dependent cell cycle arrest (Fava et al., 2017), tumor cells often carry p53 inactivating mutations. To tackle the contribution of the PIDDosome-p53 signaling axis upon occurrence of supernumerary centrosomes, the laboratory has generated isogenic hTERT-RPE1 derivatives bearing inducible PLK4 OE that lack the capability of activating this pathway either by inactivating p53 itself or distal appendage proteins critical for PIDDosome activation, namely SCLT1 and ANKRD26 (Burigotto et al., 2021) via the CRISPR/Cas9 system.

We used DXC-inducible PLK4 OE in cells as a way to provoke supernumerary centrosomes and follow the quantitative changes of centrioles. Cells were treated with DXC and subjected to immunostaining and microscopy imaging at several time points after the induction of PLK4 OE (Fig. 12 A and B). Centrioles of minimum 50 cells per condition were quantified (see Tables 8-10). The generated images taken from all clones and treatment conditions lead to the accumulation of a large amount of image data. In this collaborative effort involving several members of the laboratory, my contribution has been to assess the abundance of centrioles at different times after PLK4 OE and across several genotypes (i.e. wt, p53 KO, SCLT1 KO and ANKRD26 KO). However, visual scoring of centriole abundance is laborious and biased, due to subjective estimation of the number of centrioles. Furthermore, it is a very time-consuming approach which often requires manual changing of channels and adjustment of the brightness and contrast for each image. Thus, I decided to

analyze this data and quantify the centrioles in an automated fashion to reduce bias and increase the speed of analysis.

The automated approach needs to distinguish between the signal of the individual centriole and the surrounding background or other nearby centrioles (thereafter called centriole segmentation). In addition, it would need to distinguish the cell's contours or cell "body" (thereafter called cell body segmentation) so the quantification of centrioles can be done for each individual cell. In order to generate the binary masks for the centrioles I initially used Fiji (an open source tool for image analysis). The built-in in function of Fiji - Find Maxima (which determines the local maxima in an image and creates a binary mask) used on the Maximum intensity projection from the Z stack of a single channel would have been a simple way to quantify the centrioles. However, it required manual adjustment of the prominence (image parameter analog to topographic prominence in Fiji) necessary to detect the centrioles for each single image and lacked accuracy since it wasn't able to distinguish between individual centrioles within a centriole cluster where the Maximum intensity signals of individual centrioles overlap (Fig. 12C). In addition, it was not able to distinguish between centrioles and more prominent background signal. Moreover, the additional step of manual prominence adjustment significantly slowed down the process. The thresholding function of Fiji performed relatively well but due to the necessity of manual adjustment of the minimal and maximal threshold values for each image this approach would have slowed down the processing significantly. This led to the necessity to look for a more advanced tool for segmentation.

AI-based tools can better distinguish single centrioles even when they are in a very close proximity and their signal overlaps. A recently published easy-to-use deep learning segmentation tool – MitoS and its model MitoSegNet (Fischer et al., 2020) was tested for the segmentation of centrioles. Preliminary results showed that the AI-based tool outperform the segmentations generated with Fiji's Find Maxima and other tested segmentation approaches (Fig. 12C). Thus, I continued using the MitoS to generate the centrioles binary masks necessary for the counting. To improve the MitoS's performance I finetuned the original (MitoSegNet) model, see below. The dice coefficient (overlap index) is a statistical validation metric used as quantitative indication for a model's precision. It measures the overlapping area between the ground truth and the predictions divided by the total number of pixels so

the closer to 1 its value is the more similar to the ground truth the predictions are (Fischer et al., 2020; Taha & Hanbury, 2015; Zou et al., 2004). Model I for Centrin and for γ-Tubulin/ANKRD26 have a dice coefficient 0.68. These models are thereafter called Model I-Centrin and Model I-γ-Tubulin/ANKRD26. For the finetuning of Model I-Centrin 3 hand-labeled ground truth images were used, while for the finetuning of Model I-γ-Tubulin/ANKRD26 4 ground truth images from each antibody were used. Similarly, I also generated second models finetuning the original model for each antibody staining with larger number of ground truth images (24 for Centrin, 36 for γ-Tubulin and 92 for ANKRD26). The dice coefficient for Model II-Centrin is 0.54, for Model II-γ-Tubulin it is 0.59 and Model II-ANKRD26 has a dice coefficient 0.51. In addition, I created a Fiji macro script to prepare the files for the centriole binary mask generation. The macro processes the listed files in a user-selected directory. It runs the built-in functions of Fiji to extract the Maximum intensity Z-projection, sets the digital colors for each channel as desired, creates a 2D composite and generates 8-bit files, which are necessary for the MitoS processing.

Since the images contained only DAPI and the centriole antibody, but no cytoplasm marker I decided to manually generate the cell body binary masks in a semi-automated (SA) way using Fiji and a macro script to speed up the process. The Fiji macro is designed to assist the user in the file generation by automatically opening the file list in a selected directory. It activates Fiji's freehand tool, waits for the user to draw the region of interest (the only manual process) and creates an 8-bit inverted image (Fig. 12E). In this way I was able to visually control each image and avoid selecting mitotic cells or cells at the edges of the image, which were excluded from the analysis. I used the antibody background signal as orientation to detect the cell body edges or selected only the region of accumulated centrioles.

In order to generate the centrioles masks, few images needed to undergo pre-processing prior to the MitoS segmentation. This required to manually adjust the brightness/contrast (images counted with Models I) or to apply the Unsharp Masking filter (which uses Difference-of-Gaussian algorithm) to sharpen the images as shown in Fig. 12C. 31 images of 361 (less than 10%) were processed with the Unsharp Mask for the counts with Model II-Centrin. 28 images (of 373) had to be manually processed and masks were generated with the Thresholding Fiji function after manually removing any bleached regions of the image due to precipitations, which created regions of strong fluorescence signal. These

masks were then included in the Model II-ANKRD26 results. The predicted binary masks were then processed with the built-in classic Watershed Fiji function (uses flooding simulations described by (Soille & Vincent, 1990)) which improved the final results from Model I (Centrin and γ-Tubulin/ANRD26) and manually generated masks through thresholding but were not used for post-processing of Model II's (Centrin, γ-Tubulin and ANKRD26) predictions in order to avoid over-segmentation. Both masks - centriole and cell body were overlayed with the Speckle Inspector (Brocher, 2015) which returns a list of the counts of centrioles per cell. Schematic summary of the pipeline with each step is shown in Fig. 12D.

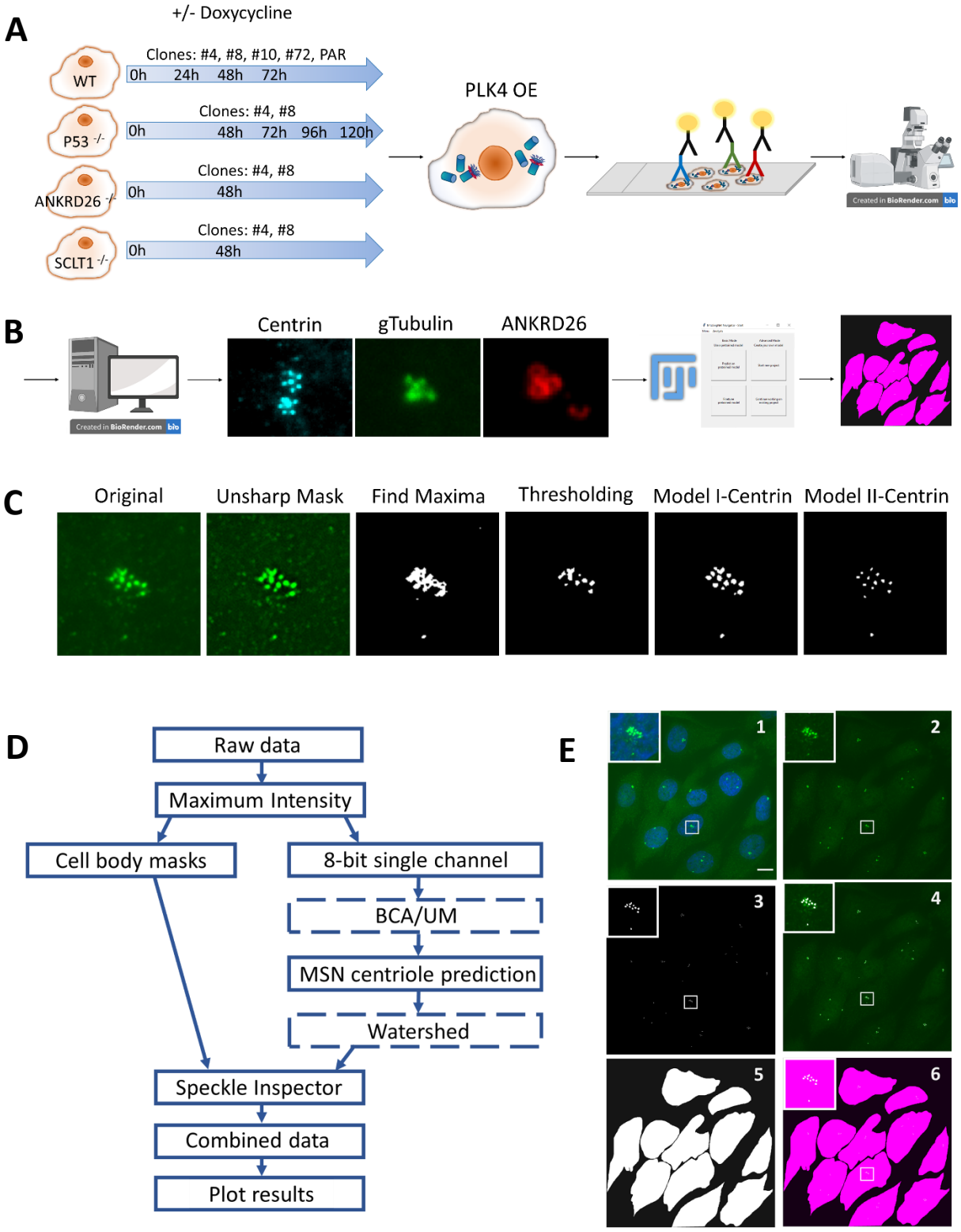
A
+/- Doxycycline
WT
Clones: #4, #8, #10, #72, PAR
0h 24h 48h 72h
P53 -/-
Clones: #4, #8
0h 48h 72h 96h 120h
ANKRD26 -/-
Clones: #4, #8
0h 48h
SCLT1 -/-
Clones: #4, #8
0h 48h
PLK4 OE
Created in BioRender.com
B
Centrin
gTubulin
ANKRD26
Created in BioRender.com
C
Original
Unsharp Mask
Find Maxima
Thresholding
Model I-Centrin
Model II-Centrin
D
Raw data
Maximum Intensity
Cell body masks
8-bit single channel
BCA/UM
MSN centriole prediction
Watershed
Speckle Inspector
Combined data
Plot results
E
1
2
3
4
5
6

Figure 12. Semi-automated pipeline for centrioles counting.

(A) Supernumerary centrosomes accumulation upon PLK4 OE. Experimental layout scheme. Four genotypes of RPE1 DXC-inducible PLK4-overexpressing cells were used: wild type, $p53^{-/-}$, $SCLT1^{-/-}$ and $ANKRD26^{-/-}$. Parental cells and several clones (indicated on the scheme) of each genotype were selected and treated with DXC for 0, 24, 48, 72, 96 or 120 hours. Upon treatment PLK4 OE resulted in accumulation of supernumerary centrosomes. Immunofluorescence microscopy-based approach was used to visualize the centrioles. Cells were stained with three different primary antibodies against: Centrin, γ-Tubulin and ANKRD26, followed by secondary antibody (with attached fluorophore - yellow circle on the scheme) staining for immunofluorescence imaging with a confocal microscope. **(B)** Example selections for the morphology of the three protein markers used are shown. Microscope images were processed with the SA pipeline in Fiji and the finetuned MitoSegNet (MSN) models and centrioles per cell were counted. **(C)** Comparison of different centrioles segmentations tools. From left to right: example from original image for Centrin positive centrioles; Unsharp Mask filter (radius 3px, mask weight 0.6); binary mask generated from Fiji's Find Maxima (prominence 150); binary mask from manual Thresholding; prediction with Model I-Centrin; prediction with Model II-Centrin. **(D)** Scheme of the steps for the SA pipeline counting. All image processing steps are performed with Fiji except the MitoS-based centrioles binary masks generation. An ImageJ Macro script is used to extract the Maximum intensity Z-projection of each image from the raw data file. The images are then used to manually generate the cell body binary masks or to create the 8-bit single channels necessary for the centriole prediction with the finetuned MSN models. If necessary (dashed line), brightness and contrast adjustments (BCA) or Unsharp Mask (UM) filter is applied to the image manually. The MSN generates the centriole binary masks. Fiji's Watershed function can then be applied to the binary masks of the centriole prediction if necessary. Using the Speckle inspector, the cell body mask and the centriole mask are overlayed and the counted centrioles per cell data is organized and plotted. **(E)** Example for each step of the image processing pipeline. 1 - Maximum intensity projection composite image for Centrin (green) and DAPI (blue) staining. 2 - Single channel for Centrin. 3 - Centrioles prediction mask generated with the finetuned MitoSegNet models. 4 - Overlay image of the Centrin single channel and Centriole prediction. 5 - Cell body mask generated manually. 6 - Speckle inspector overlay of the cell body mask and the centriole prediction mask. Selected regions with 4x zoom in digital magnification are shown at the top left corner of each image. Scale bar corresponds to 10µm.

To assess the exploitability of this pipeline, I focused on the comparison between visual scoring of centrioles performed manually and the results obtained with Models I (Centrin, γ-Tubulin/ANKRD26) or Models II (Centrin, γ-Tubulin, ANKRD26). The models need to be able to predict centrioles in parental and untreated cells representing physiological conditions so as in the independent RPE1 clones engineered to inducibly overexpress PLK4, used in this study. Results comparing the manually counted centrioles and SA counts

generated with Model I or Model II (for each antibody staining) for several DXC-dependent PLK4-overexpressing clones are shown on Fig. 13-15.

Since initial results for both models showed relatively similar data distribution (shown as dot plots), I performed a statistical analysis for the results from each antibody staining, genotype and treatment condition (Tables 8-10) in order to quantitatively estimate which of the two models performs better compared to the manual counting. I included the total number of cells per condition demonstrating that a minimum of 60 cells per condition were analyzed. A sum of the total centrioles of all cells per condition was included as a quick overview of the model's performance and it shows if the model overall overestimates or underestimates the number of centrioles. Similarly, a relative estimation of the model's performance could be taken from the mean and the standard deviations which are graphically represented in the dot plots. The mode value shows the most commonly appearing value in a data set. Thus, it demonstrates similarity or difference between the manual counts and the SA counts but it also shows how many centrioles per cell are most commonly found for each of the treatment conditions and genotypes. Additionally, a comparative evaluation between the manual counts and the SA counts of each model was done with an unpaired two-tailed t-test. The exact *p* values are given in tables 8-10, while a summary of the *p* values demonstrating statistical significance are shown on Fig. 13-15. In addition to the t-test the Cohen's *d* size effect was also calculated. Cohen's *d* is a value showing the difference between two means in standard deviations (Lakens, 2013). It is used to measure the magnitude of an experimental effect (McLeod, 2019). When the values are below 0.2 the effect size is considered to be low, between 0.2 and 0.8 - medium and above 0.8 it is considered large. Evaluation of the performance between the two models is based on all described statistical parameters but the Cohen's *d* effect size was taken as most important factor when evaluating which of the two models to be further used for the counts.

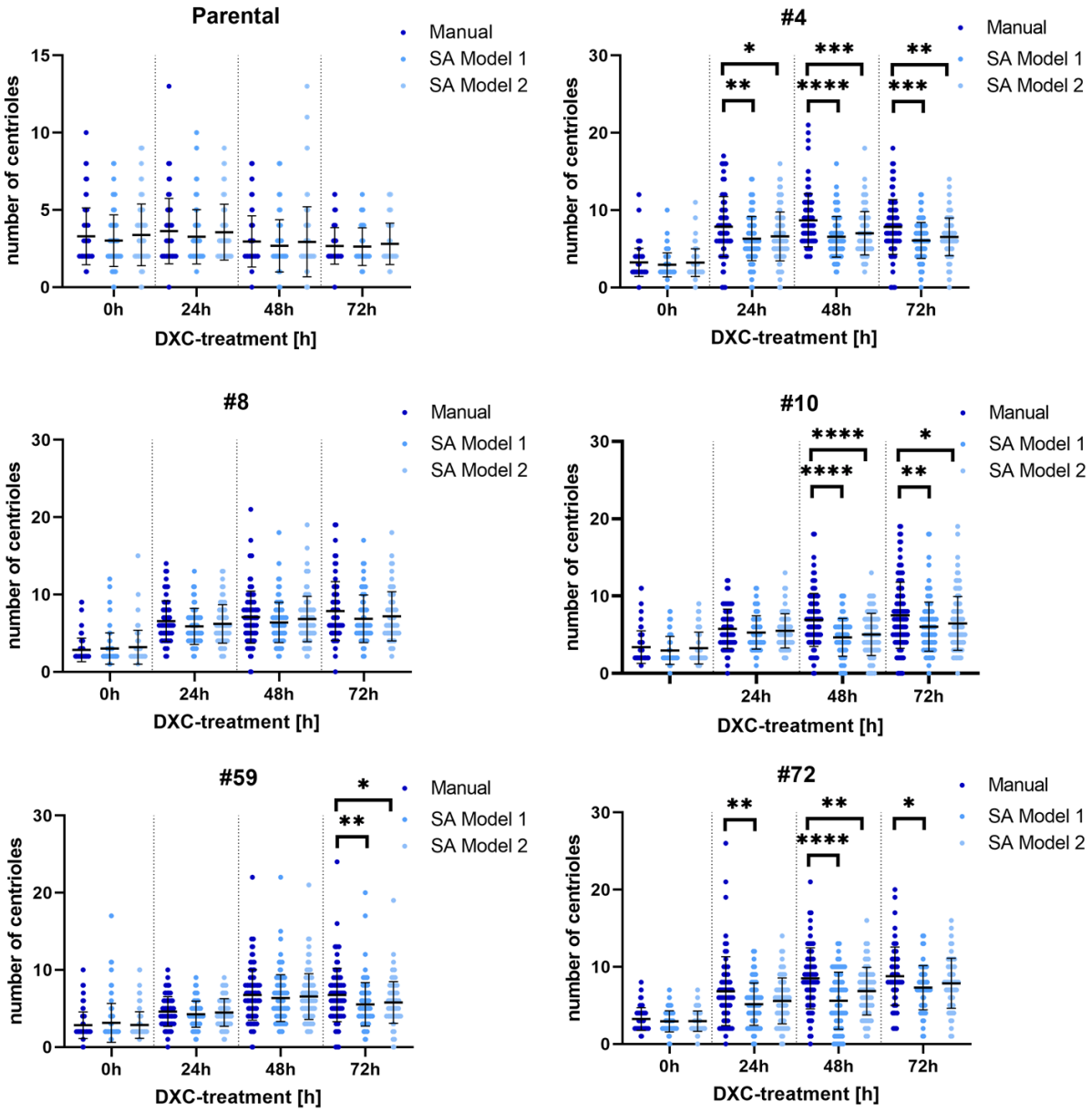

Figure 13. PLK4 overexpression in RPE1 cells - Centrin. Comparison of the finetuned MitoSegNet-based Model I and Model II.

RPE1 parental cells and DXC-inducible PLK4-overexpressing clones #4, #8, #10, #72 were treated with DXC for 0, 24, 48 and 72 hours and compared with untreated cells. Cells were labeled with anti-Centrin antibody. Centrioles/cell counting was performed manually (dark blue) and with the SA pipeline using Model I-Centrin and Model II-Centrin. Results from the three counts are compared. >50 cells were assessed for each condition. Plots show mean value with standard deviation and t-test's *p* value summary only when significant. Note, the *p* value compares manual versus SA centrioles counts.

CENTRIN												
DXC treatment	0h			24h			48h			72h		
Mode of counting	Man	Model I (SA)	Model II (SA)	Man	Model I (SA)	Model II (SA)	Man	Model I (SA)	Model II (SA)	Man	Model I (SA)	Model II (SA)
Parental												
Number of cells	78	75	75	70	68	68	78	77	77	64	62	62
Sum of total centrioles	257	226	254	254	222	242	231	206	226	171	163	174
Mode	2	2	2	2	2	2	2	2	2	2	2	2
P value		0.3239	0.7674		0.2743	0.8355		0.2894	0.9339		0.8415	0.5509
Effect size		0.2	0.0		0.2	0.0		**0.1**	**0.0**		**0.0**	**0.1**
Clone #4												
Number of cells	84	85	84	99	94	94	92	92	92	93	91	91
Sum of total centrioles	271	249	270	783	594	621	799	604	645	728	554	596
Mode	2	2	2	6	6	5	6	6	5	8	6	6
P value		0.2579	0.9660		0.0017	0.0125		<0.0001	0.0004		0.0001	0.0049
Effect size		0.2	0.0		0.5	0.4		0.7	0.5		0.6	0.4
Clone #8												
Number of cells	83	79	79	71	72	72	102	98	98	66	66	66
Sum of total centrioles	236	238	251	466	423	447	722	626	670	519	453	475
Mode	2	2	2	6	5	6	8	7	5	6	5	5
P value		0.5487	0.2615		0.0992	0.4082		0.1062	0.5885		0.0990	0.2767
Effect size		0.1	0.2		0.3	0.1		0.2	0.1		0.3	0.2
Clone #10												
Number of cells	94	100	100	73	71	71	101	106	106	115	119	119
Sum of total centrioles	319	297	327	421	376	391	699	495	534	864	719	768
Mode	2	2	2	4	4	4	7	6	4	5	7	5
P value		0.1346	0.6813		0.2349	0.5153		<0.0001	<0.0001		0.0030	0.0381
Effect size		0.2	0.1		0.2	0.1		0.8	0.6		0.4	0.3
Clone #59												
Number of cells	108	108	108	93	94	94	111	114	114	103	104	105
Sum of total centrioles	307	338	309	429	401	422	751	725	747	696	576	608
Mode	2	2	2	4	4	4	6	5	7	7	4	4
P value		0.3299	0.9371		0.1932	0.6512		0.3363	0.6091		0.0060	0.0258
Effect size		0.0	0.0		0.0	0.0		0.3	0.3		0.9	1.0
Clone #72												
Number of cells	62	63	63	72	72	72	73	70	70	62	60	60
Sum of total centrioles	201	185	187	493	372	403	621	393	480	545	438	472
Mode	2	2	2	6	6	6	8	4	8	8	7	8
P value		0.2326	0.2769		0.0075	0.0503		<0.0001	0.0063		0.0157	0.1495
Effect size		0.0	0.0		0.0	0.0		1.0	0.0		0.3	0.0

Table 8. Statistical analysis - Centrin

Statistical analysis comparing centrioles counted manually, with Model I-Centrin and Model II-Centrin for each clone and treatment condition are shown. Total number of cells and the sum of all centrioles counted per condition and genotype are given. Mode value shows the most often appearing number of centrioles per cell. *P* value from unpaired two-tailed t-test is shown. Cohen's *d* effect size highlighted in black is considered low (below 0.2), in blue-medium (between 0.2 and 0.8) and in red-large (above 0.8).

The statistical analysis shows similarities in the Model I-Centrin and Model II-Centrin performances with no statistical significance or large size effect for any of the conditions when comparing the results for the parental cells and clone #8 (Fig. 13 and Table 8). However, for the rest of the data, at later time points Model II performs better compared to Model I, visible by the higher *p* values and the lower effect size of Model II. Considering the quantitative statistical analysis and the visual data distribution, I continued the counts for Centrin positive centrioles of the rest of the data with Model II (without any post-processing).

SA counts for γ-Tubulin stained cells showed poorer performance in both models' predictions compared to the predictions for Centrin, which are more similar to the manual counts, but with similarities between the two models (Fig. 14 and Table 9). However, both models were able to detect the pattern of difference in different conditions within the data. Based on the data distribution and the statistical analysis Model I-γ-Tubulin/ANKRD26 showed lower effect size compared to the effect size of Model II-γ-Tubulin. Taking this into consideration I continued the counts for γ-Tubulin of the rest of the data with Model I-γ-Tubulin/ANKRD26 (followed by binary masks post-processing with the Watershed Fiji's function).

The statistical analysis and data distribution from the centrioles predictions for ANKRD26 shows better performance of Model II-ANKRD26 compared to Model I-γ-Tubulin/ANKRD26. The lack of statistical significance between the manual counts and the predictions from Model II-ANKRD26 for the parental cells demonstrate higher similarity of the predictions to the manual counts (Fig. 15 and Table 10). In addition, the increased occurrence of higher *p* values and lower effect size for this model compared to the *p* values and effect size of Model I-γ-Tubulin/ANKRD26 for the PLK4-overexpressing clones were considered as factor for better performance. Thus, I continued the counts for ANKRD26 of the rest of the data with Model II-ANKRD26 (without any post-processing).

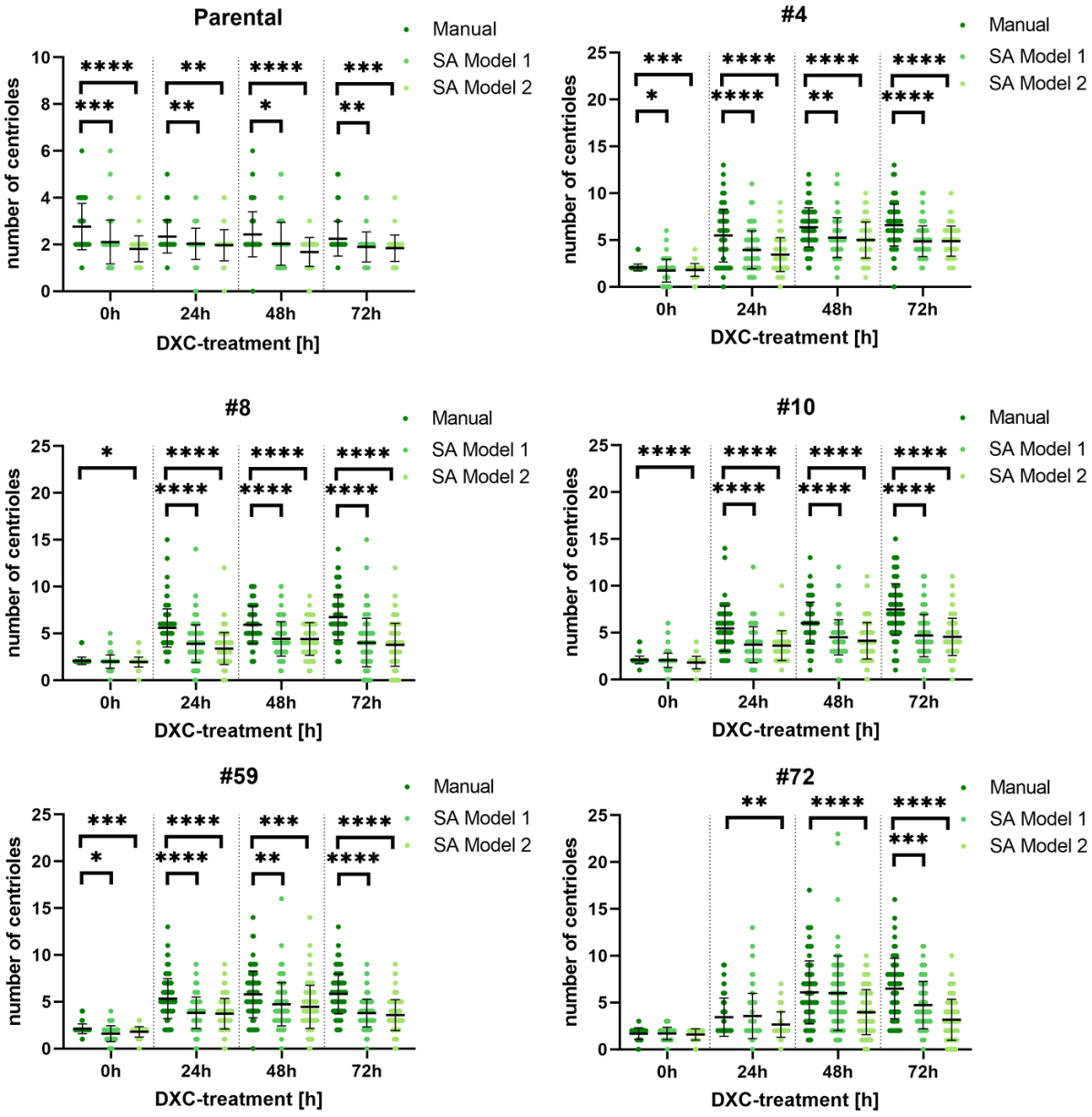

Figure 14. PLK4 overexpression in RPE1 cells – γ-Tubulin. Comparison of the finetuned MitoSegNet-based Model 1 and Model 2.

RPE1 parental cells and DXC-inducible PLK4-overexpressing clones #4, #8, #10, #72 were treated with DXC for 0, 24, 48 and 72 hours and compared with untreated cells. Cells were labeled with anti-γ-Tubulin antibody. Centrioles/cell counting was performed manually (dark green) and with the SA pipeline using Model I-γ-Tubulin/ANKRD26 and Model II-γ-Tubulin. Results from the three counts are compared. >50 cells were assessed for each condition. Plots show mean value with standard deviation and t- test's *p* value summary only when significant. Note, the *p* value compares manual versus SA centrioles counts.

γ-TUBULIN												
DXC treatment	0h			24h			48h			72h		
Mode of counting	Man	SA Model I	SA Model II	Man	SA Model I	SA Model II	Man	SA Model I	SA Model II	Man	SA Model I	SA Model II
Parental												
Number of cells	64	65	65	68	69	69	60	65	65	78	77	77
Sum of total centrioles	177	137	118	159	140	136	146	132	109	175	146	142
Mode	2	2	2	2	2	2	2	2	2	2	2	2
P value		0.0002	<0.0001		0.0091	0.0021		0.0193	<0.0001		0.0022	0.0002
Effect size		0.7	1.2		0.5	0.5		0.4	0.9		0.5	0.6
Clone #4												
Number of cells	92	93	93	102	111	111	73	80	80	111	110	110
Sum of total centrioles	190	161	167	559	439	382	464	421	400	733	536	537
Mode	2	2	2	2	2	2	7	5	5	6	5	6
P value		0.0124	0.0010		<0.0001	<0.0001		0.0017	<0.0001		<0.0001	<0.0001
Effect size		0.4	0.5		0.6	0.9		0.5	0.7		0.9	0.9
Clone #8												
Number of cells	124	131	131	120	127	129	99	101	101	111	109	109
Sum of total centrioles	258	261	254	670	496	437	587	431	446	747	438	413
Mode	2	2	2	6	4	4	5	4	4	6	4	4
P value		0.2231	0.0176		<0.0001	<0.0001		<0.0001	<0.0001		<0.0001	<0.0001
Effect size		0.2	0.3		0.8	1.2		0.9	0.8		1.1	1.2
Clone #10												
Number of cells	121	132	132	56	59	47	99	104	104	95	94	94
Sum of total centrioles	253	270	238	305	219	170	596	468	429	709	441	427
Mode	2	2	2	4	4	4	6	3	4	6	4	4
P value		0.5592	<0.0001		<0.0001	<0.0001		<0.0001	<0.0001		<0.0001	<0.0001
Effect size		0.1	0.5		0.8	0.9		0.7	0.9		1.1	1.2
Clone #59												
Number of cells	108	108	108	93	94	94	111	114	114	103	104	105
Sum of total centrioles	307	338	309	429	401	422	751	725	747	696	576	608
Mode	2	2	2	4	4	4	6	5	7	7	4	4
P value		0.3299	0.9371		0.1932	0.6512		0.3363	0.6091		0.0060	0.0258
Effect size		0.3	0.6		0.8	0.9		0.4	0.6		1.1	1.2
Clone #72												
Number of cells	76	80	81	63	76	76	69	77	77	65	71	71
Sum of total centrioles	128	136	129	217	272	202	420	462	306	422	336	225
Mode	2	2	2	2	2	2	5	4	2	8	3	3
P value		0.8779	0.3497		0.7271	0.0077		0.8877	<0.0001		0.0005	<0.0001
Effect size		0.0	0.1		0.1	0.5		0.0	0.7		0.6	1.2

Table 9. Statistical analysis – γ-Tubulin

Statistical analysis comparing centrioles counted manually, with Model I-γ-Tubulin/ANKRD26 and Model II-γ-Tubulin for each clone are shown. Total number of cells and the sum of all centrioles counted per condition and genotype are given. Mode value shows the most often appearing number of centrioles per cell. *P* value from unpaired two-tailed t-test is shown. Cohen's *d* effect size highlighted in black is considered low (below 0.2), in blue-medium (between 0.2 and 0.8) and in red-large (above 0.8).

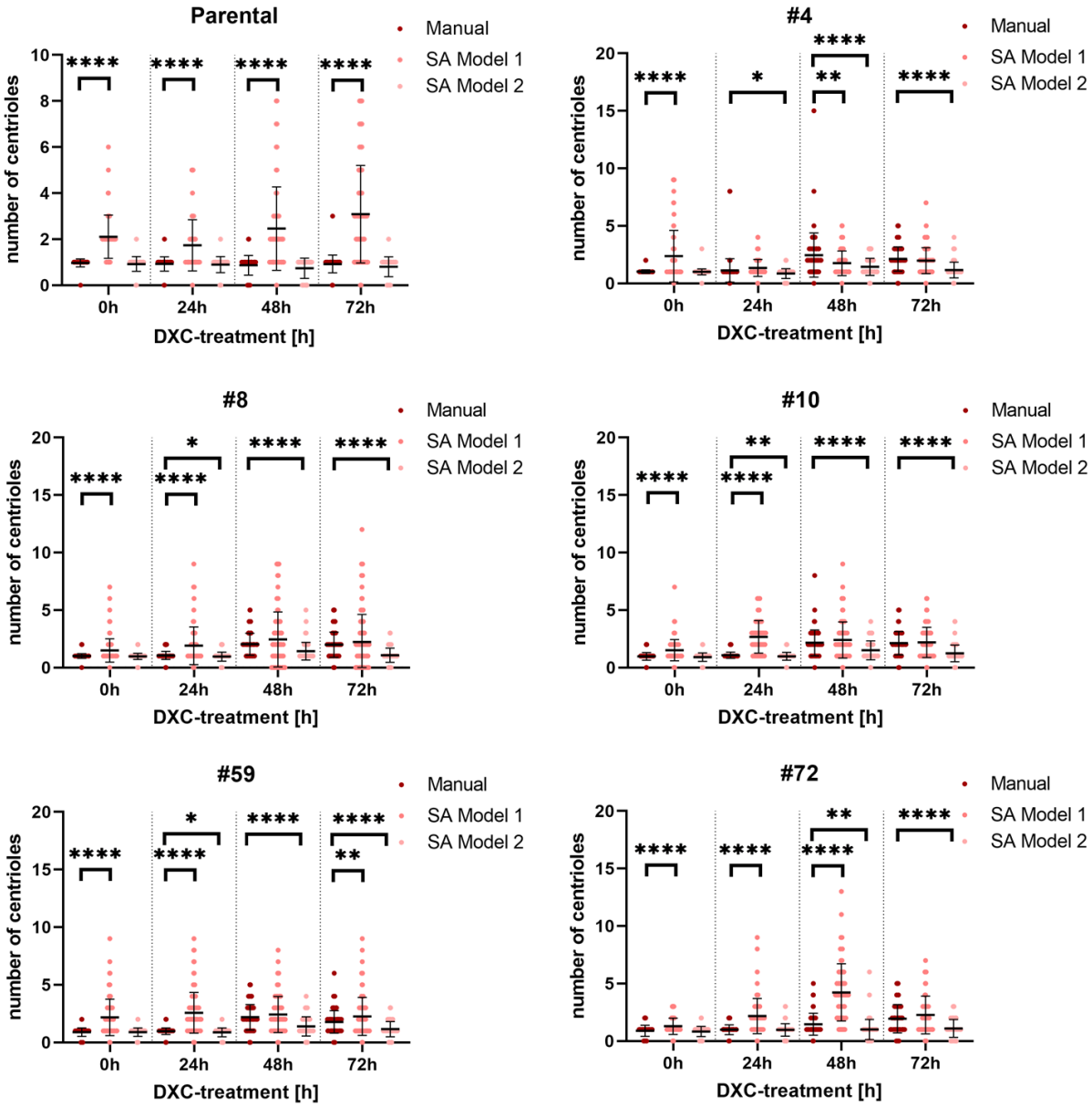

Figure 15. PLK4 overexpression in RPE1 cells - ANKRD26. Comparison of the finetuned MitoSegNet-based Model 1 and Model 2.

RPE1 parental cells and DXC-inducible PLK4-overexpressing clones #4, #8, #10, #72 were treated with DXC for 0, 24, 48 and 72 hours and compared with untreated cells. Cells were labeled with anti-ANKRD26 antibodies. Centrioles/cell counting was performed manually (dark red) and with the SA pipeline using Model I-γ-Tubulin/ANKRD26 and Model II-ANKRD26. Results from the three counts are compared. >50 cells were assessed for each condition. Plots show mean value with standard deviation and t-test's *p* value summary only when significant. Note, the *p* value compares manual versus SA centrioles counts.

ANKRD26												
DXC treatment	0h			24h			48h			72h		
Mode of counting	Man	SA Model I	SA Model II	Man	SA Model I	SA Model II	Man	SA Model I	SA Model II	Man	SA Model I	SA Model II
Parental												
Number of cells	64	65	65	68	68	69	60	65	65	78	77	77
Sum of total centrioles	62	137	60	63	118	62	52	160	48	72	238	62
Mode	1	2	1	1	1	1	1	1	1	1	1	1
P value		<0.0001	0.3195		<0.0001	0.6239		<0.0001	0.1038		<0.0001	0.0749
Effect size		1.7	0.2		1.0	0.1		1.2	0.3		1.4	0.3
Clone #4												
Number of cells	92	89	93	102	110	111	73	80	80	111	110	110
Sum of total centrioles	94	211	93	115	148	95	180	140	115	235	218	128
Mode	1	1	1	1	1	1	2	1	1	2	2	1
P value		<0.0001	0.4792		0.0743	0.0108		0.0046	<0.0001		0.3584	<0.0001
Effect size		0.9	0.1		0.2	0.4		0.5	0.7		0.1	1.1
Clone #8												
Number of cells	124	130	131	120	124	129	99	93	101	111	107	109
Sum of total centrioles	125	194	128	127	236	123	202	228	144	221	238	117
Mode	1	1	1	1	1	1	2	0	1	2	2	1
P value		<0.0001	0.2931		<0.0001	0.0275		0.1151	<0.0001		0.3550	<0.0001
Effect size		0.7	0.1		0.7	0.3		0.2	0.7		0.1	1.0
Clone #10												
Number of cells	121	132	132	75	47	59	80	100	104	95	93	94
Sum of total centrioles	118	200	120	59	126	58	172	240	156	202	204	116
Mode	1	1	1	1	3	1	2	2	1	2	1	1
P value		<0.0001	0.1288		<0.0001	0.0032		0.2336	<0.0001		0.6966	<0.0001
Effect size		0.8	0.2		1.8	0.3		0.2	0.7		0.1	1.0
Clone #59												
Number of cells	104	90	106	117	110	127	102	99	100	119	125	125
Sum of total centrioles	93	196	95	114	283	111	223	240	139	212	282	144
Mode	1	1	1	1	2	1	2	1	1	1	1	1
P value		<0.0001	0.9684		<0.0001	0.0197		0.2136	<0.0001		0.0070	<0.0001
Effect size		1.2	0.0		1.3	0.3		0.2	0.8		0.3	0.8
Clone #72												
Number of cells	76	81	81	63	72	76	69	65	77	65	71	71
Sum of total centrioles	68	104	67	62	157	74	101	275	77	126	161	78
Mode	1	1	1	1	2	1	1	4	1	1	1	1
P value		<0.0001	0.3586		<0.0001	0.9007		<0.0001	0.0027		0.1929	<0.0001
Effect size		0.6	0.1		1.0	0.0		1.5	0.5		0.2	0.8

Table 10. Statistical analysis – ANKRD26

Statistical analysis comparing centrioles counted manually, with Model I-γ-Tubulin/ANKRD26 and Model II-ANKRD26 for each clone are shown. Total number of cells and the sum of all centrioles counted per condition and genotype are given. Mode value shows the most often appearing number of centrioles per cell. *P* value from unpaired two-tailed t-test is shown. Cohen's *d* effect size highlighted in black is considered low (below 0.2), in blue-medium (between 0.2 and 0.8) and in red-large (above 0.8).

Results demonstrate that in parental and untreated control cells, thus physiological conditions, the number of centrioles is relatively constant and close to the expected number in most cells (which for interphase cells is: 2 procentrioles (positive for Centrin), 2 maturing centrioles (positive for γ-Tubulin) and 1 mature parental centriole (positive for ANKRD26)). Noticeable elevation of the number of centrioles (centriole accumulation) positive for Centrin is observed upon PLK4 OE in the DXC-dependent PLK4-overexpressing clones and it is observable already after 24 h of PLK4 OE as expected (dot plot graphs in Fig. 13 and Mode values (most often found value in a data set) shown in Table 8). However, even more significant accumulation is observable after 48 h but afterwards a plateau (no statistical significance between the groups (48 h and 72 h DXC treatment) is presented with t-test, *p* values not shown) or reduction of centriole accumulation is notable at 72 h of DXC treatment. Mature centrioles, which are γ-Tubulin positive were also accumulated after 24 h of PLK4 OE (Fig. 14) in a relatively similar pattern as Centrin-positive centrioles among clones. However, parental mature centrioles, which are ANKRD26-positive centrioles were accumulated only after 48 h in accordance with the centriole cycle. At 72 h PLK4-overexpressing cells do not show further significant increase of mature centrioles accumulation compared to cells at 48 h DXC treatment (Fig. 14 and 15). This observation is supported by the mode values shown in Tables 8-10.

In contrast, increase of centrioles accumulation is observable in PLK4-overexpressing clones with inactivated p53 in time following the cell cycle progressions compared to cells at 48 h (Fig. 16 and Table 11). This observation is notable in Centrin and γ-Tubulin counts but highlighted in ANKRD26 counts after 72 h of DXC treatment.

For the counting of this data set the adapted models for each antibody were used. However, to demonstrate the sensitivity of the SA counting pipeline in a condition different than the checked so far (thus, more than 72 h of PLK4 OE) when further centrioles

accumulation might be expected a comparison with manual counts for each antibody are shown in Fig. 16 for the time point of 96 h DXC treatment or no treatment. As noticeable statistical significance from unpaired t-test is present only between the manual counts and the SA counts of ANKRD26-positive centrioles at 96 h DXC treatment with effect size of 0.5 (medium) but not for any other of the compared groups (manual versus SA counting). This is further supported by the mode values shown in Table 11. This data demonstrates that the SA pipeline performs well for Centrin and γ-Tubulin and is able to detect centrioles in new conditions with precision similar to the visual scoring.

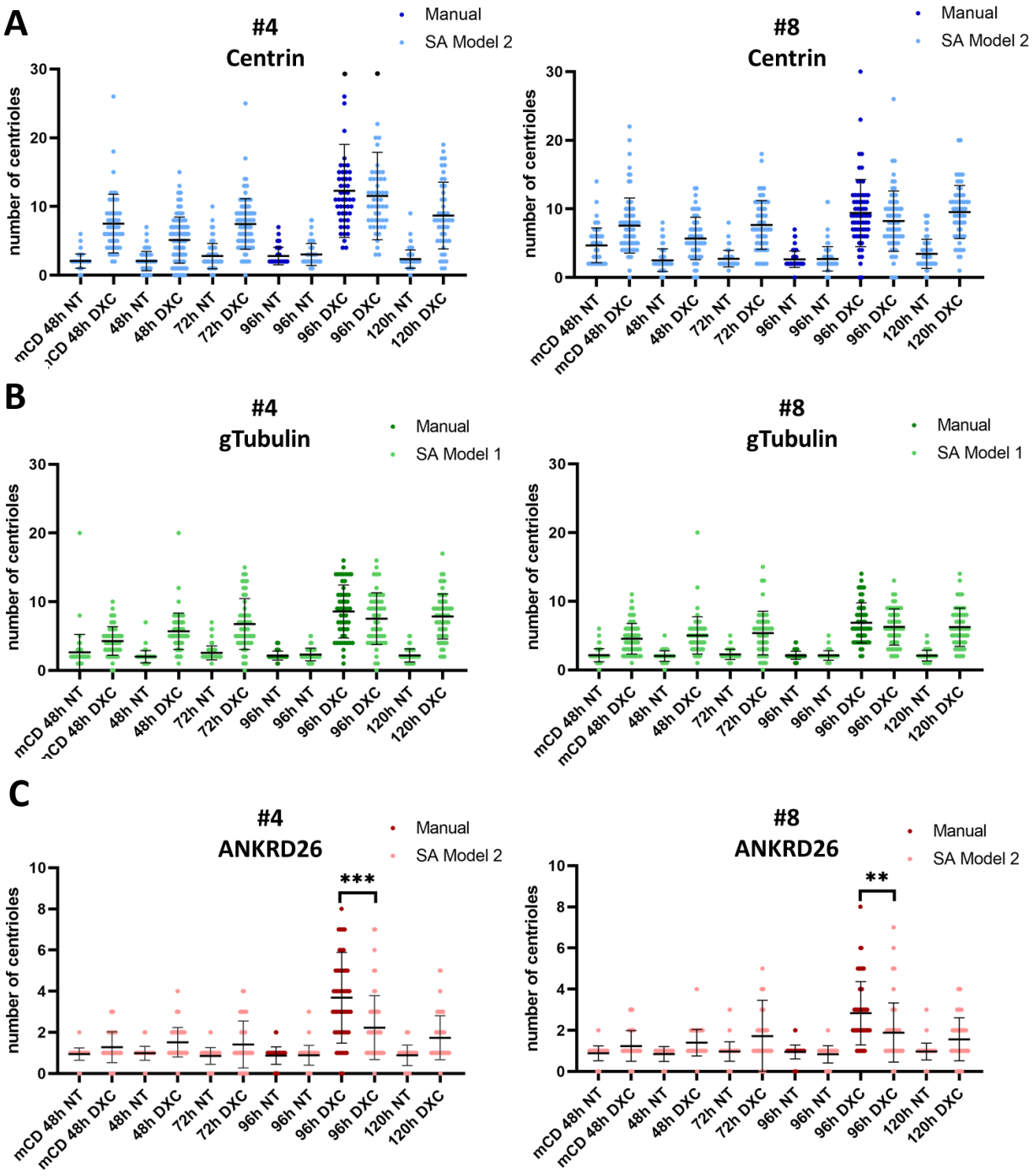

Figure 16. PLK4 overexpression in p53$^{-/-}$ RPE1 cells.

Centrioles/cell counted with the SA pipeline and manual (darker color). Two clones (#4 and #8) of DXC-inducible PLK4-overexpressing cells in which p53 is knocked out were used for this experiment. Several timepoints after DXC treatment were selected for the centrioles counts and compared to untreated cells. Results for **A)** Centrin (blue); black dots correspond to 46 (manual) and 44 (SA Model 2) centrioles/cell; **B)** γ-Tubulin (green) and **C)** ANKRD26 (red) are shown. γ-Tubulin predictions were made with Model I-γ-

Tubulin/ANKRD26, Centrin and ANKRD26 were made with Model II-Centrin and Model II-ANKRD26. Centrioles manual counts for 96 h DXC treatment or untreated cells at 96 h were compared with the SA counted centrioles. >50 cells were assessed for each condition. Plots show mean value with standard deviation and unpaired two-tailed t-test's *p* value summary only when significant. Note, the *p* value compares manual versus SA centrioles counts.

Genotype	**mCD8**		**P53 KO**									
DXC treatment	48h NT	48h DXC	48h NT	48h DXC	72h NT	72 DXC	**96h NT**	96h NT	**96h DXC**	96h DXC	120 NT	120 DXC
Centrin												
Mode Clone #4	2	6	2	6	2	9	**2**	2	**11**	12	2	8
Mode Clone #8	2	8	2	5	2	7	**2**	2	**9**	6	2	11
γ-Tubulin												
Mode Clone #4	2	5	2	5	2	5	**2**	2	**4**	4	2	9
Mode Clone #8	2	2	2	5	2	6	**2**	2	**6**	6	2	6
ANKRD26												
Mode Clone #4	1	1	1	1	1	1	**1**	1	**3**	1	1	1
Mode Clone #8	1	1	1	1	1	1	**1**	1	**2**	1	1	1

Table 11. Mode values for centrioles counts in p53$^{-/-}$ RPE1 cells. Mode values showing the most often appearing number of centrioles per cell for each treatment condition are shown. Model II-Centrin was used to count Centrin, Model I-γ-Tubulin/ANKRD26 was used to count γ-Tubulin and Model II-ANKRD26 was used to count ANKRD26. Manual counts are shown in bold.

No significant differences in the pattern of accumulation of PLK4 overexpression-induced centriole accumulation is observed upon deletion of key proteins of mature parental centrioles such as ANKRD26 or SCLT1 (Fig. 17 and Table 12) compared to the control cells. Statistical comparison between 48 h DXC treatment of the control cells – mCD and each genotype (p53 KO, ANKRD26 KO or SCLT1 KO) did not show significant differences (*p* values not shown). However, a group of cells with centrioles negative for ANKRD26 is observed in the ANKRD26 KO and SCLT1 KO cells (as expected).

In order to further check the sensitivity of the SA pipeline's performance in comparing different genotypes a comparison of manual counts and SA counts for each of the three antibodies with the corresponding models at 48 h of DXC treatment were compared. As shown in Fig. 17 statistical significance between the two approaches for centrioles

counting is noticeable for the γ-Tubulin counts of the p53 KO cells. Comparison between the manual and SA counts show low *p* values but with medium (0.6) for clone 4 and low (0.1) for clone 8 effect size. However, the mode values of the results from the two counting approaches for γ-Tubulin are similar. Comparison of manual and SA counts for ANKRD26 for the two clones also showed low *p* values (Fig. 17) but with medium effect size of 0.3. Taken into consideration: the data distribution, the mode values (Table 12) and the low to medium effect size this data demonstrates relatively good performance of the SA pipeline.

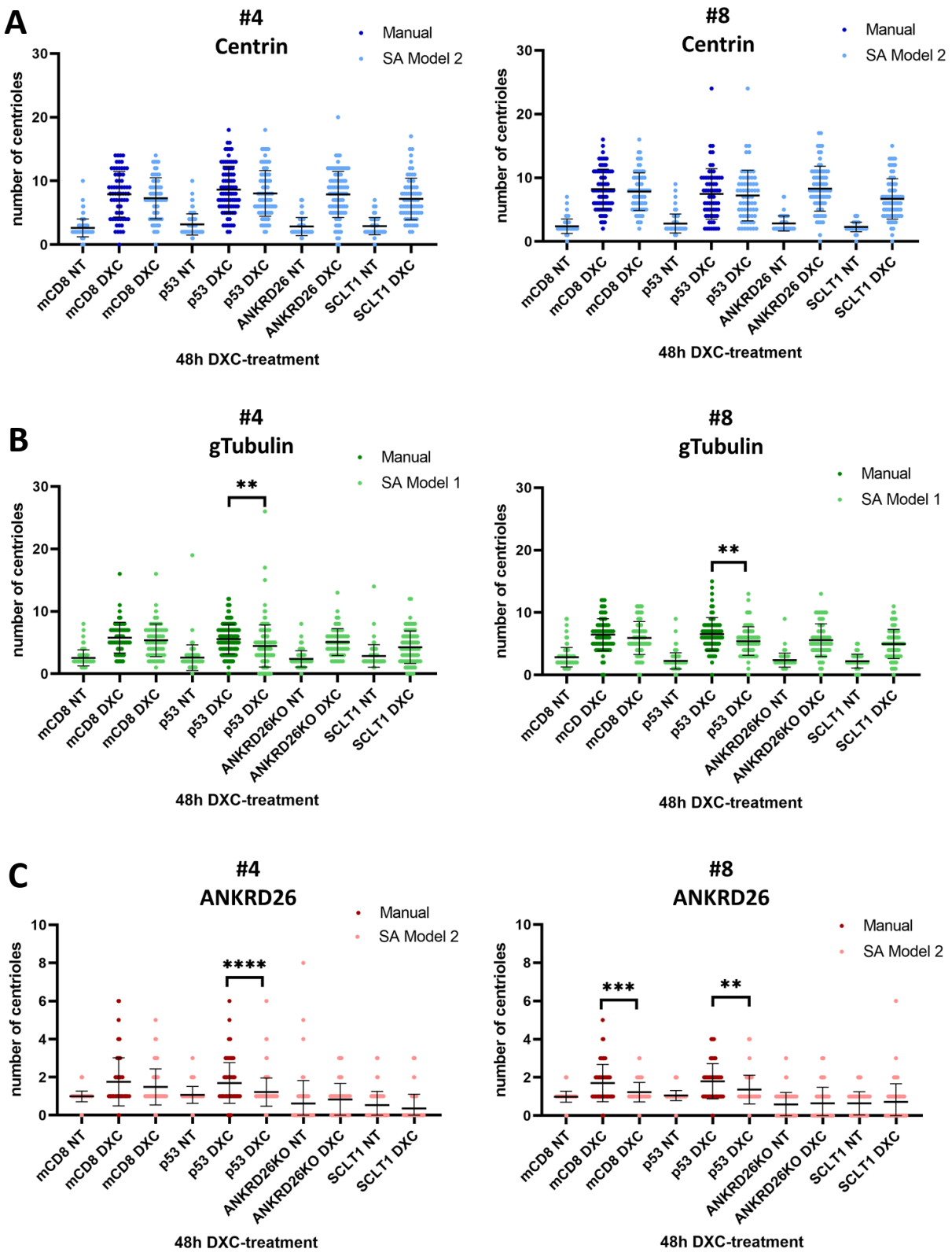
A
#4
Centrin
Manual
SA Model 2
number of centrioles
48h DXC-treatment
#8
Centrin
Manual
SA Model 2
number of centrioles
48h DXC-treatment
B
#4
gTubulin
Manual
SA Model 1
**
number of centrioles
48h DXC-treatment
#8
gTubulin
Manual
SA Model 1
**
number of centrioles
48h DXC-treatment
C
#4
ANKRD26
Manual
SA Model 2
****
number of centrioles
48h DXC-treatment
#8
ANKRD26
Manual
SA Model 2
***
**
number of centrioles
48h DXC-treatment

Figure 17. PLK4 overexpression in p53$^{-/-}$, SCLT1$^{-/-}$ and ANKRD26$^{-/-}$ RPE1 cells.

Centrioles/cell counted with the SA pipeline and manual (darker color). Untreated and treated with DXC for 48 h cells from each indicated genotype are compared. For this experiment two clones (#4 and #8) of DXC-inducible PLK4-overexpressing cells were tested. Results for **A)** Centrin (blue), **B)** γ-Tubulin (green) and **C)** ANKRD26 (red) are shown. γ-Tubulin predictions were made with Model I-γ-Tubulin/ANKRD26, Centrin and ANKRD26 were made with the respective Model II. >50 cells were assessed for each condition. Plots show mean value with standard deviation and unpaired two-tailed t-test's *p* value summary only when significant. Note, the *p* value compares manual versus SA centrioles counts.

Genotype	**mCD8**			**P53 KO**			**ANKRD26 KO**		**SCLT1 KO**	
DXC treatment	48h NT	**48h DXC**	48h DXC	48h NT	**48h DXC**	48h DXC	48h NT	48h DXC	48h NT	48h DXC
Centrin										
Mode Clone #4	2	**9**	7	2	**7**	6	2	12	2	5
Mode Clone #8	2	**8**	8	2	**10**	8	2	8	2	7
γ-Tubulin										
Mode Clone #4	2	**5**	7	2	**5**	5	2	5	2	2
Mode Clone #8	2	**5**	5	2	**6**	6	2	5	2	5
ANKRD26										
Mode Clone #4	1	**1**	1	1	**1**	1	0	1	0	0
Mode Clone #8	1	**1**	1	1	**1**	1	1	0	1	0

Table 12. Mode values for centrioles counts in p53$^{-/-}$, SCLT1$^{-/-}$ and ANKRD26$^{-/-}$ RPE1 cells. Mode values showing the most often appearing number of centrioles per cell for each treatment condition are shown. Model II-Centrin was used to count Centrin, Model I-γ-Tubulin/ANKRD26 was used to count γ-Tubulin and Model II-ANKRD26 was used to count ANKRD26. Manual counts are shown in bold.

DISCUSSION

PIDDosome-medicated Caspase-2 activation and its substrates

The main focus of this thesis is the investigation of the PIDDosome activation. In the search of fluorogenic reporter for the PIDDosome activation which would allow us to determine more precisely the localization, kinetics and timing of the PIDDosome activation several attempts were done. The reported bimolecular fluorescence complementation (BiFC) assay (Shyu et al., 2006) for analysis of protein-protein interaction in living cells was reported as an appropriate tool for measuring Caspase-2 proximity, thereby indirectly allowing to infer Caspase-2 activation (Lisa Bouchier-Hayes et al., 2009). Such approach however failed to visualize Caspase-2 activation within the PIDDosome (data not shown). Next, I tried to flank MDM2, the bona fide substrate of the PIDDosome-activated Caspase-2 (Fava et al., 2017; Pochampally et al., 1998), with fluorescent molecules (GFP and mCherry) unsuccessfully trying several cloning strategies.

As reported in many screening studies, VDVAD-based substrate is broadly used short peptide for the Caspase-2 activation measurement (Benkova et al., 2009; Kitevska et al., 2014; McStay et al., 2008; Talanian et al., 1997; Tang et al., 2011). Based on these previous studies and the broad use of VDVAD, we decided to try this commercially available fluorogenic substrates and exploit its capabilities for Caspase-2 activation detection when Caspase-2 is PIDDosome-activated. The results shown in this thesis demonstrate that VDVADase activity is measured in Caspase-2 lacking cells under apoptotic conditions (Fig. 8) controversially to some reports showing that VDVAD is specific substrate for the Caspase-2 activity measurement (McStay et al., 2008; Talanian et al., 1997). The results presented here suggest that VDVAD is able to measure apoptotic activation, which is not Caspase-2-dependent. Taken together, similarly to DEVDase activity mounting in apoptotic cells as a result of effector caspase activation, VDVADase activity measured across this thesis likely reflects the activation of effector caspases downstream to MOMP, rather than a bona fide Caspase-2 activation.

Some studies showed that the primary Caspase-2 cleavage sequence is DEVD (Julien et al., 2016) but here I did not detect any DEVDase activity form PIDDosome-activated Caspase-2 (upon ZM447439 treatment), as shown on Fig 8B. This might be due to condition-dependent substrate specificity of Caspase-2. Thus, results obtained from recombinant Caspase-2 expressed in bacteria cells could be explained with the conditions in bacteria which are different from the ones in eucaryotic cells. Furthermore, lacking the PIDDosome components or other still unknown potential factors might influence the Caspase-2 substrate preferences outcomes. It might be interesting to co-express recombinant PIDD1, RAIDD and Caspase-2 in order to examine the possibility of: 1) exogenous spontaneous PIDDosome formation in procaryote cells and 2) the Caspase-2 substrate preferences under these conditions and re-evaluate the reported VDVADase specificity of Caspase-2.

DEVD sequence is remarkably similar to the cleavage site of Caspase-3 and Caspase-7 (Julien et al., 2016; Kitevska et al., 2014; Seaman et al., 2016). Some reports even suggest it as a consensus cleavage site for caspases -2, -3 and -7 (Wejda et al., 2012). In addition, the bona fide substrate for Caspase-3 activation – PARP1 is cleaved at the DEVD sequence making the DEVD peptide classical Caspase-3 substrate (Agard et al., 2012; Boulares et al., 1999; Kaufmann et al., 1993; Nicholson et al., 1995; Tewari et al., 1995; Thornberry et al., 1997). Moreover, results shown here demonstrate DEVDase activity under apoptotic conditions, when executioner caspases like Caspase-3 and Caspase-7 are activated, independently of the Caspase-2 presence.

Considering the controversial reports about the exact Caspase-2 cleavage site and the reported similarity of caspases substrates (Wejda et al., 2012), in addition, to the fact that caspases are conservative among species, so as their active site region (S Kumar et al., 1994; Lamkanfi et al., 2002; Yuan et al., 1993) it is also likely that caspases substrates “overlap” and the reported VDVAD-based substrates are not specific enough for Caspase-2. This is consistent with previously reported studies (McStay et al., 2008) and could explain the elevated VDVADase activity in the absence of Caspase-2, measured in apoptotic cells where most likely the apoptosis executioner Caspase-3 and Caspase-7 are activated and cleave the VDVAD substrate. Moreover, this hypothesis is supported by studies demonstrating the inhibition of Caspase-3 by the commercially available inhibitors Ac-VDVAD-CHO (Schweizer et al., 2007) and the cleavage preferences of Caspase-3, although less effective

than towards DEVD, towards other substrates like: VEID, IETD, LEHD and VDVAD (McStay et al., 2008).

Interestingly, the detected increased VDVAD-AFC and DEVD-AFC signal in *Caspase-2*$^{-/-}$ cells was slightly stronger (with exception of RPE1 clone 12#2) compared to parental cells (Fig. 8). This could be due to compensatory mechanism of other initiator caspases in Caspase-2 lacking cells which under apoptosis-activating conditions compensate the Caspase-2 function with stronger cleavage effect. Caspase-2 is considered mainly an initiator caspase due to its sequence homology, the presence of long prodomain and phylogenic analysis but according to its cleavage specificity it is closer to the executioner caspases so its function is dual (Julien et al., 2016; Julien & Wells, 2017; Kitevska et al., 2014; Lamkanfi et al., 2002; Talanian et al., 1997; Tang et al., 2011; Thornberry et al., 1997; Wejda et al., 2012). When overexpressed in cells Caspase-2 was shown to cause apoptosis (S Kumar et al., 1994; L. Wang et al., 1994), but it can lead to cell cycle arrest (Fava et al., 2017) and it was shown to have many other regulatory functions different from apoptosis (Miles et al., 2017). In addition, other caspases are shown to exhibit other functions different than apoptosis like cell cycle regulation, cell survival and differentiation (Chowdhury et al., 2008; Hashimoto et al., 2011; Lamkanfi et al., 2007; Van Opdenbosch & Lamkanfi, 2019) like Caspase-2 (Miles et al., 2017). Interestingly, double KO for Caspase-2 and Caspse-9 cells are still able to undergo apoptosis (Ekert et al., 2004; Marsden et al., 2004), suggesting that other initiator caspases perform their function. This further contributes to the possibility of overlapping function between Caspase-2 and other caspases and could potentially explain the observed here results.

Caspase-2 rescue and mutations

To our surprise no VDVADase activity was detected upon PIDDosome activation, suggesting that VDVAD is not reliable reporter for PIDDosome-mediated Caspase-2 activation. However, this is controversial to all the other studies showing specificity of VDVAD as Caspase-2 substrate and at least some VDVADase activity of Caspase-2. In order to explain why VDVAD was not cleaved by the PIDDosome we hypothesized that this effect could be due to the mode of Caspase-2 activation *in vivo*. Caspase-2 could activate itself

autoproteolytically (e.g. when the concentration of procaspase-2 reaches a sufficient concentration to autoproteolytically cleave itself without the aid of additional proteins such as in a test tube) or via the PIDDosome - a multiprotein platform serving to facilitate the proximity-induced autoproteolysis (B C Baliga et al., 2004; Tinel & Tschopp, 2004). We hypothesized that the fully active heterotetramer of Caspase-2 (mature Caspase-2), similar to the recombinant one used in peptide screen studies, is capable of cleaving after the VDVAD sequence and that the PIDDosome activated Caspase-2 is the one cleaving MDM2 after the FDVPD sequence (Pochampally et al., 1998). Although uncleavable mutant Caspase-2 was reported to partially retains its activity (B C Baliga et al., 2004) the results obtained here with the uncleavable Caspase-2 indicate that the non-autoproteolytically cleavable Caspase-2 does not rescue the catalytic potential of the endogenous or the exogenous wild type PIDDosome to cleave MDM2 (Fava et al., 2017). The results shown here indicate that the exogenous wild type Caspase-2 is capable of forming the PIDDosome. Importantly, these results suggest that fully mature Caspase-2 cleaves MDM2 after the FDVPD sequence and the VDVAD peptides. To answer the question of how Caspase-2 could have such differences in the substrate specificities further investigation would be necessary. Unpublished data of our laboratory suggest the Caspase-2 mediated cleavage does not occur in classical way and the potential presence of *exo* site could explain the diversity in substrate preferences of Caspase-2.

To the best of our knowledge this is the first successful Caspase-2 rescue as no successful Caspase-2 rescue was previously reported. The new protocol established in this thesis allows the mutagenesis of Caspase-2 in life cell cultures and its exploitation for structural and functional analysis of Caspase-2. This opens vast possibilities to explore the importance and discover key residues for the functional and structural activity of Caspase-2.

We initiated this exploration by selecting several key residues which were mutated. In addition to the key residues required for the autoproteolysis of Caspase-2 we selectively mutated a putative non-canonical nuclear export sequence of Caspase-2. Caspase-2 has a unique nuclear localization among the other caspases which are strictly cytoplasmic but this unique feature and its function is still not well understood. Moreover, it was shown that Caspase-2 could trigger apoptosis from the nucleus and it is involved in an nuclear-mitochondrial apoptotic pathway (Paroni et al., 2002). The nuclear transportation function of the Caspase-2 is dependent on its prodomain and it is regulated by two nuclear NLSs in the

prodomain (required for the nuclear import of the Caspase-2) (Belinda C Baliga et al., 2003; Colussi et al., 1998). Mutations in the NLS of the cytosolic form of Caspase-2 do not prevent apoptosis upon OE of the enzyme and OE of the nuclear pool of the Caspase-2 results in apoptosis-related mitochondrial changes. Moreover, drug inhibition of the nuclear export also does not prevent the ability of Caspase-2 to trigger cytochrome *c* release (Paroni et al., 2002; Robertson et al., 2002). These data suggest that mutation of the NLS or NES does not perturb the function of Caspase-2 and consistent with our results, which show that despite the NES mutation Caspase-2 is able to form fully functional PIDDosome as demonstrated by the MDM2 cleavage (Fig. 11).

Further investigation would be necessary to assess whether Caspase-2 is indeed "locked" in the nucleus. While we still cannot conclude whether the L132D mutation effectively prevents the nuclear export of Caspase-2, the nuclear disappearance of Caspase-2 upon PIDDosome activation (Fig. 10) could be the result of an active export or of the depletion of cytoplasmic Caspase-2 via autoproteolysis.

At present however we can readily conclude that mutations of the putative NES of Caspase-2 don't affect the capability of cleaving MDM2 upon cytokinesis failure as shown on the immunoblot (Fig. 11). Although MDM2 is shown to localize in the nucleoplasm (Schuster et al., 2007) but also in the cytoplasm and its subcellular localization is of key importance, since it could be used as a prognosis marker in cancer patients (H. S. Park et al., 2014) the PIDDosome activation upon cytokinesis failure was shown to be dependent on ANKRD26 interaction with PIDD1 (Burigotto et al., 2021), which is localized on the centrosome with strictly cytoplasmic localization. It would be intriguing to further investigate and reveal if there are potential signal mechanisms that Caspase-2 might be involved in, which permit PIDDosome-activating signals in the cytoplasm to affect the nuclear located Caspase-2 and *vice versa*, similarly to the nuclear-mitochondrial signal pathway in which Caspase-2 is involved.

Semi-automatic pipeline development for centrioles counting

The SA pipeline combining the recently developed deep-learning MitoSegNet model (Fischer et al., 2020) trained and adapted to segment centrioles with Fiji outperforms other segmentation threshold-based and non-deep-learning approaches. This user-friendly pipeline is much less laborious than the manual approach of centrioles segmentation and significantly shortens the time required for centrioles quantification. Moreover, it doesn't require extensive computational skills to be used.

The predictions for Centrin show better performance compared to the predictions for the other two antibodies since Centrin, as inner centriole protein, results in small circular areas with strong fluorescent signal. Furthermore, the signal is most often relatively well separated from each other even when in a cluster as shown in Fig. 12 B and C. This also allows higher quality of the ground truth (manual annotation), which is of fundamental importance for the deep-learning model's performance.

The overall higher error for γ-Tubulin prediction compared to the manual counting is due to the nature of the γ-Tubulin lattice which doesn't have sharp edges but smear-like structure difficult to be distinguished by the models. In addition, the overlap between several centrioles further impedes the segmentation process.

The poorer performance of Model I compared to Model II for the ANKRD26 predictions is also due to the nature of the ANKRD26 protein, which as distal appendage protein results in a donut-shape signal detectable only in fully matured parental centrioles. Since centrioles could appear in different positions in an image the donut shape is not always visible as so but might be turned in different angles or appear as a short tick line. This results in signal-background-signal line which is often wrongly interpreted by the model as several separated structures and could explain the high overestimation of ANKRD26-labeled centrioles compared to the manual counting. Similarly, as with γ-Tubulin images, an additional issue arises when centrioles are physically located in very close proximity and the Maximum Intensity Signal of the individual centrioles from the same cluster overlaps. Improvement of the predictions is observed when the MitoSegNet model was finetuned with more images (training the model to recognize ANKRD26 staining viewed by different angles) in order to generate Model II-ANRD26.

The finetuned models show similar performance in many cases, however Model I shows better performance for anti-γ-Tubulin staining while Model II performs better for anti-Centrin and anti-ANKRD26 staining. Despite of the presence of differences in the models' performance compared to the manual counts the SA counting is still able to detect patterns of changes in the numbers the centrioles between the different experimental conditions/genotypes. Since the pipeline facilitates the counting of centrioles it allows the usage of even larger amount of image data (more than 10 images per experimental condition/genotype, thus more than approx. 100 cells), which will facilitate detection of differences between untreated or parental cells and treated cells.

A future aspect of this project would be to implement a segmentation tool which would use 3-Dimentional Z-stack images and distinguish the centrioles' signal in space. This will potentially overcome the overlapping issue, however the MitoSegNet is developed for the purpose of 2-Dimentional segmentation so further testing of other deep-learning tools could be considered. Alternatively, using more images or using a microscopy system with higher resolution would allow the better differentiation of individual centrioles within a cluster by eye and the generation of higher quality ground truth images, and could be used to further finetune the pretrained MitoSegNet model and improve its performance. In addition, experimental adjustments could contribute to the more accurate and precise counting.

Taken together, while the exploitation of the tool discussed here for quantifying γ-Tubulin- and ANKRD26-positive centrioles will require further adjustments, my work provides a solid base for the SA quantification of Centrin-positive centrioles, thus facilitating the characterization of experimental perturbations that impact the number of centrioles and thereby centrosomes. In fact, while the dynamics of accumulation of centrioles characterized by different maturation stages differs upon acute perturbations, at steady state the relationship between the abundance of Centrin-positive (procentrioles), γ-Tubulin-positive (centrioles) and AKRD26-positive (mature centrioles) is constant across experimental conditions.

PLK4 overexpression and supernumerary centrosomes accumulation

To investigate the impact of supernumerary centrosomes on the PIDDosome activation and the following p53 stabilization centrioles from cells with DXC-inducible

PLK4 OE were quantified in different time points. I analyzed anti-Centrin labeled images which display both immature procentrioles and mature centrioles. The results obtained using the SA quantification approach showed an increase in centriole numbers in all genotypes upon 24 h of PLK4 OE compared to the parental cells, confirming our expectations and the reported observations (P. A. Coelho et al., 2021). A further increase in centriole numbers was observed at 48 h of PLK4 OE, which is explainable by additional cell cycle passaging that lead to additional centriole duplication and further centriole accumulation. Similarly, the accumulation of supernumerary centrosomes could be observed with anti-γ-Tubulin and anti-ANKRD26 staining which displays only fully mature centrioles. Since in interphase cells only one mature centriole is present, it is necessary for the PLK4-overexpressing cells to go through at least two cell cycles, from the PLK4 OE initiation, in order to achieve higher numbers of mature centrioles. Accordingly, the increase in centriole numbers reached significance after 48 h of DXC treatment. As already reported for epidermal progenitors, centrosome amplification induced by PLK4 OE more likely leads to apoptosis or destruction of the whole cell, than centrosome degradation (Serçin et al., 2016) suggesting that cells could not eliminate the extra centrioles. In line, supernumerary centrioles further accumulated with progressing through cell cycles, indicating that cells were not able to deplete accumulated centrioles. In other cell types the centrosome accumulation error is corrected by "sensing" the presence of supernumerary centrosomes via ANKRD26-mediated PIDD1 concentration increase close to the centrosome (Burigotto et al., 2021) leading to PIDDosome activation and p53-dependent cell cycle arrest (Fava et al., 2017). This observation is further supported by immunoblot generated by our laboratory (data not shown) of the PLK4-overexpressing clones demonstrating PIDDosome activation observed by MDM2 cleavage and increase at the p53 levels at 48 h post-treatment with DXC, suggesting that at this time point when mature centrioles have accumulated the ANKRD26-dependent PIDDosome activation is unleashed. Moreover, the here shown observations of centrioles accumulation's plateau of the PLK4-overexpressing clones (highlighted by the Centrin-positive centrioles counts – Fig. 13) after completing 48 h of DXC treatment supports the immunoblot data suggesting that stabilized p53 mediates cell cycle arrest constraining the further accumulation of centrioles by perturbing the additional cycling of cells.

To investigate the impact of p53 on centrosome numbers in our model we used CRISPR/Cas9 to delete p53 in RPE1 cells in order to monitor centriole number changes upon PLK4 OE. The increase in the centriole numbers (Fig. 16) after 48 h of PLK4 OE in the p53 KO clones with further cell cycle progression indicates that p53 plays important role in controlling centrioles accumulation. Thus, when p53 is demolished the PIDDosome-p53-p21-dependent cell cycle arrest is perturbed allowing the centrioles accumulation error to be carried on and additional centrioles accumulate with each cell cycle. Since correct centrosome numbers are a prerequisite for proper chromosome segregation, the cells possessing supernumerary centrosomes may be at risk to develop aneuploidy. Importantly, it was shown that in mice lacking p53, PLK4 OE and the following centriole overduplication supports tumor formation and hyperproliferation in certain tissues like pancreas and skin (P. A. Coelho et al., 2021; Serçin et al., 2016). It should be noted however that this effect might be strictly tissue specific since centrosome amplification in p53 lacking neural stem cells lead to accumulation of highly aneuploid cells, reduction of proliferative cells and as a consequence reduced brain size (Marthiens et al., 2013). Thus, it might be interesting to compare cell growth and proliferation of $p53^{+/+}$ to $p53^{-/-}$ RPE1 cells.

Cells lacking the key centriole distal appendages proteins ANKRD26 and SCLT1 accumulated centrioles similarly as control cells, suggesting that their role in the PLK4-induced centriole accumulation is dispensable. However, the group of cells lacking any centrioles positive for ANKRD26 (Fig. 17) is expected in the ANKRD26 KO cells. The SCLT1 KO cells also show group of cells negative for ANKRD26 staining. This could be explained with the ANKRD26 recruitment downstream of SCLT1 (Burigotto et al., 2021). However, in cells negative for ANKRD26 supernumerary centrosomes were still accumulated upon PLK4 OE as visible from the γ-Tubulin and Centrin counts suggesting dispensable role of the mature centrioles proteins in the supernumerary centrosomes accumulation.

While further investigation is required to assess the role of p53 upon supernumerary centrosome accumulation, the SA pipeline developed here would facilitate the centriole quantification for any future experiment or project where this would be necessary.

REFERENCES

Abbas, T., & Dutta, A. (2009). p21 in cancer: intricate networks and multiple activities. *Nature Reviews. Cancer*, *9*(6), 400–414. https://doi.org/10.1038/nrc2657

Agard, N. J., Mahrus, S., Trinidad, J. C., Lynn, A., Burlingame, A. L., & Wells, J. A. (2012). Global kinetic analysis of proteolysis via quantitative targeted proteomics. *Proceedings of the National Academy of Sciences of the United States of America*, *109*(6), 1913–1918. https://doi.org/10.1073/pnas.1117158109

Alberts B, Johnson A, Lewis J, et al. (2002). *Molecular Biology of the Cell* (4th editio). Garland Science. https://www.ncbi.nlm.nih.gov/books/NBK21054/

Andersen, J. L., Johnson, C. E., Freel, C. D., Parrish, A. B., Day, J. L., Buchakjian, M. R., Nutt, L. K., Thompson, J. W., Moseley, M. A., & Kornbluth, S. (2009). Restraint of apoptosis during mitosis through interdomain phosphorylation of caspase-2. *The EMBO Journal*, *28*(20), 3216–3227. https://doi.org/10.1038/emboj.2009.253

Anderson, R. G., & Brenner, R. M. (1971). The formation of basal bodies (centrioles) in the Rhesus monkey oviduct. *The Journal of Cell Biology*, *50*(1), 10–34. https://doi.org/10.1083/jcb.50.1.10

Ando, K., Parsons, M. J., Shah, R. B., Charendoff, C. I., Paris, S. L., Liu, P. H., Fassio, S. R., Rohrman, B. A., Thompson, R., Oberst, A., Sidi, S., & Bouchier-Hayes, L. (2017). NPM1 directs PIDDosome-dependent caspase-2 activation in the nucleolus. *The Journal of Cell Biology*, *216*(6), 1795–1810. https://doi.org/10.1083/jcb.201608095

Aravind, L., Dixit, V. M., & Koonin, E. V. (1999). The domains of death: evolution of the apoptosis machinery. *Trends in Biochemical Sciences*, *24*(2), 47–53. https://doi.org/10.1016/s0968-0004(98)01341-3

Arellano, M., & Moreno, S. (1997). Regulation of CDK/cyclin complexes during the cell cycle. *The International Journal of Biochemistry & Cell Biology*, *29*(4), 559–573. https://doi.org/10.1016/s1357-2725(96)00178-1

Atlas, S. J., & Lin, S. (1978). Dihydrocytochalasin B. Biological effects and binding to 3T3 cells. *The Journal of Cell Biology*, *76*(2), 360–370. https://doi.org/10.1083/jcb.76.2.360

Baliga, B C, Read, S. H., & Kumar, S. (2004). The biochemical mechanism of caspase-2 activation. *Cell Death & Differentiation*, *11*(11), 1234–1241. https://doi.org/10.1038/sj.cdd.4401492

Baliga, Belinda C, Colussi, P. A., Read, S. H., Dias, M. M., Jans, D. A., & Kumar, S. (2003). Role of prodomain in importin-mediated nuclear localization and activation of caspase-2. *The Journal of Biological Chemistry*, *278*(7), 4899–4905. https://doi.org/10.1074/jbc.M211512200

Barak, Y., & Oren, M. (1992). Enhanced binding of a 95 kDa protein to p53 in cells undergoing p53-mediated growth arrest. *The EMBO Journal*, *11*(6), 2115–2121. https://pubmed.ncbi.nlm.nih.gov/1600943

Barnum, K. J., & O'Connell, M. J. (2014). Cell cycle regulation by checkpoints. *Methods in Molecular Biology (Clifton, N.J.)*, *1170*, 29–40. https://doi.org/10.1007/978-1-4939-0888-2_2

Baron, A. T., Greenwood, T. M., Bazinet, C. W., & Salisbury, J. L. (1992). Centrin is a component of the periocentriola lattice. *Biology of the Cell*, *76*(3), 383–388. https://doi.org/https://doi.org/10.1016/0248-4900(92)90442-4

Barr, F. A., Silljé, H. H. W., & Nigg, E. A. (2004). Polo-like kinases and the orchestration of cell division. *Nature Reviews Molecular Cell Biology*, *5*(6), 429–441. https://doi.org/10.1038/nrm1401

Beaudouin, J., Gerlich, D., Daigle, N., Eils, R., & Ellenberg, J. (2002). Nuclear Envelope Breakdown Proceeds by Microtubule-Induced Tearing of the Lamina. *Cell*, *108*(1), 83–96. https://doi.org/10.1016/S0092-8674(01)00627-4

Ben-David, U., & Amon, A. (2020). Context is everything: aneuploidy in cancer. *Nature Reviews Genetics*, *21*(1), 44–62. https://doi.org/10.1038/s41576-019-0171-x

Benkova, B., Lozanov, V., Ivanov, I. P., & Mitev, V. (2009). Evaluation of recombinant caspase specificity by competitive substrates. *Analytical Biochemistry*, *394*(1), 68–74. https://doi.org/10.1016/j.ab.2009.07.012

Benson, E. K., Mungamuri, S. K., Attie, O., Kracikova, M., Sachidanandam, R., Manfredi, J. J., & Aaronson, S. A. (2014). p53-dependent gene repression through p21 is mediated by recruitment of E2F4 repression complexes. *Oncogene*, *33*(30), 3959–3969. https://doi.org/10.1038/onc.2013.378

Bergeron, L., Perez, G. I., Macdonald, G., Shi, L., Sun, Y., Jurisicova, A., Varmuza, S., Latham, K. E., Flaws, J. A., Salter, J. C., Hara, H., Moskowitz, M. A., Li, E., Greenberg, A., Tilly, J. L., & Yuan, J. (1998). Defects in regulation of apoptosis in caspase-2-deficient mice. *Genes & Development*, *12*(9), 1304–1314. https://doi.org/10.1101/gad.12.9.1304

Berube, C., Boucher, L.-M., Ma, W., Wakeham, A., Salmena, L., Hakem, R., Yeh, W.-C., Mak, T. W., & Benchimol, S. (2005). Apoptosis caused by p53-induced protein with death domain (PIDD) depends on the death adapter protein RAIDD. *Proceedings of the National Academy of Sciences of the United States of America*, *102*(40), 14314–14320. https://doi.org/10.1073/pnas.0506475102

Bettencourt-Dias, M., Rodrigues-Martins, A., Carpenter, L., Riparbelli, M., Lehmann, L., Gatt, M. K., Carmo, N., Balloux, F., Callaini, G., & Glover, D. M. (2005). SAK/PLK4 is required for centriole duplication and flagella development. *Current Biology : CB*, *15*(24), 2199–2207. https://doi.org/10.1016/j.cub.2005.11.042

Bieging, K. T., & Attardi, L. D. (2012). Deconstructing p53 transcriptional networks in tumor suppression. *Trends in Cell Biology*, *22*(2), 97–106. https://doi.org/10.1016/j.tcb.2011.10.006

Blow, J. J., & Laskey, R. A. (1988). A role for the nuclear envelope in controlling DNA replication within the cell cycle. *Nature*, *332*(6164), 546–548. https://doi.org/10.1038/332546a0

Boatright, K. M., & Salvesen, G. S. (2003). Mechanisms of caspase activation. *Current Opinion in Cell Biology*, *15*(6), 725–731.

Bodrug, T., Welsh, K. A., Hinkle, M., Emanuele, M. J., & Brown, N. G. (2021). Intricate Regulatory Mechanisms of the Anaphase-Promoting Complex/Cyclosome and Its Role in Chromatin Regulation. *Frontiers in Cell and Developmental Biology*, *9*, 687515. https://doi.org/10.3389/fcell.2021.687515

Bonzon, C., Bouchier-Hayes, L., Pagliari, L. J., Green, D. R., & Newmeyer, D. D. (2006). Caspase-2-induced apoptosis requires bid cleavage: a physiological role for bid in heat shock-induced death. *Molecular Biology of the Cell*, *17*(5), 2150–2157. https://doi.org/10.1091/mbc.e05-12-1107

Bouchier-Hayes, L, & Green, D. R. (2012). Caspase-2: the orphan caspase. *Cell Death and Differentiation*, *19*(1), 51–57. https://doi.org/10.1038/cdd.2011.157

Bouchier-Hayes, Lisa. (2010). The role of caspase-2 in stress-induced apoptosis. *Journal of Cellular and Molecular Medicine*, *14*(6A), 1212–1224. https://doi.org/10.1111/j.1582-4934.2010.01037.x

Bouchier-Hayes, Lisa, Oberst, A., McStay, G. P., Connell, S., Tait, S. W. G., Dillon, C. P., Flanagan, J. M., Beere, H. M., & Green, D. R. (2009). Characterization of cytoplasmic caspase-2 activation by induced proximity. *Molecular Cell*, *35*(6), 830–840. https://doi.org/10.1016/j.molcel.2009.07.023

Boulares, A. H., Yakovlev, A. G., Ivanova, V., Stoica, B. A., Wang, G., Iyer, S., & Smulson, M. (1999). Role of Poly(ADP-ribose) Polymerase (PARP) Cleavage in Apoptosis: CASPASE 3-RESISTANT PARP MUTANT INCREASES RATES OF APOPTOSIS IN TRANSFECTED CELLS *. *Journal of Biological Chemistry*, *274*(33), 22932–22940. https://doi.org/10.1074/jbc.274.33.22932

Boveri, T. (1887). Ueber den Antheil des Spermatozoon an der Teilung des Eies. Sitzungsber. *Ges. Morph. Physiol. München*, *3*, 151–164.

Boveri, T. (1888). Die Befruchtung und Teilung des Eies von Ascaris megalocephala. *Zellen-Studien, Jena*, *Heft 2*.

Boveri, T. (1900). *Zellen-Studien: Über die Natur der Centrosomen*. G. Fischer. https://books.google.it/books?id=gfQYAAAAYAAJ

Boveri, Theodor. (1914). *Zur Frage der Entstehung maligner Tumoren.* Gustav Fischer.

Boveri, Theodor. (2008). Concerning the origin of malignant tumours by Theodor Boveri. Translated and annotated by Henry Harris. *Journal of Cell Science*, *121 Suppl*, 1–84. https://doi.org/10.1242/jcs.025742

Bower, J. J., Vance, L. D., Psioda, M., Smith-Roe, S. L., Simpson, D. A., Ibrahim, J. G., Hoadley, K. A., Perou, C. M., & Kaufmann, W. K. (2017). Patterns of cell cycle checkpoint deregulation associated with intrinsic molecular subtypes of human breast cancer cells. *Npj Breast Cancer*, *3*(1), 9. https://doi.org/10.1038/s41523-017-0009-7

Bowler, M., Kong, D., Sun, S., Nanjundappa, R., Evans, L., Farmer, V., Holland, A., Mahjoub, M. R., Sui, H., & Loncarek, J. (2019). High-resolution characterization of centriole distal appendage morphology and dynamics by correlative STORM and electron microscopy. *Nature Communications*, *10*(1), 993. https://doi.org/10.1038/s41467-018-08216-4

Breslow, D. K., & Holland, A. J. (2019). Mechanism and Regulation of Centriole and Cilium Biogenesis. *Annual Review of Biochemistry*, *88*, 691–724. https://doi.org/10.1146/annurev-biochem-013118-111153

Brocher, J. (2015). The BioVoxxel Image Processing and Analysis Toolbox. In *EuBIAS-Conference* (Vols. 2015, Jan).

Burigotto, M., Mattivi, A., Migliorati, D., Magnani, G., Valentini, C., Roccuzzo, M., Offterdinger, M., Pizzato, M., Schmidt, A., Villunger, A., Maffini, S., & Fava, L. L. (2021). Centriolar distal appendages activate the centrosome-PIDDosome-p53 signalling axis via ANKRD26. *The EMBO Journal*, *40*(4), e104844. https://doi.org/https://doi.org/10.15252/embj.2020104844

Butt, A. J., Harvey, N. L., Parasivam, G., & Kumar, S. (1998). Dimerization and Autoprocessing of the Nedd2

(Caspase-2) Precursor Requires both the Prodomain and the Carboxyl-terminal Regions *. *Journal of Biological Chemistry*, *273*(12), 6763–6768. https://doi.org/10.1074/jbc.273.12.6763
Cai, J., Yang, J., & Jones, D. P. (1998). Mitochondrial control of apoptosis: the role of cytochrome c. *Biochimica et Biophysica Acta*, *1366*(1–2), 139–149. https://doi.org/10.1016/s0005-2728(98)00109-1
Castedo, M., Perfettini, J.-L., Roumier, T., Andreau, K., Medema, R., & Kroemer, G. (2004). Cell death by mitotic catastrophe: a molecular definition. *Oncogene*, *23*(16), 2825–2837. https://doi.org/10.1038/sj.onc.1207528
Castedo, M., Perfettini, J.-L., Roumier, T., Valent, A., Raslova, H., Yakushijin, K., Horne, D., Feunteun, J., Lenoir, G., Medema, R., Vainchenker, W., & Kroemer, G. (2004). Mitotic catastrophe constitutes a special case of apoptosis whose suppression entails aneuploidy. *Oncogene*, *23*(25), 4362–4370. https://doi.org/10.1038/sj.onc.1207572
Chan, J. Y. (2011). A clinical overview of centrosome amplification in human cancers. *International Journal of Biological Sciences*, *7*(8), 1122–1144. https://doi.org/10.7150/ijbs.7.1122
Chen, J., Saha, P., Kornbluth, S., Dynlacht, B. D., & Dutta, A. (1996). Cyclin-binding motifs are essential for the function of p21CIP1. *Molecular and Cellular Biology*, *16*(9), 4673–4682. https://doi.org/10.1128/mcb.16.9.4673
Chen, J., Wu, X., Lin, J., & Levine, A. J. (1996). mdm-2 inhibits the G1 arrest and apoptosis functions of the p53 tumor suppressor protein. *Molecular and Cellular Biology*, *16*(5), 2445–2452. https://doi.org/10.1128/mcb.16.5.2445
Cheng, T.-H., & Cohen, S. N. (2007). Human MDM2 isoforms translated differentially on constitutive versus p53-regulated transcripts have distinct functions in the p53/MDM2 and TSG101/MDM2 feedback control loops. *Molecular and Cellular Biology*, *27*(1), 111–119. https://doi.org/10.1128/MCB.00235-06
Chinnaiyan, A. M. (1999). The apoptosome: heart and soul of the cell death machine. *Neoplasia (New York, N.Y.)*, *1*(1), 5–15. https://doi.org/10.1038/sj.neo.7900003
Chong, W. M., Wang, W.-J., Lo, C.-H., Chiu, T.-Y., Chang, T.-J., Liu, Y.-P., Tanos, B., Mazo, G., Tsou, M.-F. B., Jane, W.-N., Yang, T. T., & Liao, J.-C. (2020). Super-resolution microscopy reveals coupling between mammalian centriole subdistal appendages and distal appendages. *ELife*, *9*, e53580. https://doi.org/10.7554/eLife.53580
Chowdhury, I., Tharakan, B., & Bhat, G. K. (2008). Caspases - an update. *Comparative Biochemistry and Physiology. Part B, Biochemistry & Molecular Biology*, *151*(1), 10–27. https://doi.org/10.1016/j.cbpb.2008.05.010
Cizmecioglu, O., Arnold, M., Bahtz, R., Settele, F., Ehret, L., Haselmann-Weiss, U., Antony, C., & Hoffmann, I. (2010). Cep152 acts as a scaffold for recruitment of Plk4 and CPAP to the centrosome. *The Journal of Cell Biology*, *191*(4), 731–739. https://doi.org/10.1083/jcb.201007107
Coelho, L. P., Shariff, A., & Murphy, R. F. (2009). Nuclear segmentation in microscope cell images: A hand-segmented dataset and comparison of algorithms. *2009 IEEE International Symposium on Biomedical Imaging: From Nano to Macro*, 518–521. https://doi.org/10.1109/ISBI.2009.5193098
Coelho, P. A., Bury, L., Shahbazi, M. N., Liakath-Ali, K., Tate, P. H., Wormald, S., Hindley, C. J., Huch, M., Archer, J., Skarnes, W. C., Zernicka-Goetz, M., & Glover, D. M. (2021). Over-expression of Plk4 induces centrosome amplification, loss of primary cilia and associated tissue hyperplasia in the mouse. *Open Biology*, *5*(12), 150209. https://doi.org/10.1098/rsob.150209
Colussi, P. A., Harvey, N. L., & Kumar, S. (1998). Prodomain-dependent nuclear localization of the caspase-2 (Nedd2) precursor. A novel function for a caspase prodomain. *The Journal of Biological Chemistry*, *273*(38), 24535–24542. https://doi.org/10.1074/jbc.273.38.24535
Conduit, P. T., Wainman, A., & Raff, J. W. (2015). Centrosome function and assembly in animal cells. *Nature Reviews. Molecular Cell Biology*, *16*(10), 611–624. https://doi.org/10.1038/nrm4062
Cook, D. R., Solski, P. A., Bultman, S. J., Kauselmann, G., Schoor, M., Kuehn, R., Friedman, L. S., Cowley, D. O., Van Dyke, T., Yeh, J. J., Johnson, L., & Der, C. J. (2011). The ect2 rho Guanine nucleotide exchange factor is essential for early mouse development and normal cell cytokinesis and migration. *Genes & Cancer*, *2*(10), 932–942. https://doi.org/10.1177/1947601912437035
Coons, A. H., & Kaplan, M. H. (1950). Localization of antigen in tissue cells; improvements in a method for the detection of antigen by means of fluorescent antibody. *The Journal of Experimental Medicine*, *91*(1), 1–13. https://doi.org/10.1084/jem.91.1.1
Cory, S., & Adams, J. M. (2002). The Bcl2 family: regulators of the cellular life-or-death switch. *Nature Reviews Cancer*, *2*(9), 647–656. https://doi.org/10.1038/nrc883
Crasta, K., Ganem, N. J., Dagher, R., Lantermann, A. B., Ivanova, E. V, Pan, Y., Nezi, L., Protopopov, A.,

Chowdhury, D., & Pellman, D. (2012). DNA breaks and chromosome pulverization from errors in mitosis. *Nature*, *482*(7383), 53–58. https://doi.org/10.1038/nature10802
Dalal, Y. (2009). Epigenetic specification of centromeres. *Biochemistry and Cell Biology = Biochimie et Biologie Cellulaire*, *87*(1), 273–282. https://doi.org/10.1139/O08-135
Dawar, S., Lim, Y., Puccini, J., White, M., Thomas, P., Bouchier-Hayes, L., Green, D. R., Dorstyn, L., & Kumar, S. (2017). Caspase-2-mediated cell death is required for deleting aneuploid cells. *Oncogene*, *36*(19), 2704–2714. https://doi.org/10.1038/onc.2016.423
Delaval, B., & Doxsey, S. J. (2010). Pericentrin in cellular function and disease. *The Journal of Cell Biology*, *188*(2), 181–190. https://doi.org/10.1083/jcb.200908114
Deng, C., Zhang, P., Harper, J. W., Elledge, S. J., & Leder, P. (1995). Mice lacking p21CIP1/WAF1 undergo normal development, but are defective in G1 checkpoint control. *Cell*, *82*(4), 675–684. https://doi.org/10.1016/0092-8674(95)90039-x
Diamantis, A., Magiorkinis, E., Sakorafas, G. H., & Androutsos, G. (2008). A Brief History of Apoptosis: From Ancient to Modern Times. *Oncology Research and Treatment*, *31*(12), 702–706. https://doi.org/10.1159/000165071
Dictenberg, J. B., Zimmerman, W., Sparks, C. A., Young, A., Vidair, C., Zheng, Y., Carrington, W., Fay, F. S., & Doxsey, S. J. (1998). Pericentrin and gamma-tubulin form a protein complex and are organized into a novel lattice at the centrosome. *The Journal of Cell Biology*, *141*(1), 163–174. https://doi.org/10.1083/jcb.141.1.163
Diffley, J. (1996). Once and only once upon a time: Specifying and regulating origins of DNA replication in eukaryotic cells. *Genes & Development*, *10*, 2819–2830. https://doi.org/10.1101/gad.10.22.2819
Ditchfield, C., Johnson, V. L., Tighe, A., Ellston, R., Haworth, C., Johnson, T., Mortlock, A., Keen, N., & Taylor, S. S. (2003). Aurora B couples chromosome alignment with anaphase by targeting BubR1, Mad2, and Cenp-E to kinetochores. *The Journal of Cell Biology*, *161*(2), 267–280. https://doi.org/10.1083/jcb.200208091
Dorn, J. F., & Maddox, A. S. (2011). Cytokinesis: cells go back and forth about division. *Current Biology : CB*, *21*(20), R848-50. https://doi.org/10.1016/j.cub.2011.09.012
Dorstyn, L., Puccini, J., Wilson, C. H., Shalini, S., Nicola, M., Moore, S., & Kumar, S. (2012). Caspase-2 deficiency promotes aberrant DNA-damage response and genetic instability. *Cell Death and Differentiation*, *19*(8), 1288–1298. https://doi.org/10.1038/cdd.2012.36
Du, C., Fang, M., Li, Y., Li, L., & Wang, X. (2000). Smac, a mitochondrial protein that promotes cytochrome c-dependent caspase activation by eliminating IAP inhibition. *Cell*, *102*(1), 33–42. https://doi.org/10.1016/s0092-8674(00)00008-8
Duan, H., & Dixit, V. M. (1997). RAIDD is a new "death" adaptor molecule. *Nature*, *385*(6611), 86–89. https://doi.org/10.1038/385086a0
Earnshaw, W. C., Martins, L. M., & Kaufmann, S. H. (1999). Mammalian Caspases: Structure, Activation, Substrates, and Functions During Apoptosis. *Annual Review of Biochemistry*, *68*(1), 383–424. https://doi.org/10.1146/annurev.biochem.68.1.383
Edelheit, O., Hanukoglu, A., & Hanukoglu, I. (2009). Simple and efficient site-directed mutagenesis using two single-primer reactions in parallel to generate mutants for protein structure-function studies. *BMC Biotechnology*, *9*(1), 61. https://doi.org/10.1186/1472-6750-9-61
Ekert, P. G., Read, S. H., Silke, J., Marsden, V. S., Kaufmann, H., Hawkins, C. J., Gerl, R., Kumar, S., & Vaux, D. L. (2004). Apaf-1 and caspase-9 accelerate apoptosis, but do not determine whether factor-deprived or drug-treated cells die. *The Journal of Cell Biology*, *165*(6), 835–842. https://doi.org/10.1083/jcb.200312031
Elmore, S. (2007). Apoptosis: A Review of Programmed Cell Death. *Toxicologic Pathology*, *35*(4), 495–516. https://doi.org/10.1080/01926230701320337
Evans, L. T., Anglen, T., Scott, P., Lukasik, K., Loncarek, J., & Holland, A. J. (2021). ANKRD26 recruits PIDD1 to centriolar distal appendages to activate the PIDDosome following centrosome amplification. *The EMBO Journal*, *40*(4), e105106. https://doi.org/https://doi.org/10.15252/embj.2020105106
Evans, T., Rosenthal, E. T., Youngblom, J., Distel, D., & Hunt, T. (1983). Cyclin: a protein specified by maternal mRNA in sea urchin eggs that is destroyed at each cleavage division. *Cell*, *33*(2), 389–396. https://doi.org/10.1016/0092-8674(83)90420-8
Fakharzadeh, S. S., Trusko, S. P., & George, D. L. (1991). Tumorigenic potential associated with enhanced expression of a gene that is amplified in a mouse tumor cell line. *The EMBO Journal*, *10*(6), 1565–1569. https://pubmed.ncbi.nlm.nih.gov/2026149
Fava, L. L., Bock, F. J., Geley, S., & Villunger, A. (2012). Caspase-2 at a glance. *Journal of Cell Science*, *125*(Pt 24), 5911–5915. https://doi.org/10.1242/jcs.115105

Fava, L. L., Schuler, F., Sladky, V., Haschka, M. D., Soratroi, C., Eiterer, L., Demetz, E., Weiss, G., Geley, S., Nigg, E. A., & Villunger, A. (2017). The PIDDosome activates p53 in response to supernumerary centrosomes. *Genes & Development*, *31*(1), 34–45. https://doi.org/10.1101/gad.289728.116

Fischer, C. A., Besora-Casals, L., Rolland, S. G., Haeussler, S., Singh, K., Duchen, M., Conradt, B., & Marr, C. (2020). MitoSegNet: Easy-to-use Deep Learning Segmentation for Analyzing Mitochondrial Morphology. *IScience*, *23*(10), 101601. https://doi.org/https://doi.org/10.1016/j.isci.2020.101601

Fisher R., Perkins S., Walker A., W. E. (2004). *The Hypermedia Image Processing Reference*. https://homepages.inf.ed.ac.uk/rbf/HIPR2/hipr_top.htm

Flemming, W. (1878). "Zur Kenntniss der Zelle und ihrer Theilungs-Erscheinungen." *Schriften Des Naturwissenschaftlichen Vereins Für Schleswig-Holstein*, *3*, 23–27.

Franklin, E. E., & Robertson, J. D. (2007). Requirement of Apaf-1 for mitochondrial events and the cleavage or activation of all procaspases during genotoxic stress-induced apoptosis. *The Biochemical Journal*, *405*(1), 115–122. https://doi.org/10.1042/BJ20061576

Fürst, E. (1898). Ueber Centrosomen bei Ascaris megalocephala. *Archiv Für Mikroskopische Anatomie*, *52*(1), 97–133. https://doi.org/10.1007/BF02976211

Gall, J. G. (2004). Early Studies on Centrioles and Centrosomes. In *Centrosomes in Development and Disease* (pp. 1–15). https://doi.org/https://doi.org/10.1002/3527603808.ch1

Ganem, N. J., Godinho, S. A., & Pellman, D. (2009). A mechanism linking extra centrosomes to chromosomal instability. *Nature*, *460*(7252), 278–282. https://doi.org/10.1038/nature08136

Gascoigne, K. E., & Taylor, S. S. (2008). Cancer cells display profound intra- and interline variation following prolonged exposure to antimitotic drugs. *Cancer Cell*, *14*(2), 111–122. https://doi.org/10.1016/j.ccr.2008.07.002

Gerschenson, L. E., & Geske, F. J. (2001). Virchow and apoptosis. *The American Journal of Pathology*, *158*(4), 1543. https://doi.org/10.1016/S0002-9440(10)64105-3

Ghetti, S., Burigotto, M., Mattivi, A., Magnani, G., Casini, A., Bianchi, A., Cereseto, A., & Fava, L. L. (2021). CRISPR/Cas9 ribonucleoprotein-mediated knockin generation in hTERT-RPE1 cells. *STAR Protocols*, *2*(2), 100407. https://doi.org/10.1016/j.xpro.2021.100407

Godinho, S. A., Picone, R., Burute, M., Dagher, R., Su, Y., Leung, C. T., Polyak, K., Brugge, J. S., Théry, M., & Pellman, D. (2014). Oncogene-like induction of cellular invasion from centrosome amplification. *Nature*, *510*(7503), 167–171. https://doi.org/10.1038/nature13277

Gönczy, P. (2012). Towards a molecular architecture of centriole assembly. *Nature Reviews. Molecular Cell Biology*, *13*(7), 425–435. https://doi.org/10.1038/nrm3373

Gordon, D. J., Resio, B., & Pellman, D. (2012). Causes and consequences of aneuploidy in cancer. *Nature Reviews Genetics*, *13*(3), 189–203. https://doi.org/10.1038/nrg3123

Green, R. A., Paluch, E., & Oegema, K. (2012). Cytokinesis in animal cells. *Annual Review of Cell and Developmental Biology*, *28*, 29–58. https://doi.org/10.1146/annurev-cellbio-101011-155718

Greenblatt, M. S., Bennett, W. P., Hollstein, M., & Harris, C. C. (1994). Mutations in the p53 tumor suppressor gene: clues to cancer etiology and molecular pathogenesis. *Cancer Research*, *54*(18), 4855–4878.

Gregoli, P. A., & Bondurant, M. C. (1999). Function of caspases in regulating apoptosis caused by erythropoietin deprivation in erythroid progenitors. *Journal of Cellular Physiology*, *178*(2), 133–143. https://doi.org/10.1002/(SICI)1097-4652(199902)178:2<133::AID-JCP2>3.0.CO;2-5

Guichard, P., Hamel, V., & Gönczy, P. (2018). The Rise of the Cartwheel: Seeding the Centriole Organelle. *BioEssays : News and Reviews in Molecular, Cellular and Developmental Biology*, *40*(4), e1700241. https://doi.org/10.1002/bies.201700241

Guidotti, J.-E., Brégerie, O., Robert, A., Debey, P., Brechot, C., & Desdouets, C. (2003). Liver cell polyploidization: a pivotal role for binuclear hepatocytes. *The Journal of Biological Chemistry*, *278*(21), 19095–19101. https://doi.org/10.1074/jbc.M300982200

Gully, C. P., Velazquez-Torres, G., Shin, J.-H., Fuentes-Mattei, E., Wang, E., Carlock, C., Chen, J., Rothenberg, D., Adams, H. P., Choi, H. H., Guma, S., Phan, L., Chou, P.-C., Su, C.-H., Zhang, F., Chen, J.-S., Yang, T.-Y., Yeung, S.-C. J., & Lee, M.-H. (2012). Aurora B kinase phosphorylates and instigates degradation of p53. *Proceedings of the National Academy of Sciences of the United States of America*, *109*(24), E1513-22. https://doi.org/10.1073/pnas.1110287109

Guo, Y., Srinivasula, S. M., Druilhe, A., Fernandes-Alnemri, T., & Alnemri, E. S. (2002). Caspase-2 Induces Apoptosis by Releasing Proapoptotic Proteins from Mitochondria *. *Journal of Biological Chemistry*, *277*(16), 13430–13437. https://doi.org/10.1074/jbc.M108029200

Gupta, A., & Kitagawa, D. (2018). Ultrastructural diversity between centrioles of eukaryotes. *The Journal of Biochemistry*, *164*(1), 1–8. https://doi.org/10.1093/jb/mvy031
Habedanck, R., Stierhof, Y.-D., Wilkinson, C. J., & Nigg, E. A. (2005). The Polo kinase Plk4 functions in centriole duplication. *Nature Cell Biology*, *7*(11), 1140–1146. https://doi.org/10.1038/ncb1320
Hainaut, P., Hernandez, T., Robinson, A., Rodriguez-Tome, P., Flores, T., Hollstein, M., Harris, C. C., & Montesano, R. (1998). IARC Database of p53 gene mutations in human tumors and cell lines: updated compilation, revised formats and new visualisation tools. *Nucleic Acids Research*, *26*(1), 205–213. https://doi.org/10.1093/nar/26.1.205
Hall, M., Bates, S., & Peters, G. (1995). Evidence for different modes of action of cyclin-dependent kinase inhibitors: p15 and p16 bind to kinases, p21 and p27 bind to cyclins. *Oncogene*, *11*(8), 1581–1588.
Hamoir, G. (1992). The discovery of meiosis by E. Van Beneden, a breakthrough in the morphological phase of heredity. *The International Journal of Developmental Biology*, *36*(1), 9–15.
Harper, J. W., Adami, G. R., Wei, N., Keyomarsi, K., & Elledge, S. J. (1993). The p21 Cdk-interacting protein Cip1 is a potent inhibitor of G1 cyclin-dependent kinases. *Cell*, *75*(4), 805–816. https://doi.org/10.1016/0092-8674(93)90499-g
Harris, P. (1961). Electron microscope study of mitosis in sea urchin blastomeres. *The Journal of Biophysical and Biochemical Cytology*, *11*(2), 419–431. https://doi.org/10.1083/jcb.11.2.419
Hartwell, L. H., & Weinert, T. A. (1989). Checkpoints: controls that ensure the order of cell cycle events. *Science (New York, N.Y.)*, *246*(4930), 629–634. https://doi.org/10.1126/science.2683079
Harvey, N. L., Butt, A. J., & Kumar, S. (1997). Functional activation of Nedd2/ICH-1 (caspase-2) is an early process in apoptosis. *The Journal of Biological Chemistry*, *272*(20), 13134–13139. https://doi.org/10.1074/jbc.272.20.13134
Hashimoto, T., Kikkawa, U., & Kamada, S. (2011). Contribution of caspase(s) to the cell cycle regulation at mitotic phase. *PloS One*, *6*(3), e18449–e18449. https://doi.org/10.1371/journal.pone.0018449
Hauf, S., Cole, R. W., LaTerra, S., Zimmer, C., Schnapp, G., Walter, R., Heckel, A., van Meel, J., Rieder, C. L., & Peters, J.-M. (2003). The small molecule Hesperadin reveals a role for Aurora B in correcting kinetochore-microtubule attachment and in maintaining the spindle assembly checkpoint. *The Journal of Cell Biology*, *161*(2), 281–294. https://doi.org/10.1083/jcb.200208092
Haupt, Y., Maya, R., Kazaz, A., & Oren, M. (1997). Mdm2 promotes the rapid degradation of p53. *Nature*, *387*(6630), 296–299. https://doi.org/10.1038/387296a0
Hertwig, W. A. O. (1876). Beitrage zur Kenntnis der Bildung, Befruchtung und Theilung des thierisches Eies. *Morphologisches Jahrbuch*, *1*, 347–434. doi:10.2307/1411521
Hill, M. M., Adrain, C., Duriez, P. J., Creagh, E. M., & Martin, S. J. (2004). Analysis of the composition, assembly kinetics and activity of native Apaf-1 apoptosomes. *The EMBO Journal*, *23*(10), 2134–2145. https://doi.org/10.1038/sj.emboj.7600210
Hinchcliffe, E. H., Li, C., Thompson, E. A., Maller, J. L., & Sluder, G. (1999). Requirement of Cdk2-cyclin E activity for repeated centrosome reproduction in Xenopus egg extracts. *Science (New York, N.Y.)*, *283*(5403), 851–854. https://doi.org/10.1126/science.283.5403.851
Ho, L H, Read, S. H., Dorstyn, L., Lambrusco, L., & Kumar, S. (2008). Caspase-2 is required for cell death induced by cytoskeletal disruption. *Oncogene*, *27*(24), 3393–3404. https://doi.org/10.1038/sj.onc.1211005
Ho, Lien Ha, Taylor, R., Dorstyn, L., Cakouros, D., Bouillet, P., & Kumar, S. (2009). A tumor suppressor function for caspase-2. *Proceedings of the National Academy of Sciences of the United States of America*, *106*(13), 5336–5341. https://doi.org/10.1073/pnas.0811928106
Hofmann, K., Bucher, P., & Tschopp, J. (1997). The CARD domain: a new apoptotic signalling motif. *Trends in Biochemical Sciences*, *22*(5), 155–156. https://doi.org/10.1016/s0968-0004(97)01043-8
Honda, R., Tanaka, H., & Yasuda, H. (1997). Oncoprotein MDM2 is a ubiquitin ligase E3 for tumor suppressor p53. *FEBS Letters*, *420*(1), 25–27. https://doi.org/10.1016/s0014-5793(97)01480-4
Howard, A. & Pelc, S. (1953). Synthesis of deoxyribonucleic acid in normal and irradiatedcells and its relation to chromosome breakage. *Heredity*, *6 (Suppl.)*, 261–273.
Howard, A., & Pelc, S. R. (1986). Synthesis of Desoxyribonucleic Acid in Normal and Irradiated Cells and Its Relation to Chromosome Breakage. *International Journal of Radiation Biology and Related Studies in Physics, Chemistry and Medicine*, *49*(2), 207–218. https://doi.org/10.1080/09553008514552501
Iglesias, L. L., Bellón, P. S., Del Barrio, A. P., Fernández-Miranda, P. M., González, D. R., Vega, J. A., Mandly, A. A. G., & Blanco, J. A. P. (2021). A primer on deep learning and convolutional neural networks for clinicians. *Insights into Imaging*, *12*(1), 117. https://doi.org/10.1186/s13244-021-01052-z

Igney, F. H., & Krammer, P. H. (2002). Death and anti-death: tumour resistance to apoptosis. *Nature Reviews. Cancer*, *2*(4), 277–288. https://doi.org/10.1038/nrc776
Israels, E. D., & Israels, L. G. (2001). The cell cycle. *Stem Cells (Dayton, Ohio)*, *19*(1), 88–91. https://doi.org/10.1634/stemcells.19-1-88
Iyer, D. R., & Rhind, N. (2017). The Intra-S Checkpoint Responses to DNA Damage. *Genes*, *8*(2), 74. https://doi.org/10.3390/genes8020074
Johnson, D. G., & Walker, C. L. (1999). Cyclins and cell cycle checkpoints. *Annual Review of Pharmacology and Toxicology*, *39*, 295–312. https://doi.org/10.1146/annurev.pharmtox.39.1.295
Jonathan Long, Evan Shelhamer, T. D. (2015). Fully convolutional networks for semantic segmentation. *Proceedings of the IEEE Conference on Computer Vision and Pattern Recognition (CVPR), pp. 3431-3440*.
Joshi, H. C., & Zhou, J. B. T.-M. in C. B. (2001). Gamma tubulin and microtubule nucleation in mammalian cells. In *Centrosomes and Spindle Pole Bodies* (Vol. 67, pp. 179–193). Academic Press. https://doi.org/https://doi.org/10.1016/S0091-679X(01)67013-4
Julien, O., & Wells, J. A. (2017). Caspases and their substrates. *Cell Death & Differentiation*, *24*(8), 1380–1389. https://doi.org/10.1038/cdd.2017.44
Julien, O., Zhuang, M., Wiita, A. P., O'Donoghue, A. J., Knudsen, G. M., Craik, C. S., & Wells, J. A. (2016). Quantitative MS-based enzymology of caspases reveals distinct protein substrate specificities, hierarchies, and cellular roles. *Proceedings of the National Academy of Sciences of the United States of America*, *113*(14), E2001-10. https://doi.org/10.1073/pnas.1524900113
Karsenti, E., & Vernos, I. (2001). The mitotic spindle: a self-made machine. *Science (New York, N.Y.)*, *294*(5542), 543–547. https://doi.org/10.1126/science.1063488
Kastenhuber, E. R., & Lowe, S. W. (2017). Putting p53 in Context. *Cell*, *170*(6), 1062–1078. https://doi.org/10.1016/j.cell.2017.08.028
Kaufmann, S. H., Desnoyers, S., Ottaviano, Y., Davidson, N. E., & Poirier, G. G. (1993). Specific Proteolytic Cleavage of Poly(ADP-ribose) Polymerase: An Early Marker of Chemotherapy-induced Apoptosis. *Cancer Research*, *53*(17), 3976 LP – 3985. http://cancerres.aacrjournals.org/content/53/17/3976.abstract
Keoni, C. L., & Brown, T. L. (2015). Inhibition of Apoptosis and Efficacy of Pan Caspase Inhibitor, Q-VD-OPh, in Models of Human Disease. *Journal of Cell Death*, *8*, 1–7. https://doi.org/10.4137/JCD.S23844
Kerr, J. F., Wyllie, A. H., & Currie, A. R. (1972). Apoptosis: a basic biological phenomenon with wide-ranging implications in tissue kinetics. *British Journal of Cancer*, *26*(4), 239–257. https://doi.org/10.1038/bjc.1972.33
Kersse, K., Verspurten, J., Vanden Berghe, T., & Vandenabeele, P. (2011). The death-fold superfamily of homotypic interaction motifs. *Trends in Biochemical Sciences*, *36*(10), 541–552. https://doi.org/10.1016/j.tibs.2011.06.006
Khodjakov, A., & Rieder, C. L. (1999). The sudden recruitment of gamma-tubulin to the centrosome at the onset of mitosis and its dynamic exchange throughout the cell cycle, do not require microtubules. *The Journal of Cell Biology*, *146*(3), 585–596. https://doi.org/10.1083/jcb.146.3.585
Kiefer, B., Sakai, H., Solari, A. J., & Mazia, D. (1966). The molecular unit of the microtubules of the mitotic apparatus. *Journal of Molecular Biology*, *20*(1), 75–79. https://doi.org/https://doi.org/10.1016/0022-2836(66)90118-5
Kitevska, T., Roberts, S. J., Pantaki-Eimany, D., Boyd, S. E., Scott, F. L., & Hawkins, C. J. (2014). Analysis of the minimal specificity of caspase-2 and identification of Ac-VDTTD-AFC as a caspase-2-selective peptide substrate. *Bioscience Reports*, *34*(2), e00100. https://doi.org/10.1042/BSR20140025
Kleylein-Sohn, J., Westendorf, J., Le Clech, M., Habedanck, R., Stierhof, Y.-D., & Nigg, E. A. (2007). Plk4-induced centriole biogenesis in human cells. *Developmental Cell*, *13*(2), 190–202. https://doi.org/10.1016/j.devcel.2007.07.002
Kollman, J. M., Merdes, A., Mourey, L., & Agard, D. A. (2011). Microtubule nucleation by γ-tubulin complexes. *Nature Reviews. Molecular Cell Biology*, *12*(11), 709–721. https://doi.org/10.1038/nrm3209
Krenn, V., & Musacchio, A. (2015). The Aurora B Kinase in Chromosome Bi-Orientation and Spindle Checkpoint Signaling . In *Frontiers in Oncology* (Vol. 5). https://www.frontiersin.org/article/10.3389/fonc.2015.00225
Krumschnabel, G., Sohm, B., Bock, F., Manzl, C., & Villunger, A. (2008). The enigma of caspase-2: The laymen's view. *Cell Death and Differentiation*, *16*, 195–207. https://doi.org/10.1038/cdd.2008.170
Kubbutat, M. H., Jones, S. N., & Vousden, K. H. (1997). Regulation of p53 stability by Mdm2. *Nature*, *387*(6630), 299–303. https://doi.org/10.1038/387299a0
Kudryavtsev, B. N., Kudryavtseva, M. V, Sakuta, G. A., & Stein, G. I. (1993). Human hepatocyte polyploidization kinetics in the course of life cycle. *Virchows Archiv. B, Cell Pathology Including Molecular Pathology*, *64*(6),

387–393. https://doi.org/10.1007/BF02915139
Kumar, S, Kinoshita, M., Noda, M., Copeland, N. G., & Jenkins, N. A. (1994). Induction of apoptosis by the mouse Nedd2 gene, which encodes a protein similar to the product of the Caenorhabditis elegans cell death gene ced-3 and the mammalian IL-1 beta-converting enzyme. *Genes & Development*, *8*(14), 1613–1626. https://doi.org/10.1101/gad.8.14.1613
Kumar, Sharad. (2009). Caspase 2 in apoptosis, the DNA damage response and tumour suppression: enigma no more? *Nature Reviews. Cancer*, *9*(12), 897–903. https://doi.org/10.1038/nrc2745
Lacey, K. R., Jackson, P. K., & Stearns, T. (1999). Cyclin-dependent kinase control of centrosome duplication. *Proceedings of the National Academy of Sciences of the United States of America*, *96*(6), 2817–2822. https://doi.org/10.1073/pnas.96.6.2817
Lakens, D. (2013). Calculating and reporting effect sizes to facilitate cumulative science: a practical primer for t-tests and ANOVAs. *Frontiers in Psychology*, *4*, 863. https://doi.org/10.3389/fpsyg.2013.00863
Lamkanfi, M., Declercq, W., Kalai, M., Saelens, X., & Vandenabeele, P. (2002). Alice in caspase land. A phylogenetic analysis of caspases from worm to man. In *Cell death and differentiation* (Vol. 9, Issue 4, pp. 358–361). https://doi.org/10.1038/sj.cdd.4400989
Lamkanfi, M., Festjens, N., Declercq, W., Berghe, T. Vanden, & Vandenabeele, P. (2007). Caspases in cell survival, proliferation and differentiation. *Cell Death & Differentiation*, *14*(1), 44–55. https://doi.org/10.1038/sj.cdd.4402047
Lampson, M. A., Renduchitala, K., Khodjakov, A., & Kapoor, T. M. (2004). Correcting improper chromosome-spindle attachments during cell division. *Nature Cell Biology*, *6*(3), 232–237. https://doi.org/10.1038/ncb1102
Lawo, S., Hasegan, M., Gupta, G. D., & Pelletier, L. (2012). Subdiffraction imaging of centrosomes reveals higher-order organizational features of pericentriolar material. *Nature Cell Biology*, *14*(11), 1148–1158. https://doi.org/10.1038/ncb2591
Lee, Y., Pei, J., Baumhardt, J. M., Chook, Y. M., & Grishin, N. V. (2019). Structural prerequisites for CRM1-dependent nuclear export signaling peptides: accessibility, adapting conformation, and the stability at the binding site. *Scientific Reports*, *9*(1), 6627. https://doi.org/10.1038/s41598-019-43004-0
Lens, S. M. A., & Medema, R. H. (2019). Cytokinesis defects and cancer. *Nature Reviews Cancer*, *19*(1), 32–45. https://doi.org/10.1038/s41568-018-0084-6
Levine, M. S., Bakker, B., Boeckx, B., Moyett, J., Lu, J., Vitre, B., Spierings, D. C., Lansdorp, P. M., Cleveland, D. W., Lambrechts, D., Foijer, F., & Holland, A. J. (2017). Centrosome Amplification Is Sufficient to Promote Spontaneous Tumorigenesis in Mammals. *Developmental Cell*, *40*(3), 313-322.e5. https://doi.org/10.1016/j.devcel.2016.12.022
Liccardi, G., Ramos Garcia, L., Tenev, T., Annibaldi, A., Legrand, A. J., Robertson, D., Feltham, R., Anderton, H., Darding, M., Peltzer, N., Dannappel, M., Schünke, H., Fava, L. L., Haschka, M. D., Glatter, T., Nesvizhskii, A., Schmidt, A., Harris, P. A., Bertin, J., … Meier, P. (2019). RIPK1 and Caspase-8 Ensure Chromosome Stability Independently of Their Role in Cell Death and Inflammation. *Molecular Cell*, *73*(3), 413-428.e7. https://doi.org/10.1016/j.molcel.2018.11.010
Lichtman, J. W., & Conchello, J.-A. (2005). Fluorescence microscopy. *Nature Methods*, *2*(12), 910–919. https://doi.org/10.1038/nmeth817
Lim, Y., De Bellis, D., Sandow, J. J., Capalbo, L., D'Avino, P. P., Murphy, J. M., Webb, A. I., Dorstyn, L., & Kumar, S. (2021). Phosphorylation by Aurora B kinase regulates caspase-2 activity and function. *Cell Death and Differentiation*, *28*(1), 349–366. https://doi.org/10.1038/s41418-020-00604-y
Lin, Y., Ma, W., & Benchimol, S. (2000). Pidd, a new death-domain-containing protein, is induced by p53 and promotes apoptosis. *Nature Genetics*, *26*(1), 122–127. https://doi.org/10.1038/79102
Livneh, I., Cohen-Kaplan, V., Cohen-Rosenzweig, C., Avni, N., & Ciechanover, A. (2016). The life cycle of the 26S proteasome: from birth, through regulation and function, and onto its death. *Cell Research*, *26*(8), 869–885. https://doi.org/10.1038/cr.2016.86
Lohrum, M. A. E., & Vousden, K. H. (1999). Regulation and activation of p53 and its family members. *Cell Death & Differentiation*, *6*(12), 1162–1168. https://doi.org/10.1038/sj.cdd.4400625
Los, M., Mozoluk, M., Ferrari, D., Stepczynska, A., Stroh, C., Renz, A., Herceg, Z., Wang, Z.-Q., & Schulze-Osthoff, K. (2002). Activation and caspase-mediated inhibition of PARP: a molecular switch between fibroblast necrosis and apoptosis in death receptor signaling. *Molecular Biology of the Cell*, *13*(3), 978–988. https://doi.org/10.1091/mbc.01-05-0272
Luca, F. C., & Ruderman, J. V. (1989). Control of programmed cyclin destruction in a cell-free system. *The Journal of Cell Biology*, *109*(5), 1895–1909. https://doi.org/10.1083/jcb.109.5.1895

Luo, Q., Beaver, J. M., Liu, Y., & Zhang, Z. (2017). Dynamics of p53: A Master Decider of Cell Fate. *Genes*, *8*(2), 66. https://doi.org/10.3390/genes8020066

Maag, R. S., Mancini, M., Rosen, A., & Machamer, C. E. (2005). Caspase-resistant Golgin-160 Disrupts Apoptosis Induced by Secretory Pathway Stress and Ligation of Death Receptors. *Molecular Biology of the Cell*, *16*(6), 3019–3027. https://doi.org/10.1091/mbc.e04-11-0971

Maillard, M. C., Brookfield, F. A., Courtney, S. M., Eustache, F. M., Gemkow, M. J., Handel, R. K., Johnson, L. C., Johnson, P. D., Kerry, M. A., Krieger, F., Meniconi, M., Muñoz-Sanjuán, I., Palfrey, J. J., Park, H., Schaertl, S., Taylor, M. G., Weddell, D., & Dominguez, C. (2011). Exploiting differences in caspase-2 and -3 S_2 subsites for selectivity: structure-based design, solid-phase synthesis and in vitro activity of novel substrate-based caspase-2 inhibitors. *Bioorganic & Medicinal Chemistry*, *19*(19), 5833–5851. https://doi.org/10.1016/j.bmc.2011.08.020

Malumbres, M., Harlow, E., Hunt, T., Hunter, T., Lahti, J. M., Manning, G., Morgan, D. O., Tsai, L.-H., & Wolgemuth, D. J. (2009). Cyclin-dependent kinases: a family portrait. *Nature Cell Biology*, *11*(11), 1275–1276. https://doi.org/10.1038/ncb1109-1275

Mancini, M., Machamer, C. E., Roy, S., Nicholson, D. W., Thornberry, N. A., Casciola-Rosen, L. A., & Rosen, A. (2000). Caspase-2 is localized at the Golgi complex and cleaves golgin-160 during apoptosis. *The Journal of Cell Biology*, *149*(3), 603–612. https://doi.org/10.1083/jcb.149.3.603

Manfredi, J. J. (2010). The Mdm2-p53 relationship evolves: Mdm2 swings both ways as an oncogene and a tumor suppressor. *Genes & Development*, *24*(15), 1580–1589. https://doi.org/10.1101/gad.1941710

Manzl, C, Peintner, L., Krumschnabel, G., Bock, F., Labi, V., Drach, M., Newbold, A., Johnstone, R., & Villunger, A. (2012). PIDDosome-independent tumor suppression by Caspase-2. *Cell Death and Differentiation*, *19*(10), 1722–1732. https://doi.org/10.1038/cdd.2012.54

Manzl, Claudia, Krumschnabel, G., Bock, F., Sohm, B., Labi, V., Baumgartner, F., Logette, E., Tschopp, J., & Villunger, A. (2009). Caspase-2 activation in the absence of PIDDosome formation. *The Journal of Cell Biology*, *185*(2), 291–303. https://doi.org/10.1083/jcb.200811105

Marsden, V. S., Ekert, P. G., Van Delft, M., Vaux, D. L., Adams, J. M., & Strasser, A. (2004). Bcl-2-regulated apoptosis and cytochrome c release can occur independently of both caspase-2 and caspase-9. *The Journal of Cell Biology*, *165*(6), 775–780. https://doi.org/10.1083/jcb.200312030

Marthiens, V., Rujano, M. A., Pennetier, C., Tessier, S., Paul-Gilloteaux, P., & Basto, R. (2013). Centrosome amplification causes microcephaly. *Nature Cell Biology*, *15*(7), 731–740. https://doi.org/10.1038/ncb2746

Matsumoto, Y., Hayashi, K., & Nishida, E. (1999). Cyclin-dependent kinase 2 (Cdk2) is required for centrosome duplication in mammalian cells. *Current Biology : CB*, *9*(8), 429–432. https://doi.org/10.1016/s0960-9822(99)80191-2

Mazzi, S., Lordier, L., Debili, N., Raslova, H., & Vainchenker, W. (2018). Megakaryocyte and polyploidization. *Experimental Hematology*, *57*, 1–13. https://doi.org/10.1016/j.exphem.2017.10.001

McLeod, S. A. (2019). *What does effect size tell you?* https://www.simplypsychology.org/effect-size.html

McLuskey, K., & Mottram, J. C. (2015). Comparative structural analysis of the caspase family with other clan CD cysteine peptidases. *The Biochemical Journal*, *466*(2), 219–232. https://doi.org/10.1042/BJ20141324

McStay, G. P., Salvesen, G. S., & Green, D. R. (2008). Overlapping cleavage motif selectivity of caspases: implications for analysis of apoptotic pathways. *Cell Death and Differentiation*, *15*(2), 322–331. https://doi.org/10.1038/sj.cdd.4402260

Mennella, V., Keszthelyi, B., McDonald, K. L., Chhun, B., Kan, F., Rogers, G. C., Huang, B., & Agard, D. A. (2012). Subdiffraction-resolution fluorescence microscopy reveals a domain of the centrosome critical for pericentriolar material organization. *Nature Cell Biology*, *14*(11), 1159–1168. https://doi.org/10.1038/ncb2597

Meraldi, P, & Nigg, E. A. (2002). The centrosome cycle. *FEBS Letters*, *521*(1), 9–13. https://doi.org/https://doi.org/10.1016/S0014-5793(02)02865-X

Meraldi, Patrick, Lukas, J., Fry, A. M., Bartek, J., & Nigg, E. A. (1999). Centrosome duplication in mammalian somatic cells requires E2F and Cdk2–Cyclin A. *Nature Cell Biology*, *1*(2), 88–93. https://doi.org/10.1038/10054

Miles, M. A., Kitevska-Ilioski, T., & Hawkins, C. J. (2017). Old and Novel Functions of Caspase-2. *International Review of Cell and Molecular Biology*, *332*, 155–212. https://doi.org/10.1016/bs.ircmb.2016.12.002

Mitchell, T. (1997). *Machine Learning*. McGraw Hill.

Mohl, H. (1837). Ueber die Vermehrung der Pflanzen-Zellen durch Theilung. *Flora; Oder Allgemeine Botanische Zeitung*, *20(1)*, 1–32.

Moll, U. M., & Petrenko, O. (2003). The MDM2-p53 Interaction. *Molecular Cancer Research*, *1*(14), 1001 LP –

1008. http://mcr.aacrjournals.org/content/1/14/1001.abstract
Momand, J., Zambetti, G. P., Olson, D. C., George, D., & Levine, A. J. (1992). The mdm-2 oncogene product forms a complex with the p53 protein and inhibits p53-mediated transactivation. *Cell*, *69*(7), 1237–1245. https://doi.org/10.1016/0092-8674(92)90644-R
Moyer, T. C., & Holland, A. J. (2019). PLK4 promotes centriole duplication by phosphorylating STIL to link the procentriole cartwheel to the microtubule wall. *ELife*, *8*. https://doi.org/10.7554/eLife.46054
Musacchio, A., & Salmon, E. D. (2007). The spindle-assembly checkpoint in space and time. *Nature Reviews. Molecular Cell Biology*, *8*(5), 379–393. https://doi.org/10.1038/nrm2163
Nag, S., Qin, J., Srivenugopal, K. S., Wang, M., & Zhang, R. (2013). The MDM2-p53 pathway revisited. *Journal of Biomedical Research*, *27*(4), 254–271. https://doi.org/10.7555/JBR.27.20130030
Nasmyth, K. (1999). Separating sister chromatids. *Trends in Biochemical Sciences*, *24*(3), 98–104. https://doi.org/10.1016/s0968-0004(99)01358-4
Nazockdast, E., & Redemann, S. (2020). Mechanics of the spindle apparatus. *Seminars in Cell & Developmental Biology*, *107*, 91–102. https://doi.org/10.1016/j.semcdb.2020.06.018
Nicholson, D. W., Ali, A., Thornberry, N. A., Vaillancourt, J. P., Ding, C. K., Gallant, M., Gareau, Y., Griffin, P. R., Labelle, M., Lazebnik, Y. A., Munday, N. A., Raju, S. M., Smulson, M. E., Yamin, T.-T., Yu, V. L., & Miller, D. K. (1995). Identification and inhibition of the ICE/CED-3 protease necessary for mammalian apoptosis. *Nature*, *376*(6535), 37–43. https://doi.org/10.1038/376037a0
Nicklas, R. B. (1997). How cells get the right chromosomes. *Science (New York, N.Y.)*, *275*(5300), 632–637. https://doi.org/10.1126/science.275.5300.632
Nigg, E A. (1995). Cyclin-dependent protein kinases: key regulators of the eukaryotic cell cycle. *BioEssays : News and Reviews in Molecular, Cellular and Developmental Biology*, *17*(6), 471–480. https://doi.org/10.1002/bies.950170603
Nigg, Erich A, & Holland, A. J. (2018). Once and only once: mechanisms of centriole duplication and their deregulation in disease. *Nature Reviews. Molecular Cell Biology*, *19*(5), 297–312. https://doi.org/10.1038/nrm.2017.127
Nigg, Erich A, & Stearns, T. (2011). The centrosome cycle: Centriole biogenesis, duplication and inherent asymmetries. *Nature Cell Biology*, *13*(10), 1154–1160. https://doi.org/10.1038/ncb2345
Normand, G., & King, R. W. (2010). Understanding cytokinesis failure. *Advances in Experimental Medicine and Biology*, *676*, 27–55. https://doi.org/10.1007/978-1-4419-6199-0_3
Nurse, P. (1990). Universal control mechanism regulating onset of M-phase. *Nature*, *344*(6266), 503–508. https://doi.org/10.1038/344503a0
Nurse, P. (2000). A Long Twentieth Century of the Cell Cycle and Beyond. *Cell*, *100*(1), 71–78. https://doi.org/10.1016/S0092-8674(00)81684-0
Nutt, L. K., Margolis, S. S., Jensen, M., Herman, C. E., Dunphy, W. G., Rathmell, J. C., & Kornbluth, S. (2005). Metabolic regulation of oocyte cell death through the CaMKII-mediated phosphorylation of caspase-2. *Cell*, *123*(1), 89–103. https://doi.org/10.1016/j.cell.2005.07.032
Nyberg, K. A., Michelson, R. J., Putnam, C. W., & Weinert, T. A. (2002). Toward maintaining the genome: DNA damage and replication checkpoints. *Annual Review of Genetics*, *36*, 617–656. https://doi.org/10.1146/annurev.genet.36.060402.113540
O'Connell, C. B., & Khodjakov, A. L. (2007). Cooperative mechanisms of mitotic spindle formation. *Journal of Cell Science*, *120*(Pt 10), 1717–1722. https://doi.org/10.1242/jcs.03442
O'Reilly, L. A., Ekert, P., Harvey, N., Marsden, V., Cullen, L., Vaux, D. L., Hacker, G., Magnusson, C., Pakusch, M., Cecconi, F., Kuida, K., Strasser, A., Huang, D. C. S., & Kumar, S. (2002). Caspase-2 is not required for thymocyte or neuronal apoptosis even though cleavage of caspase-2 is dependent on both Apaf-1 and caspase-9. *Cell Death and Differentiation*, *9*(8), 832–841. https://doi.org/10.1038/sj.cdd.4401033
O'Shaughnessy, B., & Thiyagarajan, S. (2018). Mechanisms of contractile ring tension production and constriction. *Biophysical Reviews*, *10*(6), 1667–1681. https://doi.org/10.1007/s12551-018-0476-6
Oakley, B. R., Oakley, C. E., Yoon, Y., & Jung, M. K. (1990). Gamma-tubulin is a component of the spindle pole body that is essential for microtubule function in Aspergillus nidulans. *Cell*, *61*(7), 1289–1301. https://doi.org/10.1016/0092-8674(90)90693-9
Oliner, J. D., Pietenpol, J. A., Thiagalingam, S., Gyuris, J., Kinzler, K. W., & Vogelstein, B. (1993). Oncoprotein MDM2 conceals the activation domain of tumour suppressor p53. *Nature*, *362*(6423), 857–860. https://doi.org/10.1038/362857a0
Oliver, T. G., Meylan, E., Chang, G. P., Xue, W., Burke, J. R., Humpton, T. J., Hubbard, D., Bhutkar, A., & Jacks,

T. (2011). Caspase-2-mediated cleavage of Mdm2 creates a p53-induced positive feedback loop. *Molecular Cell*, *43*(1), 57–71. https://doi.org/10.1016/j.molcel.2011.06.012
Paoletti, A., Moudjou, M., Paintrand, M., Salisbury, J. L., & Bornens, M. (1996). Most of centrin in animal cells is not centrosome-associated and centrosomal centrin is confined to the distal lumen of centrioles. *Journal of Cell Science*, *109 (Pt 1*, 3089–3102.
Pardee, A. B. (1989). G1 events and regulation of cell proliferation. *Science*, *246*(4930), 603 LP – 608. https://doi.org/10.1126/science.2683075
Park, H. H., Logette, E., Raunser, S., Cuenin, S., Walz, T., Tschopp, J., & Wu, H. (2007). Death domain assembly mechanism revealed by crystal structure of the oligomeric PIDDosome core complex. *Cell*, *128*(3), 533–546. https://doi.org/10.1016/j.cell.2007.01.019
Park, H. S., Park, J. M., Park, S., Cho, J., Kim, S. Il, & Park, B.-W. (2014). Subcellular localization of Mdm2 expression and prognosis of breast cancer. *International Journal of Clinical Oncology*, *19*(5), 842–851. https://doi.org/10.1007/s10147-013-0639-1
Paroni, G., Henderson, C., Schneider, C., & Brancolini, C. (2001). Caspase-2-induced Apoptosis Is Dependent on Caspase-9, but Its Processing during UV- or Tumor Necrosis Factor-dependent Cell Death Requires Caspase-3 *. *Journal of Biological Chemistry*, *276*(24), 21907–21915. https://doi.org/10.1074/jbc.M011565200
Paroni, G., Henderson, C., Schneider, C., & Brancolini, C. (2002). Caspase-2 can trigger cytochrome C release and apoptosis from the nucleus. *The Journal of Biological Chemistry*, *277*(17), 15147–15161. https://doi.org/10.1074/jbc.M112338200
Parsons, M. J., McCormick, L., Janke, L., Howard, A., Bouchier-Hayes, L., & Green, D. R. (2013). Genetic deletion of caspase-2 accelerates MMTV/c-neu-driven mammary carcinogenesis in mice. *Cell Death & Differentiation*, *20*(9), 1174–1182. https://doi.org/10.1038/cdd.2013.38
Peintner, L., Dorstyn, L., Kumar, S., Aneichyk, T., Villunger, A., & Manzl, C. (2015). The tumor-modulatory effects of Caspase-2 and Pidd1 do not require the scaffold protein Raidd. *Cell Death and Differentiation*, *22*(11), 1803–1811. https://doi.org/10.1038/cdd.2015.31
Picksley, S. M., & Lane, D. P. (1993). The p53-mdm2 autoregulatory feedback loop: a paradigm for the regulation of growth control by p53? *BioEssays : News and Reviews in Molecular, Cellular and Developmental Biology*, *15*(10), 689–690. https://doi.org/10.1002/bies.950151008
Pietenpol, J. A., & Stewart, Z. A. (2002). Cell cycle checkpoint signaling: cell cycle arrest versus apoptosis. *Toxicology*, *181–182*, 475–481. https://doi.org/10.1016/s0300-483x(02)00460-2
Pizzato, M., Erlwein, O., Bonsall, D., Kaye, S., Muir, D., & McClure, M. O. (2009). A one-step SYBR Green I-based product-enhanced reverse transcriptase assay for the quantitation of retroviruses in cell culture supernatants. *Journal of Virological Methods*, *156*(1–2), 1–7. https://doi.org/10.1016/j.jviromet.2008.10.012
Pochampally, R., Fodera, B., Chen, L., Shao, W., Levine, E. A., & Chen, J. (1998). A 60 kd MDM2 isoform is produced by caspase cleavage in non-apoptotic tumor cells. *Oncogene*, *17*(20), 2629–2636. https://doi.org/10.1038/sj.onc.1202206
Poreba, M., Rut, W., Groborz, K., Snipas, S. J., Salvesen, G. S., & Drag, M. (2019). Potent and selective caspase-2 inhibitor prevents MDM-2 cleavage in reversine-treated colon cancer cells. *Cell Death and Differentiation*, *26*(12), 2695–2709. https://doi.org/10.1038/s41418-019-0329-2
Porter, A. G., & Jänicke, R. U. (1999). Emerging roles of caspase-3 in apoptosis. *Cell Death and Differentiation*, *6*(2), 99–104. https://doi.org/10.1038/sj.cdd.4400476
Prestige, M. (1972). THE BIOLOGY OF THE CELL CYCLE. By J. M. Mitchison. Cambridge University Press, 1971. Pp. 313. £4.60. Also issued as a paperback. *Quarterly Journal of Experimental Physiology and Cognate Medical Sciences*, *57*(3), 346–347. https://doi.org/https://doi.org/10.1113/expphysiol.1972.sp002169
Prives, C., & Hall, P. A. (1999). The p53 pathway. *The Journal of Pathology*, *187*(1), 112–126. https://doi.org/10.1002/(SICI)1096-9896(199901)187:1<112::AID-PATH250>3.0.CO;2-3
Ramirez, M. L. G., & Salvesen, G. S. (2018). A primer on caspase mechanisms. *Seminars in Cell & Developmental Biology*, *82*, 79–85. https://doi.org/https://doi.org/10.1016/j.semcdb.2018.01.002
Read, S. H., Baliga, B. C., Ekert, P. G., Vaux, D. L., & Kumar, S. (2002). A novel Apaf-1-independent putative caspase-2 activation complex. *The Journal of Cell Biology*, *159*(5), 739–745. https://doi.org/10.1083/jcb.200209004
Rhee, Y., Gurel, F., Gafni, Y., Dingwall, C., & Citovsky, V. (2000). A genetic system for detection of protein nuclear import and export. *Nature Biotechnology*, *18*(4), 433–437. https://doi.org/10.1038/74500
Ribe, E. M., Jean, Y. Y., Goldstein, R. L., Manzl, C., Stefanis, L., Villunger, A., & Troy, C. M. (2012). Neuronal caspase 2 activity and function requires RAIDD, but not PIDD. *The Biochemical Journal*, *444*(3), 591–599.

https://doi.org/10.1042/BJ20111588
Riedl, S. J., & Salvesen, G. S. (2007). The apoptosome: signalling platform of cell death. *Nature Reviews. Molecular Cell Biology*, *8*(5), 405–413. https://doi.org/10.1038/nrm2153
Robertson, J. D., Enoksson, M., Suomela, M., Zhivotovsky, B., & Orrenius, S. (2002). Caspase-2 acts upstream of mitochondria to promote cytochrome c release during etoposide-induced apoptosis. *The Journal of Biological Chemistry*, *277*(33), 29803–29809. https://doi.org/10.1074/jbc.M204185200
Robeson, A. C., Lindblom, K. R., Wojton, J., Kornbluth, S., & Matsuura, K. (2018). Dimer-specific immunoprecipitation of active caspase-2 identifies TRAF proteins as novel activators. *The EMBO Journal*, *37*(14), e97072. https://doi.org/https://doi.org/10.15252/embj.201797072
Ronneberger, O., Fischer, P., & Brox, T. (2015). *U-Net: Convolutional Networks for Biomedical Image Segmentation BT - Medical Image Computing and Computer-Assisted Intervention – MICCAI 2015* (N. Navab, J. Hornegger, W. M. Wells, & A. F. Frangi (eds.); pp. 234–241). Springer International Publishing.
Roth, J., Dobbelstein, M., Freedman, D. A., Shenk, T., & Levine, A. J. (1998). Nucleo-cytoplasmic shuttling of the hdm2 oncoprotein regulates the levels of the p53 protein via a pathway used by the human immunodeficiency virus rev protein. *The EMBO Journal*, *17*(2), 554–564. https://doi.org/10.1093/emboj/17.2.554
Roussel, M. F. (1999). The INK4 family of cell cycle inhibitors in cancer. *Oncogene*, *18*(38), 5311–5317. https://doi.org/10.1038/sj.onc.1202998
Salvesen, G. S., & Dixit, V. M. (1999). Caspase activation: The induced-proximity model. *Proceedings of the National Academy of Sciences*, *96*(20), 10964 LP – 10967. https://doi.org/10.1073/pnas.96.20.10964
Schafer, K. A. (1998). The Cell Cycle: A Review. *Veterinary Pathology*, *35*(6), 461–478. https://doi.org/10.1177/030098589803500601
Schatten, H. (2008). The mammalian centrosome and its functional significance. *Histochemistry and Cell Biology*, *129*(6), 667–686. https://doi.org/10.1007/s00418-008-0427-6
Schechter, I., & Berger, A. (1967). On the size of the active site in proteases. I. Papain. *Biochemical and Biophysical Research Communications*, *27*(2), 157–162. https://doi.org/10.1016/s0006-291x(67)80055-x
Scheer, U. (2014). Historical roots of centrosome research: discovery of Boveri's microscope slides in Würzburg. *Philosophical Transactions of the Royal Society of London. Series B, Biological Sciences*, *369*(1650), 20130469. https://doi.org/10.1098/rstb.2013.0469
Schmelz, K., Wieder, T., Tamm, I., Müller, A., Essmann, F., Geilen, C.-C., Schulze-Osthoff, K., Dörken, B., & Daniel, P.-T. (2004). Tumor necrosis factor α sensitizes malignant cells to chemotherapeutic drugs via the mitochondrial apoptosis pathway independently of caspase-8 and NF-κB. *Oncogene*, *23*(40), 6743–6759. https://doi.org/10.1038/sj.onc.1207848
Schuster, K., Fan, L., & Harris, L. C. (2007). MDM2 splice variants predominantly localize to the nucleoplasm mediated by a COOH-terminal nuclear localization signal. *Molecular Cancer Research : MCR*, *5*(4), 403–412. https://doi.org/10.1158/1541-7786.MCR-06-0146
Schweizer, A., Briand, C., & Grutter, M. G. (2003). Crystal structure of caspase-2, apical initiator of the intrinsic apoptotic pathway. *The Journal of Biological Chemistry*, *278*(43), 42441–42447. https://doi.org/10.1074/jbc.M304895200
Schweizer, A., Roschitzki-Voser, H., Amstutz, P., Briand, C., Gulotti-Georgieva, M., Prenosil, E., Binz, H. K., Capitani, G., Baici, A., Plückthun, A., & Grütter, M. G. (2007). Inhibition of caspase-2 by a designed ankyrin repeat protein: specificity, structure, and inhibition mechanism. *Structure (London, England : 1993)*, *15*(5), 625–636. https://doi.org/10.1016/j.str.2007.03.014
Seaman, J. E., Julien, O., Lee, P. S., Rettenmaier, T. J., Thomsen, N. D., & Wells, J. A. (2016). Cacidases: caspases can cleave after aspartate, glutamate and phosphoserine residues. *Cell Death and Differentiation*, *23*(10), 1717–1726. https://doi.org/10.1038/cdd.2016.62
Serçin, Ö., Larsimont, J.-C., Karambelas, A. E., Marthiens, V., Moers, V., Boeckx, B., Le Mercier, M., Lambrechts, D., Basto, R., & Blanpain, C. (2016). Transient PLK4 overexpression accelerates tumorigenesis in p53-deficient epidermis. *Nature Cell Biology*, *18*(1), 100–110. https://doi.org/10.1038/ncb3270
Shalini, S, Dorstyn, L., Dawar, S., & Kumar, S. (2015). Old, new and emerging functions of caspases. *Cell Death and Differentiation*, *22*(4), 526–539. https://doi.org/10.1038/cdd.2014.216
Shalini, Sonia, & Kumar, S. (2015). Caspase-2 and the oxidative stress response. *Molecular & Cellular Oncology*, *2*(4), e1004956–e1004956. https://doi.org/10.1080/23723556.2015.1004956
Shaw, P. H. (1996). The role of p53 in cell cycle regulation. *Pathology, Research and Practice*, *192*(7), 669–675. https://doi.org/10.1016/S0344-0338(96)80088-4
Shin, S., Lee, Y., Kim, W., Ko, H., Choi, H., & Kim, K. (2005). Caspase-2 primes cancer cells for TRAIL-mediated

apoptosis by processing procaspase-8. *The EMBO Journal*, *24*(20), 3532–3542. https://doi.org/10.1038/sj.emboj.7600827
Shintomi, K., & Hirano, T. (2010). Sister chromatid resolution: a cohesin releasing network and beyond. *Chromosoma*, *119*(5), 459–467. https://doi.org/10.1007/s00412-010-0271-z
Shyu, Y. J., Liu, H., Deng, X., & Hu, C.-D. (2006). Identification of new fluorescent protein fragments for bimolecular fluorescence complementation analysis under physiological conditions. *BioTechniques*, *40*(1), 61–66. https://doi.org/10.2144/000112036
Silkworth, W. T., Nardi, I. K., Scholl, L. M., & Cimini, D. (2009). Multipolar spindle pole coalescence is a major source of kinetochore mis-attachment and chromosome mis-segregation in cancer cells. *PloS One*, *4*(8), e6564. https://doi.org/10.1371/journal.pone.0006564
Sladky, V. C., Knapp, K., Soratroi, C., Heppke, J., Eichin, F., Rocamora-Reverte, L., Szabo, T. G., Bongiovanni, L., Westendorp, B., Moreno, E., van Liere, E. A., Bakker, B., Spierings, D. C. J., Wardenaar, R., Pereyra, D., Starlinger, P., Schultze, S., Trauner, M., Stojakovic, T., … Villunger, A. (2020). E2F-Family Members Engage the PIDDosome to Limit Hepatocyte Ploidy in Liver Development and Regeneration. *Developmental Cell*, *52*(3), 335-349.e7. https://doi.org/https://doi.org/10.1016/j.devcel.2019.12.016
Sladky, V. C., & Villunger, A. (2020). Uncovering the PIDDosome and caspase-2 as regulators of organogenesis and cellular differentiation. *Cell Death and Differentiation*, *27*(7), 2037–2047. https://doi.org/10.1038/s41418-020-0556-6
Soille, P., & Vincent, L. M. (1990). Determining watersheds in digital pictures via flooding simulations. *Proc.SPIE*, *1360*. https://doi.org/10.1117/12.24211
Sommer, C., & Gerlich, D. W. (2013). Machine learning in cell biology - teaching computers to recognize phenotypes. *Journal of Cell Science*, *126*(Pt 24), 5529–5539. https://doi.org/10.1242/jcs.123604
Sonnen, K. F., Schermelleh, L., Leonhardt, H., & Nigg, E. A. (2012). 3D-structured illumination microscopy provides novel insight into architecture of human centrosomes. *Biology Open*, *1*(10), 965–976. https://doi.org/10.1242/bio.20122337
Sorokin, S. (1962). Centrioles and the formation of rudimentary cilia by fibroblasts and smooth muscle cells. *The Journal of Cell Biology*, *15*(2), 363–377. https://doi.org/10.1083/jcb.15.2.363
Spoerri, L., Oo, Z. Y., Larsen, J. E., Haass, N. K., Gabrielli, B., & Pavey, S. (2015). *Cell Cycle Checkpoint and DNA Damage Response Defects as Anticancer Targets: From Molecular Mechanisms to Therapeutic Opportunities BT - Stress Response Pathways in Cancer: From Molecular Targets to Novel Therapeutics* (G. T. Wondrak (ed.); pp. 29–49). Springer Netherlands. https://doi.org/10.1007/978-94-017-9421-3_3
Storchova, Z., & Pellman, D. (2004). From polyploidy to aneuploidy, genome instability and cancer. *Nature Reviews. Molecular Cell Biology*, *5*(1), 45–54. https://doi.org/10.1038/nrm1276
Strnad, P., Leidel, S., Vinogradova, T., Euteneuer, U., Khodjakov, A., & Gönczy, P. (2007). Regulated HsSAS-6 levels ensure formation of a single procentriole per centriole during the centrosome duplication cycle. *Developmental Cell*, *13*(2), 203–213. https://doi.org/10.1016/j.devcel.2007.07.004
Sullenberger, C., Vasquez-Limeta, A., Kong, D., & Loncarek, J. (2020). With Age Comes Maturity: Biochemical and Structural Transformation of a Human Centriole in the Making. *Cells*, *9*(6). https://doi.org/10.3390/cells9061429
Taha, A. A., & Hanbury, A. (2015). Metrics for evaluating 3D medical image segmentation: analysis, selection, and tool. *BMC Medical Imaging*, *15*(1), 29. https://doi.org/10.1186/s12880-015-0068-x
Talanian, R. V, Quinlan, C., Trautz, S., Hackett, M. C., Mankovich, J. A., Banach, D., Ghayur, T., Brady, K. D., & Wong, W. W. (1997). Substrate specificities of caspase family proteases. *The Journal of Biological Chemistry*, *272*(15), 9677–9682. https://doi.org/10.1074/jbc.272.15.9677
Tan, C. H., Gasic, I., Huber-Reggi, S. P., Dudka, D., Barisic, M., Maiato, H., & Meraldi, P. (2015). The equatorial position of the metaphase plate ensures symmetric cell divisions. *ELife*, *4*, e05124. https://doi.org/10.7554/eLife.05124
Tanaka, T. U. (2002). Bi-orienting chromosomes on the mitotic spindle. *Current Opinion in Cell Biology*, *14*(3), 365–371. https://doi.org/10.1016/s0955-0674(02)00328-9
Tanaka, T. U. (2005). Chromosome bi-orientation on the mitotic spindle. *Philosophical Transactions of the Royal Society of London. Series B, Biological Sciences*, *360*(1455), 581–589. https://doi.org/10.1098/rstb.2004.1612
Tanaka, T. U. (2008). Bi-orienting chromosomes: acrobatics on the mitotic spindle. *Chromosoma*, *117*(6), 521–533. https://doi.org/10.1007/s00412-008-0173-5
Tang, Y., Wells, J. A., & Arkin, M. R. (2011). Structural and enzymatic insights into caspase-2 protein substrate recognition and catalysis. *The Journal of Biological Chemistry*, *286*(39), 34147–34154.

https://doi.org/10.1074/jbc.M111.247627
Taylor, A. M., Shih, J., Ha, G., Gao, G. F., Zhang, X., Berger, A. C., Schumacher, S. E., Wang, C., Hu, H., Liu, J., Lazar, A. J., Cherniack, A. D., Beroukhim, R., & Meyerson, M. (2018). Genomic and Functional Approaches to Understanding Cancer Aneuploidy. *Cancer Cell*, *33*(4), 676-689.e3. https://doi.org/10.1016/j.ccell.2018.03.007
Telliez, J. B., Bean, K. M., & Lin, L. L. (2000). LRDD, a novel leucine rich repeat and death domain containing protein. *Biochimica et Biophysica Acta*, *1478*(2), 280–288. https://doi.org/10.1016/s0167-4838(00)00029-7
Tewari, M., Quan, L. T., O'Rourke, K., Desnoyers, S., Zeng, Z., Beidler, D. R., Poirier, G. G., Salvesen, G. S., & Dixit, V. M. (1995). Yama/CPP32 beta, a mammalian homolog of CED-3, is a CrmA-inhibitable protease that cleaves the death substrate poly(ADP-ribose) polymerase. *Cell*, *81*(5), 801–809. https://doi.org/10.1016/0092-8674(95)90541-3
Thornberry, N. A., Rano, T. A., Peterson, E. P., Rasper, D. M., Timkey, T., Garcia-Calvo, M., Houtzager, V. M., Nordstrom, P. A., Roy, S., Vaillancourt, J. P., Chapman, K. T., & Nicholson, D. W. (1997). A combinatorial approach defines specificities of members of the caspase family and granzyme B. Functional relationships established for key mediators of apoptosis. *The Journal of Biological Chemistry*, *272*(29), 17907–17911. https://doi.org/10.1074/jbc.272.29.17907
Tinel, A., Janssens, S., Lippens, S., Cuenin, S., Logette, E., Jaccard, B., Quadroni, M., & Tschopp, J. (2007). Autoproteolysis of PIDD marks the bifurcation between pro-death caspase-2 and pro-survival NF-kappaB pathway. *The EMBO Journal*, *26*(1), 197–208. https://doi.org/10.1038/sj.emboj.7601473
Tinel, A., & Tschopp, J. (2004). The PIDDosome, a protein complex implicated in activation of caspase-2 in response to genotoxic stress. *Science (New York, N.Y.)*, *304*(5672), 843–846. https://doi.org/10.1126/science.1095432
Tischer, J., Carden, S., & Gergely, F. (2021). Accessorizing the centrosome: new insights into centriolar appendages and satellites. *Current Opinion in Structural Biology*, *66*, 148–155. https://doi.org/10.1016/j.sbi.2020.10.021
Torborg, C. L., & Feller, M. B. (2004). Unbiased analysis of bulk axonal segregation patterns. *Journal of Neuroscience Methods*, *135*(1–2), 17–26. https://doi.org/10.1016/j.jneumeth.2003.11.019
Toyoda, H., Bregerie, O., Vallet, A., Nalpas, B., Pivert, G., Brechot, C., & Desdouets, C. (2005). Changes to hepatocyte ploidy and binuclearity profiles during human chronic viral hepatitis. *Gut*, *54*(2), 297–302. https://doi.org/10.1136/gut.2004.043893
Troy, C. M., & Shelanski, M. L. (2003). Caspase-2 redux. *Cell Death & Differentiation*, *10*(1), 101–107. https://doi.org/10.1038/sj.cdd.4401175
Turing, A. M. (1950). Computing machinery and intelligence. *Mind*, *59*(October).
Uchida, S. (2013). Image processing and recognition for biological images. *Development, Growth & Differentiation*, *55*(4), 523–549. https://doi.org/10.1111/dgd.12054
Ullman, K. S., Powers, M. A., & Forbes, D. J. (1997). Nuclear Export Receptors: From Importin to Exportin. *Cell*, *90*(6), 967–970. https://doi.org/10.1016/S0092-8674(00)80361-X
Upton, J.-P., Austgen, K., Nishino, M., Coakley, K. M., Hagen, A., Han, D., Papa, F. R., & Oakes, S. A. (2008). Caspase-2 cleavage of BID is a critical apoptotic signal downstream of endoplasmic reticulum stress. *Molecular and Cellular Biology*, *28*(12), 3943–3951. https://doi.org/10.1128/MCB.00013-08
Uzbekov, R., & Alieva, I. (2010). *Centriole Duplication or DNA Replication - What Starts Earlier? In: Cytoskeleton: Cell Movement, Cytokinesis and Organelles Organization* (p. pp.127-138).
Uzbekov, R., & Alieva, I. (2018). Who are you, subdistal appendages of centriole? *Open Biology*, *8*(7). https://doi.org/10.1098/rsob.180062
Uzbekov, R. E. (2007). Centriole duplication in PE (SPEV) cells starts before the beginning of the DNA replication. *Biochemistry (Moscow) Supplement Series A: Membrane and Cell Biology*, *1*(3), 206–211. https://doi.org/10.1134/S1990747807030026
Vakifahmetoglu-Norberg, H., & Zhivotovsky, B. (2010). The unpredictable caspase-2: what can it do? *Trends in Cell Biology*, *20*(3), 150–159. https://doi.org/10.1016/j.tcb.2009.12.006
van Beneden E, N. A. (1887). Nouvelle recherches sur la fécondation et la division mitosique chez l'Ascaride mégalocéphale. *Bull. Acad. Royale Belgique 3éme Sér.*, *14*, 215–295.
Van de Craen, M., Declercq, W., Van den brande, I., Fiers, W., & Vandenabeele, P. (1999). The proteolytic procaspase activation network: an in vitro analysis. *Cell Death & Differentiation*, *6*(11), 1117–1124. https://doi.org/10.1038/sj.cdd.4400589
Van Opdenbosch, N., & Lamkanfi, M. (2019). Caspases in Cell Death, Inflammation, and Disease. *Immunity*, *50*(6), 1352–1364. https://doi.org/https://doi.org/10.1016/j.immuni.2019.05.020

Vasquez-Limeta, A., & Loncarek, J. (2021). Human centrosome organization and function in interphase and mitosis. *Seminars in Cell & Developmental Biology*. https://doi.org/https://doi.org/10.1016/j.semcdb.2021.03.020
Vasudevan, A., Schukken, K. M., Sausville, E. L., Girish, V., Adebambo, O. A., & Sheltzer, J. M. (2021). Aneuploidy as a promoter and suppressor of malignant growth. *Nature Reviews Cancer*, *21*(2), 89–103. https://doi.org/10.1038/s41568-020-00321-1
Veronese, E., Castellani, U., Peruzzo, D., Bellani, M., & Brambilla, P. (2013). Machine learning approaches: from theory to application in schizophrenia. *Computational and Mathematical Methods in Medicine*, *2013*, 867924. https://doi.org/10.1155/2013/867924
Vertii, A., Hung, H.-F., Hehnly, H., & Doxsey, S. (2016). Human basal body basics. *Cilia*, *5*, 13. https://doi.org/10.1186/s13630-016-0030-8
Vigneswara, V., & Ahmed, Z. (2020). The Role of Caspase-2 in Regulating Cell Fate. *Cells*, *9*(5). https://doi.org/10.3390/cells9051259
Villunger, A., Michalak, E. M., Coultas, L., Müllauer, F., Böck, G., Ausserlechner, M. J., Adams, J. M., & Strasser, A. (2003). p53- and drug-induced apoptotic responses mediated by BH3-only proteins puma and noxa. *Science (New York, N.Y.)*, *302*(5647), 1036–1038. https://doi.org/10.1126/science.1090072
Viol, L. (2020). *Behavior and regulation of centriolar appendage proteins during mitosis*.
Vitale, I., Manic, G., Castedo, M., & Kroemer, G. (2017). Caspase 2 in mitotic catastrophe: The terminator of aneuploid and tetraploid cells. *Molecular & Cellular Oncology*, *4*(3), e1299274. https://doi.org/10.1080/23723556.2017.1299274
Voorhees, J. J., Duell, E. A., Chambers, D. A., & Marcelo, C. L. (1976). Regulation of cell cycles. *The Journal of Investigative Dermatology*, *67*(1), 15–19. https://doi.org/10.1111/1523-1747.ep12512472
Wang, G., Jiang, Q., & Zhang, C. (2014). The role of mitotic kinases in coupling the centrosome cycle with the assembly of the mitotic spindle. *Journal of Cell Science*, *127*(Pt 19), 4111–4122. https://doi.org/10.1242/jcs.151753
Wang, J. T., & Stearns, T. (2017). The ABCs of Centriole Architecture: The Form and Function of Triplet Microtubules. *Cold Spring Harbor Symposia on Quantitative Biology*, *82*, 145–155. https://doi.org/10.1101/sqb.2017.82.034496
Wang, L., Miura, M., Bergeron, L., Zhu, H., & Yuan, J. (1994). Ich-1, an Ice/ced-3-related gene, encodes both positive and negative regulators of programmed cell death. *Cell*, *78*(5), 739–750. https://doi.org/10.1016/s0092-8674(94)90422-7
Wang, W.-J., Soni, R. K., Uryu, K., & Tsou, M.-F. B. (2011). The conversion of centrioles to centrosomes: essential coupling of duplication with segregation. *The Journal of Cell Biology*, *193*(4), 727–739. https://doi.org/10.1083/jcb.201101109
Watson, J. D., & Crick, F. H. (1953). Molecular structure of nucleic acids; a structure for deoxyribose nucleic acid. *Nature*, *171*(4356), 737–738. https://doi.org/10.1038/171737a0
Wei, M. C., Lindsten, T., Mootha, V. K., Weiler, S., Gross, A., Ashiya, M., Thompson, C. B., & Korsmeyer, S. J. (2000). tBID, a membrane-targeted death ligand, oligomerizes BAK to release cytochrome c. *Genes & Development*, *14*(16), 2060–2071.
Wejda, M., Impens, F., Takahashi, N., Van Damme, P., Gevaert, K., & Vandenabeele, P. (2012). Degradomics reveals that cleavage specificity profiles of caspase-2 and effector caspases are alike. *The Journal of Biological Chemistry*, *287*(41), 33983–33995. https://doi.org/10.1074/jbc.M112.384552
Wilson, E. (1925). The Cell in Development and Heredity. *New York: Macmillan*.
Woodruff, J. B., Wueseke, O., & Hyman, A. A. (2014). Pericentriolar material structure and dynamics. *Philosophical Transactions of the Royal Society of London. Series B, Biological Sciences*, *369*(1650). https://doi.org/10.1098/rstb.2013.0459
Wu, J., & Akhmanova, A. (2017). Microtubule-Organizing Centers. *Annual Review of Cell and Developmental Biology*, *33*(1), 51–75. https://doi.org/10.1146/annurev-cellbio-100616-060615
Wu, X., Bayle, J. H., Olson, D., & Levine, A. J. (1993). The p53-mdm-2 autoregulatory feedback loop. *Genes & Development*, *7*(7A), 1126–1132. https://doi.org/10.1101/gad.7.7a.1126
Xiong, Y. (1996). Why are there so many CDK inhibitors? *Biochimica et Biophysica Acta*, *1288*(1), 1–5. https://doi.org/10.1016/0304-419x(96)00012-1
Xu, B., Kim, S.-T., Lim, D.-S., & Kastan, M. B. (2002). Two molecularly distinct G(2)/M checkpoints are induced by ionizing irradiation. *Molecular and Cellular Biology*, *22*(4), 1049–1059. https://doi.org/10.1128/mcb.22.4.1049-1059.2002
Xu, D., Farmer, A., Collett, G., Grishin, N. V, & Chook, Y. M. (2012). Sequence and structural analyses of nuclear

export signals in the NESdb database. *Molecular Biology of the Cell*, *23*(18), 3677–3693. https://doi.org/10.1091/mbc.E12-01-0046

Xue, J. Z., & Funabiki, H. (2014). Nuclear assembly shaped by microtubule dynamics. *Nucleus (Austin, Tex.)*, *5*(1), 40–46. https://doi.org/10.4161/nucl.28168

Yadav, P., Yadav, R., Jain, S., & Vaidya, A. (2021). Caspase-3, a primary target for natural and synthetic compounds for cancer therapy. *Chemical Biology & Drug Design*. https://doi.org/10.1111/cbdd.13860

Yang, J., & Yang, J. (2009). *Image Pattern Recognition BT - Encyclopedia of Biometrics* (S. Z. Li & A. Jain (eds.); pp. 726–729). Springer US. https://doi.org/10.1007/978-0-387-73003-5_223

Yang, T. T., Chong, W. M., Wang, W.-J., Mazo, G., Tanos, B., Chen, Z., Tran, T. M. N., Chen, Y.-D., Weng, R. R., Huang, C.-E., Jane, W.-N., Tsou, M.-F. B., & Liao, J.-C. (2018). Super-resolution architecture of mammalian centriole distal appendages reveals distinct blade and matrix functional components. *Nature Communications*, *9*(1), 2023. https://doi.org/10.1038/s41467-018-04469-1

Yuan, J., Shaham, S., Ledoux, S., Ellis, H. M., & Horvitz, H. R. (1993). The C. elegans cell death gene ced-3 encodes a protein similar to mammalian interleukin-1 beta-converting enzyme. *Cell*, *75*(4), 641–652. https://doi.org/10.1016/0092-8674(93)90485-9

Zhivotovsky, B, Samali, A., Gahm, A., & Orrenius, S. (1999). Caspases: their intracellular localization and translocation during apoptosis. *Cell Death and Differentiation*, *6*(7), 644–651. https://doi.org/10.1038/sj.cdd.4400536

Zhivotovsky, Boris, & Orrenius, S. (2005). Caspase-2 function in response to DNA damage. *Biochemical and Biophysical Research Communications*, *331*(3), 859–867. https://doi.org/10.1016/j.bbrc.2005.03.191

Zimmerman, W. C., Sillibourne, J., Rosa, J., & Doxsey, S. J. (2004). Mitosis-specific anchoring of gamma tubulin complexes by pericentrin controls spindle organization and mitotic entry. *Molecular Biology of the Cell*, *15*(8), 3642–3657. https://doi.org/10.1091/mbc.e03-11-0796

Zorman, M., & Verlic, M. (2009). Explanatory approach for evaluation of machine learning-induced knowledge. *The Journal of International Medical Research*, *37*(5), 1543–1551. https://doi.org/10.1177/147323000903700532

Zou, K. H., Warfield, S. K., Bharatha, A., Tempany, C. M. C., Kaus, M. R., Haker, S. J., Wells, W. M. 3rd, Jolesz, F. A., & Kikinis, R. (2004). Statistical validation of image segmentation quality based on a spatial overlap index. *Academic Radiology*, *11*(2), 178–189. https://doi.org/10.1016/s1076-6332(03)00671-8